Winter 2-2-2021

Cape Gooseberry Husk for the Removal of CECs from Wastewater: A Biosorption Study

Jehan Abdel Salam
j.abdelsalam@aucegypt.edu

The American University in Cairo

School of Science and Engineering

Department of Chemistry

Cape Gooseberry Husk for the removal of CECs from Wastewater: A biosorption study

Master Thesis Project

By:

Jehan Abdel Salam

Under the Supervision of:

Dr. Mayyada El-Sayed

January 2021

Abstract

Food and beverage industries produce large amounts of fruit wastes that are normally discarded every year. Meanwhile, these industries along with the pharmaceutical industries discharge wastewater effluents that are loaded with contaminants of emerging concern (CECs). Recent research is directed towards finding alternative cost effective and sustainable solutions for treating wastewater. In this regard, we investigated cape gooseberry husk as a potential biosorbent for the removal of caffeine (CA) and salicylic acid (SA), as examples of CECs, from wastewater. Three different types of husk were investigated; un-activated husk (H), and chemically activated husks (H350 and H500) prepared by acid treatment and heating at 350^{o}C and 500^{o}C, respectively. The husks were characterized using Fourier transform infrared (FTIR) spectroscopy, scanning electron microscopy (SEM), CHNS analysis, Brunauer- Emmet- Teller (BET), zeta potential (ZP) and point of zero charge (PZC) measurements. All three types of husks were primarily mesoporous and negatively charged. The activation of the husk resulted in an increase in the surface area, pore volume and average pore size. The activation also led to the disappearance of some functional groups due to husk carbonization, as confirmed by FTIR. The single-component adsorption of SA and CA onto the three husks was investigated at different pHs and pH 6.5 was selected as the optimal pH for operation. The effect of initial concentration was also examined at the optimal pH. At the low range of concentrations of up to 70 mg/L, the maximum removal efficiencies reached up to 59%, 85%, and 85% for H, H350 and H500, respectively. At the higher concentration range (70-280 mg/L), the percent removal averaged around 55% for the three husks. Similarly for CA, up to 56%, 65% and 63% respective removal efficiencies were obtained for H, H350, and H500, below 85 mg/L. They, as well, averaged around 55% similar to SA adsorption, in most of the employed range of concentrations (82-400 mg/L). Adsorption was influenced by the textural properties along with the surface charge on the adsorbent. The adsorption of SA and CA onto all different types of husk was best described by the pseudo-second-order kinetic model. H350 exhibited high rates of adsorption towards SA and CA, since adsorption was likely governed by fast surface reaction kinetics. The adsorption isotherms for CA onto H, H350 and H500 were best fitted to the Linear adsorption model, and same applied for SA adsorption onto H. For the adsorption of SA onto H350 and H500, the Freundlich isotherm model was a better fit. The isotherm parameters along with energies of adsorption suggested physisorption with higher

favorability for the activated husks, as well as stronger binding of CA onto the husk as compared to SA binding. It was proposed that CA interacts electrostatically with the husk, while SA binds through weak physical interactions like van der Waals' and H-bonding. H350 was chosen as the optimal husk for further binary studies since it offered rapid adsorption with efficient removal towards SA and CA. In binary systems, CA adsorption was highly favored over SA adsorption, possibly owing to its electrostatic interactions. Additionally, the husk was successfully regenerated and re-used for up to 4 consecutive cycles.

Acknowledgments

I would like to express my utter and sincere appreciation and gratitude to my supervisor Dr. Mayyada ElSayed whom without her supervision, guidance and constant support this graduate thesis would not have seen light. She provided me with all the help and advice. I really appreciate it. Thank you.

I would also like to thank my beloved family and friends for their continuous and genuine support they provided me throughout this whole process. It would not have been possible without. I know it was not an easy process and I cannot thank my family enough for the financial support they have offered me.

Last but not least, a special gratitude I give to Khaled Abdel Rahim without his support this would not have been possible. He was always there for assistance. He made sure that it was an easy and smooth process.

I would like to extend my sincere thanks to all of them.

Table of Contents

List of Figures:

List of Tables:

List of Abbreviations:

ATWP	: Advanced Wastewater Treatment Plant
BET	: Brunauer- Emmet- Teller
C_e	: solution concentration at equilibrium
CA	: Caffeine
CEC	: Contaminants of emerging concern
EDC	: endocrine disruptive compounds
Fig	: Figure
FTIR	: Fourier Transform Infrared Spectroscopy
H	: un-activated cape gooseberry husk
H350	: activated cape gooseberry husk at 350°C
H500	: activated cape gooseberry husk at 500°C
HPLC	: High Performance Liquid Chromatography
M-PMD-P-A	: magnetic polar post-cross-linked resin
PCP	: Personal Care Products
PGDpc_D	: polar-modified post-cross-linked polystyrene
pK_a	: acid dissociation constant
PZC	: Point of zero charge
q	: quantity adsorbed in the solid phase
q_e	: equilibrium adsorbed quantity
R^2	: correlation factor
SA	: Salicylic Acid
SE	: Secondary electrons
SEM	: Scanning Electron Microscopy
TNT	: titania nanotublar
WWTP	: Wastewater Treatment Plant
WRRF	: Water Resource Recovery Facility
ZP	: Zeta potential

Chapter 1
Introduction

1. Introduction

Contaminants of emerging concern (CECs), also known as emerging contaminants include any chemical, synthetic or natural, or microorganism that is present in the environment but is not commonly monitored. The accumulation of CECs in the environment causes disruptions to the ecosystem as well as health hazards to humans. These contaminants have been present and released into the environment for a very long time. However, they were not properly detected due to lack of knowledge on their appropriate detection methods. In addition, their adverse health effects have not been fully examined or elucidated, especially those relevant to the long-term exposure. Some emerging contaminants are also new chemicals that were recently introduced and have not yet been detected. [1, 2]

The current Wastewater Treatment Plants (WWTPs) are not designed to remove CECs from water and there are still no current regulations that companies need to abide by for the discharge of these contaminants. In fact, there are thousands of different compounds which are being employed in industry and their removal from industrial effluents depends on their chemical and physical properties such as their solubility, volatility, absorbance and biodegradability. Therefore, various adsorbent materials and adsorption techniques are currently being examined for the safe removal of CECs.[3]

Over the last few decades, the production and the use of medications has increased tremendously with the advanced medical science and with the population's increase. It is assumed that around 3000 different compounds are being used in the pharmaceutical industry. As a result, hundreds of tons are being produced annually. However, unfortunately, massive amounts of these pharmaceuticals are being discarded in the water system. Samples of urban, livestock agricultural water and surface water have been examined and traces of these pharmaceuticals have been detected.[4] According to a document issued by the WHO Organization, the presence of these pharmaceuticals in water should not be of concern since the concentration of these pharmaceuticals

is much less than their minimum therapeutic dose. However, as previously mentioned, there is an increased concern with the long-term exposure to these pharmaceuticals on the human health and the ecosystem, even at these minimal concentrations. [4, 5]

Of the common compounds used in pharmaceutical industries are Salicylic Acid (SA) and Caffeine (CA). Salicylic acid is used in medications that treat acne, dandruff, calluses, among others. It is used commonly in the pharmaceutical industry as an antiseptic and disinfecting agent. It is also used in skin care products such as oils, creams, facial cleansers and gels. As for caffeine, it is an important ingredient in food and pharmaceutical industries. Specifically, it is most commonly used in the beverage industry as a stimulant which belongs to the group of xanthines. It, thus, has potency to fight fatigue and sleepiness. Therefore in the pharmaceutical industry, CA is used in many painkillers and other drugs to counteract the effect of drowsiness. CA is also used as a vasodilator (an ingredient that relaxes blood vessels) and a as diuretic (an ingredient that increases urination). [6, 7]

There are a number of physical, chemical and biological processes employed to treat the wastewater effluents before they are released into the environment. Some of the physical techniques include membrane filtration, coagulation, physisorption, and ion exchange. Oxidation, advanced oxidation and electrochemical methods are common chemical techniques. Biological processes include aerobic, anaerobic or enzymatic treatments. These conventional techniques still suffer from some technical issues as well as environmental and economic disadvantages. Biosorption proposes an alternative technique for wastewater treatment that is potentially eco-friendly and cost-effective, since the utilized adsorbents are derived from a natural bio-based origin. Several agricultural wastes have been successfully used for treating CECs such as rice husk, coconut husk and fruit peels. In this work, we investigate the use of the agricultural waste cape gooseberry husk in removing SA and CA from water via biosorption. The origin of the Cape gooseberry, or *Physalis peruviana*, is Peru and Chile however, it is currently being cultivated in other countries such as: Kenya, South Africa, India, Egypt and New Zealand, among others. Although it is still considered as a backyard fruit, it is drawing a lot of attention and becoming more important over the last few years due to several factors: fast growing nature, productivity, adaptability to different soil conditions and high nutritional values of the fruit. In Egypt, it is mostly found in Al-Nubaria region in ElBaheira governate, which is part of the Nile Delta. Cape

gooseberry husk is commonly produced from domestic wastes or effluents of food and beverage industries where the fruit is used to make puree or for jam production. [8, 9, 10, 11, 12, 13, 14]

1.1 Statement of Purpose

The aim of this work is to examine the possibility of using cape gooseberry husk as a novel biosorbent for the efficient removal of different CECs like CA and SA from wastewater. To the best of our knowledge, this is the first report to deploy cape gooseberry husk as a sorbent. Adsorption will be conducted for each of the untreated husk and the chemically activated husk under various operating conditions. Thus, we propose a facile, environmentally-friendly and cost-effective process to be used in wastewater treatment plants (WWTPs) for the removal of CECs. This process could be integrated in WWTPs as an add-on polishing process or as an alternative to existing tertiary processes. Hence, the specific objectives of this work are the following:

- Preparation and characterization of the untreated and the chemically activated husks.
- Investigating the different parameters affecting the sorption of SA and CA onto the prepared husks in single-component systems.
- Studying and modeling the equilibrium and kinetics of SA and CA sorption onto the prepared husks in single-component systems.
- Selection of the optimal husk in terms of sorption performance.
- Assessing sorption in binary systems of SA and CA using the selected husk.
- Evaluating husk regeneration in binary systems.

Chapter 2
Literature Review

2. Literature review

2.1 Contaminants of Emerging Concern

There are a huge number of emerging contaminants that are very unrelated and diverse in their structure, synthesis, use and health effects. Thus, they are usually categorized according to their use, purpose or other common categories. In Table 2.1, the main categories of CECs are being listed based on their use, place of detection and suspected health effects.[1]

Table 2..1 Different categories of CECs, place of occurrence and possible health effects.[1]

Category	**Place of Detection**	**Suspected Health Effects**
Antibiotics	Groundwater, surface water, WWTP effluent, land applied biosolids, recycled water	Antibiotic resistance in disease causing bacteria, thus complicating treatment of infections
Disinfectants	Wastewater, WWTP effluent, surface and ground water	Genotoxicity, cytotoxicity carcinogenicity
Fire Retardants	Sewage sludge, natural waterways, accumulation in bioorganisms such as fishes, whales and other aquatic lives	Endocrine disruption, higher risk of cancer
Industrial Additives	Industrial and household waste	possible toxicity to ecosystem, animals and humans
Life-style products (Nicotine and Caffeine)	Ground water, surface water and WWTP effluent	Possible cellular stress and negative impact on the reproductive activity of animals
Nonprescription drugs	WWTP effluent, surface water and recycled water	Still unknown
Other prescription drugs	Ground water, surface water, and recycled water	Higher rates of cancer and organ damage

Over the last decade, a number of studies have been performed on CECs in order to examine their fate, occurrence and ecotoxicology. Studies were conducted in soil, marine sediments, wastewater and in aquatic environments. Fig. 2.1 depicts the number of research studies published per pollutant up to the year 2017. "White" represents "conventional" pollutants, or in other words, pollutants that have long been examined. "Gray" represents re-emerging contaminants and "black" emerging ones. Thus as indicated in Fig. 2.1, CECs have not been as extensively studied as other pollutants, however, they are gaining a wide popularity with relevant amount of research increasing tremendously over the last decade.[15]

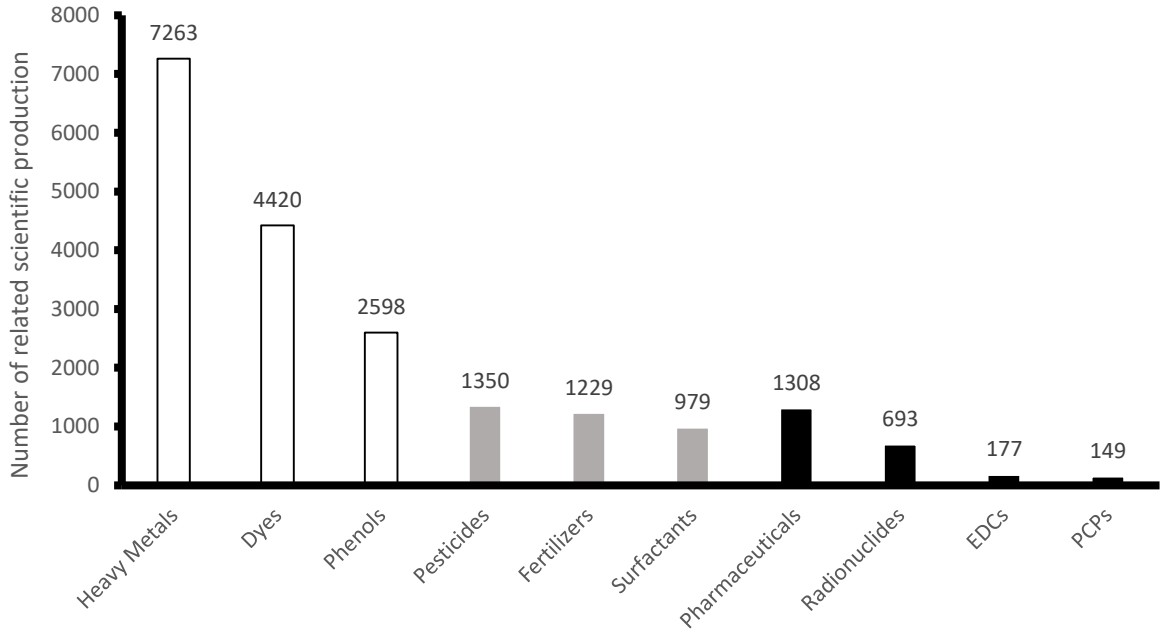

Figure 2.1 Number of scientific articles published per each group of pollutants [15]. EDCs are short for endocrine disruptive compounds and PCPs for personal care products.

In this work, we focus on the removal of two pharmaceutical compounds, SA and CA, from wastewater. Thus, we will give an overview of these compounds in the following lines.

2.1.1 Salicylic Acid

According to the IUPAC naming system, salicylic acid (SA) is monohydroxybenzoic acid ($C_7H_6O_3$) whose structure is shown in Fig. 2.2. It is a white, crystalline powder that could be

extracted from several plants such as willow and myrtle trees. However, it needs further treatment such as separation and purification in order to obtain pure SA.

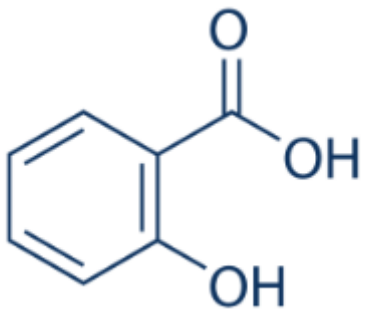

Figure 2.2 Molecular Structure of SA.[16]

The synthesis of SA is carried out via a series of reactions where sodium hydroxide reacts first with a phenol to give water and sodium phenate (Eq. 2.1). In the next step, the sodium phenate is left to react with carbon dioxide yielding sodium salicylate (Eq. 2.2). At last, sulfuric acid is added to the sodium salicylate giving salicylic acid as indicated by (Eq. 2.3). The relevant chemical equations could be written as follows [16]:

$C_6H_5OH + NaOH \rightarrow C_6H_5ONa + H_2O$ Eq. (2.1)

$C_6H_5ONa + CO_2 \rightarrow C_7H_5NaO_3$ Eq. (2.2)

$C_7H_5NaO_3 \rightarrow C_7H_6O_3$ in H_2SO_4 Eq. (2.3)

SA is the main ingredient in aspirin (acetylsalicylic acid). Aspirin is a common medication consumed for the treatment of fever, inflammation and pain. SA is also used in agriculture for the protection of the plants from insects and germs. The compound is commonly found in wastewater effluents of pharmaceutical, cosmetic, paper milling industries and others. It was reported that SA could have negative effects on human health when consumed constantly as it causes headaches, nausea and its accumulation in the human body affects the kidney and liver. In the structure of SA, a benzene ring is attached to a carboxylic group as illustrated in Fig. 2.2 This carboxylic group is an electron-withdrawing group resulting in SA being a non-degradable persistent contaminant. Therefore, there is a great interest in removing SA from water cycles.[16,17,18]

2.1.2 Caffeine

1,3,7 – Trimethylpurine- 2.6-dione is the IUPAC name for Caffeine (CA). It is a stimulant to the nervous system and is most commonly used as a psychoactive drug. CA is one of the most versatile compounds, being a constituent in numerous beverages and medicines. It is one of the oldest known stimulants that provide alertness and dodge sleep, and could sometimes be addictive. In medicine, CA aids with mild respiratory depression cases and helps in the treatment of circulatory failures. Additionally, it is sometimes added in the aspirin or ergotamine preparations for the treatment of headaches and migraines. CA is a natural alkaloid that is found in the leaves, fruits or seeds of around 63 plant species. The amount of CA present varies from one plant to another, however, the Cacao and guarana trees possess high caffeine content. Fig. 2.3a portrays the chemical structure of CA and Fig.2.3b is protonated CA. [19]

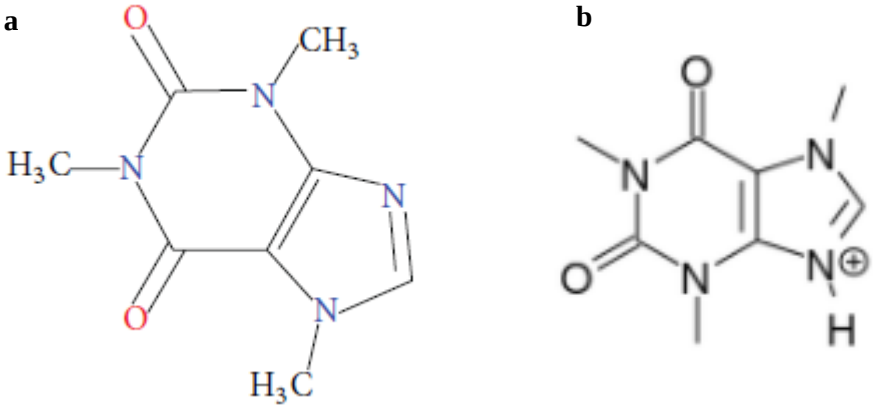

Figure 2.3 Chemical Structure of Caffeine (a) and protonated Caffeine (b). [19]

CA can also be synthesized from dimethylurea and malonic acid. However, CA is not commonly synthesized but is obtained as a byproduct of decaffeination. Decaffeination is the extraction of CA from coffee beans. There are various solvents that could be employed in the extraction process. One of the most commonly used extraction techniques is water extraction. Green coffee is soaked in water until CA is completely dissolved. Afterward, the CA-containing water is passed through a filter made out of activated carbon. The filter allows water and other solid particles to pass through, but rejects CA molecules which are relatively large. The mixture of water with coffee flavored solids is then placed in a fresh coffee batch. Due to simple law of diffusion, the caffeine

migrates from the fresh coffee beans to the mixture. This yields coffee beans that are completely decaffeinated and CA that could be then recovered. [20]

Another commonly used method in the decaffeination process is supercritical carbon dioxide processing. Carbon dioxide supercritical fluid has both gas and liquid properties. It can permeate a porous substance and at the same time dissolve its constituents. Since carbon dioxide supercritical fluid is nonpolar, it is mixed with a polar solvent, water, in order to dissolve the caffeine. At first, the coffee beans are steamed till they start to swell. Afterward, the steamed coffee beans are introduced to the carbon dioxide supercritical fluid. Since the CO_2 supercritical fluid is mixed with water and it has gaseous properties, it starts penetrating the coffee beans and dissolves the caffeine in the beans releasing almost 97% of the total amount of CA present. Thus, the flavor in the beans remains intact. The CO_2 supercritical fluid mixture is then passed through a charcoal membrane and the caffeine molecule is separated based on its size. CA is finally obtained as a white powder which is then used in the beverage and pharmaceutical industries. [20]

In the following lines, we will discuss wastewater treatment methods in general. Afterward, we will focus on biosorption and its application in the removal of CECs.

2.2 Wastewater Treatment

Wastewater treatment (WWT) is the process of removing contaminants from wastewater, thus producing an effluent which could be of use. The main target of treating wastewater is to make domestic and industrial effluents safer by removing organic and inorganic solids. Wastewater could then be disposed into different water bodies such as rivers, lakes or oceans, without imposing any danger on the human health. Wastewater is always subject to treatment, even in basic forms, before it is used again as in the case of irrigation. The treatment process takes place in a Wastewater Treatment Plant (WWTP) also known as Water Resource Recovery Facility (WRRF).

The influent of a WWTP contains traces of organic contaminants. However, most of the WWTPs are only designed to eliminate biochemical oxygen demand (BOD), suspended solids and other nutrients. Individual organic chemicals are not considered. The current set-up of a WWTP can only remove a percentage of these contaminants. After treatment, the effluent of the WWTP is

discharged in any nearby river, lake...etc. The process of wastewater treatment generally consists of four stages; namely, preliminary, primary, secondary, and tertiary/advanced treatment. [6, 21]

Preliminary treatment removes large objects such as rags and wood pieces. These objects could destroy the plant equipment. Primary treatment occurs in some kind of basin or settling tank where heavy objects settle at the bottom and other foreign bodies such as plastic bags float at the top. Suspended solids are mainly removed in this step. In the secondary treatment, a biological system is deployed where microorganisms clarify the water by digesting its organic matter content and decreasing its BOD. In most cases, these microorganisms are aerobic and the basin is aerated by constant stirring. This process is also referred to as activated sludge process and some CECs might biodegrade and metabolize or partition into the sludge during this process. CO_2, NO_3 and H_2O are the main products of this step. Another sedimentation basin and a recycle system are used after the biological treatment. In some plants, there is a nitrification-denitrification process. Nitrification is the conversion of ammonia to nitrate and then nitrite. In the denitrification step, nitrite is converted to nitrogen and other gases. Tertiary Treatment is not present in all plants. It is necessary in order to reduce the level of nitrogen, phosphorous and halides remaining in the water after the secondary stage. It is also needed to remove other nutrients and the microorganisms that were used in the secondary stage. Advanced treatment methods such as adsorption, filtration, advanced oxidation can be used as polishing steps to remove trace and toxic pollutants that might include CECs. Fig. 2.4 is a schematic diagram of a WWTP. [21, 22, 23]

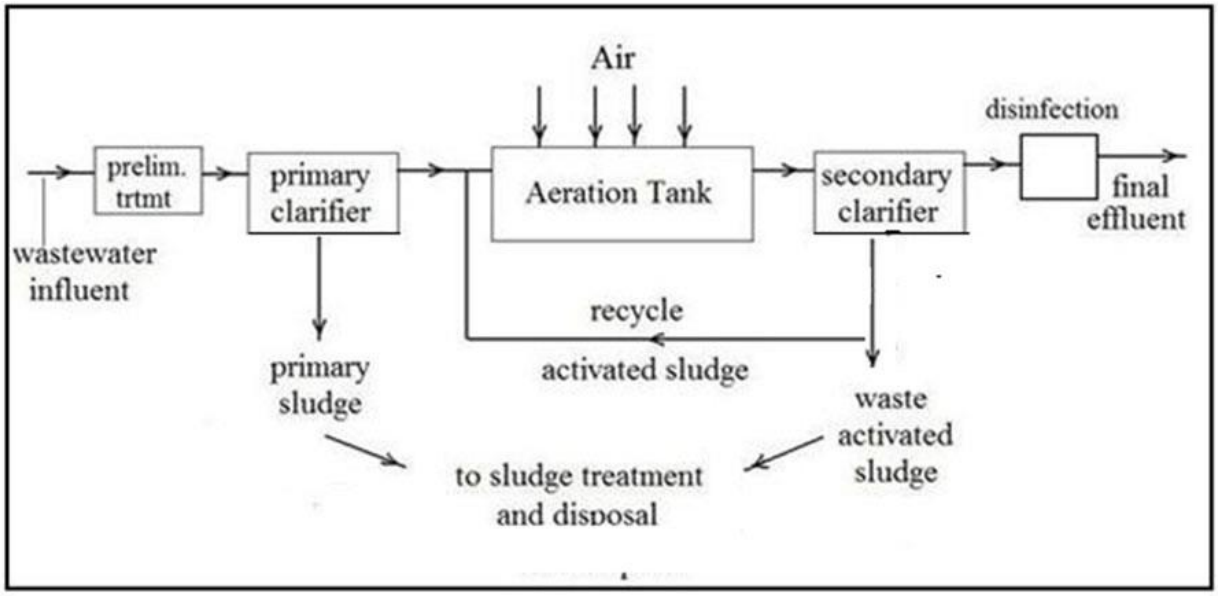

Figure 2.4 Schematic Diagram of a WWTP [21]

A WWTP produces waste solids which are often termed as sludge or biosolids. This sludge needs to be managed and requires further treatment before it is being discharged. Each country, presumably, has its own set of regulations and limits for disposing of the effluents. The main parameters which are monitored are the following: suspended solids, biochemical oxygen demand after 5-day incubation (BOD_5), pH, temperature, grease and oil. Sometimes, other parameters are added based on the industry. Treated wastewater could have multiple applications depending on the requirement and the degree of treatment, examples are firefighting supply, irrigation and sometimes groundwater recharge. [21]

2.2.1 Wastewater Treatment in Egypt

In Egypt, the River Nile is the primary source of water. With the construction of the Grand Ethiopian Renaissance Dam, water supply to Egypt might be at risk. Additionally, Egypt's demand for water is growing due to the following reasons: population growth, urbanization, better living standards and expansion of agricultural areas to match the needs. Since Nile water and

groundwater are better allocated for drinking and domestic uses, treatment of wastewater is crucial to fill in the void in the agricultural sector. [24]

In 2011, there was approximately 7.1 BCM (Billion Cubic Meters) of produced wastewater in Egypt. However, unfortunately, 3.7 BCM out of the 7.1 BCM remain untreated. About 2.4 BCM undergo secondary treatment, while 0.9 BCM go through primary treatment and 0.068 BCM through tertiary treatment. Alas, with a total of 3.368 BCM of treated water, only 0.271 BCM are directly used in agriculture whereas the rest is discarded. As part of the 2030 National Vison for Wastewater Reuse in Egypt, it is planned to upgrade all primary treatment plants to secondary treatment ones. With this vision, it is predicted that, in 2030, Egypt will produce 11.673 BCM of wastewater; 11.607 BCM will undergo secondary treatment and the rest of the quantity will pass through tertiary treatment. It is also planned that 5.82 BCM will be directly utilized in agriculture. This development is necessary in order to irrigate the planned expansion of 1.45 Million Feddans in agricultural lands. [24]

As of 2018, there are 409 WWTPs in Egypt belonging to the Holding Company for drinking water and sanitary drainage which falls under the Ministry of Housing, Utilities and Urban Communities. They cover only 59.7% of the wastewater in Egypt. Wastewater treatment process in Egypt follows primarily the same process mentioned above while activated sludge is the most commonly employed secondary stage. [24]

2.3 Removal of SA via sorption

Several studies used polymeric adsorbents for the removal of SA from water. The adsorption of SA onto different polymeric resins was studied and results were compared to those obtained with activated charcoal as an adsorbent. Activated charcoal, however, showed better performance than the polymeric resins. The adsorption isotherm was fitted to both the Langmuir and the Natta multisite model, while adsorption kinetics followed the pseudo-first order model. The effect of temperature was also tested where higher temperature decreased the quantity of SA adsorbed. [5] Another novel polymeric adsorbent which is the polar-modified post-cross-linked polystyrene (PGDpc_D) was investigated for the adsorption of SA, then compared to adsorption using the

precursors of PGDpc_D and the nonpolar counterpart. Results showed that PGDpc_D was the most efficient adsorbent for SA at the optimal pH of 3. Equilibrium data fitted both Langmuir and Freundlich isotherm models. The reaction was very fast as diffusion in the micropores was the rate determining step. Thus, PGDpc_D was proven to be efficient in the removal of SA from aqueous solutions. [25] Other workers synthesized a novel resin, magnetic polar post-cross-linked resin (M-PMD-P-A) for the adsorption of SA. The resin was characterized by FT-IR, BET surface area, pore volume, TEM and powder X-Ray diffraction. Adsorption equilibrium fitted both Langmuir and Freundlich isotherm models. The reaction was rapid and its kinetics followed the pseudo-second- order model. Adsorption was influenced by pH. Depending on the pH of the solution, SA was present in its molecular, mono-anion or di-anion form. When pH lied between 2.2 and 10.67, adsorption was more favorable towards the molecular form of SA due to the presence of polar amide and amino groups on the resins. A removal efficiency of about 77% was achieved at an initial SA concentration of 988.1 mg/L. Desorption was conducted using a mixture of NaOH and ethanol to obtain a percentage recovery of 95.4%. The regenerated M-PMD-P-A was reused while its efficiency was reduced to 91.4% after five cycles of adsorption- desorption. [17]

In an attempt to increase the removal efficiency of SA from wastewater, a combined process of adsorption and photodegradation of SA was studied using a biofilm immobilized onto activated carbon (AC). The biofilm was made out of *Pseudomonas putida* bacteria which can biodegrade phenolic groups. AC was employed as the adsorbent, while *P. putida* bacteria was used for the biodegradation of SA. The presence of the biofilm reduced the adsorption capacity of AC as it blocked the active sites for SA. However, the use of a free-cells system resulted in an increase in the adsorption of SA. Almost 100% of SA was adsorbed using this system. With respect to the adsorption/biodegradation process, the biofilm yielded very promising results that surpassed the individual performance of each of AC and the biological treatment, especially when the initial concentrations were high. [26] In addition to single-component systems, the same workers examined the adsorption of SA in multi-component systems using charcoal produced from pulp mill sludge. The adsorptive capacity of charcoal was evaluated for the removal of SA along with other pharmaceuticals of diclofenac, ibuprofen and acetaminophen from real wastewater. For a better understanding of the adsorptive behavior of each pharmaceutical, the equilibrium and the kinetics of their adsorption from wastewater was compared to that from ultrapure water and there was no significant difference between the two. Kinetics of adsorption of SA followed the pseudo-second-

order model. However, salicylic acid had the lowest equilibrium adsorption capacity relative to other pharmaceuticals. [27]

A large-scale study examined the removal of five different contaminants, one hormone; 17a-ethinylestradiol, two pharmaceuticals; salicylic acid (SA) and trimethoprim, a drug; carbamazepine, and one surfactant metabolite; nonylphenol from wastewater. The study was performed at a large-scale Advanced Wastewater Treatment Plant (AWTP) located in Washington, DC, USA. Samples were collected from the different stages of the AWTP where they underwent solid phase extraction (SPE) to extract the contaminants from the liquid phase. Then, HPLC was used in order to separate the individual contaminants. The aim was to study the efficiency of removing the above mentioned contaminants in each of the wastewater treatment stages, and to identify the mechanism for their removal as being sorption or biodegradation. About 94% of SA was removed in the secondary stage. The acidic nature of SA allowed it to be adsorbed. Thus, its sorption was more favorable than its biodegradation. [6]

2.4 Removal of CA via sorption

The adsorption of CA and diclofenac onto activated carbon in aqueous column systems was studied. The effects of initial concentration, volumetric flow rate and column length on adsorption were examined. Results showed that diclofenac had a better affinity to activated carbon than CA and thus it exhibited a higher adsorption capacity of 233.9 mg/g compared to 190.9 mg/g for CA. In a binary system, the adsorption capacity was reduced due to competition over the available active sites. Adsorption of both contaminants onto activated carbon was best described by the Freundlich isotherm. [28]

Along with adsorption, the photocatalytic degradation of both SA and CA was investigated using titania nanotubular (TNT**)** films. The films of 20 μm length were prepared using an electrochemical anodization process and had a growth rate of 10 μm/h. Upon comparing them to the commercial TiO_2 nanoparticulate films (Evonik P25), TNT films showed a larger surface area and a highly porous structure allowing for efficient adsorption of both emerging contaminants. The TNT films

were also calcinated at 450°C rendering them an anatase crystal structure that led to high degradation rates for both SA and CA. The effect of pH on the photocatalytic degradation of SA and CA was examined as well. The photocatalytic degradation of both contaminants was best at the neutral pH (around 6). The produced TNT films were characterized by high endurance and, therefore, an ability to sustain multiple photocatalytic cycles. The study, thus, concluded that photocatalytic degradation on TNT films can be a suitable and efficient add-on process to the already existing wastewater treatment methods. [29]

2.5 Biosorption

In biosorption, the adsorption occurs on a compound of biological origin. Low cost, high efficiency, reduction of the chemical and biological sludge, and regeneration of the adsorbent are considered to be some of the advantages of this process when compared to other more conventional methods. Additionally, it does not follow one type of mechanism and could be used for the removal of several pollutants. For a biosorbent to be considered cheap, it must satisfy these conditions: 1) being abundant in nature, 2) being a waste product or a by-product, and 3) should only undergo minimal treatments. The biggest challenge in biosorption is to find a biosorbent which satisfies the above mentioned characteristics, while, at the same time, having a high affinity towards the desired pollutant. Several parameters affect biosorption such as the nature of the pollutant, the mechanism of removal of the pollutant and cost of the whole process. This is just to name a few of these parameters. [8]

The biosorption process involves an adsorbent as the solid-phase and an adsorbate dissolved in the liquid-phase, usually water. [30] Biosorbents could be grouped into the following categories: living biomass, dead biomass, agricultural wastes, industrial wastes and natural residues. Examples of agricultural wastes are fruit peels, fibers, leaves, rice husk and wheat bran. Fig. 2.5 shows the different categories of adsorbents. Numerous studies reported the use of rice husk, different nut shells, fruit peels, wheat bran, chitin and chitosan as biosorbents for heavy metals and dyes. However, unfortunately, less research has been published on utilizing industrial wastes from food or pharmaceutical industries as biosorbents for CECs. [8]

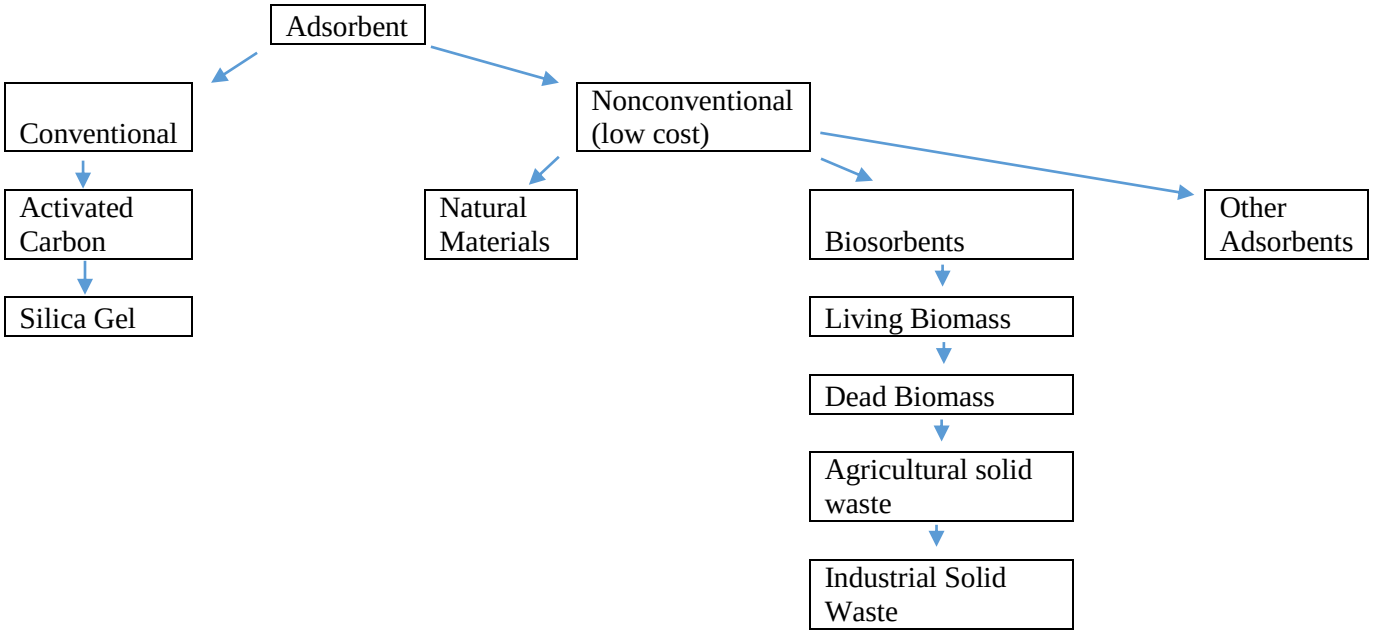

Figure 2.5 Different categories of adsorbents. [8]

2.5.1 Influencing parameters

There are different operating factors that affect biosorption:

1. Solution pH and the ionic strength,
2. Adsorbate concentration and the adsorbent dose,
3. Temperature,
4. Particle size of the sorbent,
5. Agitation speed,
6. Mode of operation, and
7. Competition of other co-ions [8]

1) **pH and ionic strength**

The pH of the sorbate solution is an important factor in biosorption. It affects the charge of the functional groups of the adsorbent and the dissociation of the adsorbates. In addition to that, it also influences the solubility of the adsorbate and the degree of ionization. [8]

2) **Adsorbate concentration and adsorbent dose**

Higher adsorbate concentration results in less mass transfer resistance which, in turn, enhances the adsorption capacity. The same is also true for the adsorbent dose. The higher the dose of the adsorbent, the higher the uptake amount of adsorbate. Higher adsorbent dose means more active sites available for the adsorbate to bind to.[8] In some cases, the adsorption capacity decreases at very high adsorbent doses due to agglomeration of the adsorbent particles.

3) **Temperature**

Temperature plays an important role in wastewater treatment. Wastewater effluents sometimes have high temperatures as a result of the processing steps. The effect of temperature on biosorption depends on the thermodynamics of the reaction taking place between the adsorbent and adsorbate. An exothermic reaction results in a decrease in the biosorption capacity due a decrease in the surface activity. The opposite is true for an endothermic reaction. [8]

4) **Particle size of the sorbent**

Most of the studies have shown, that the surface reaction is the rate limiting step in biosorption. In these studies, the initial rate of sorption was highest at the beginning and then decreased gradually until it reached a plateau. This indicates that other steps such as film or pore diffusion are negligible or are very fast. In case where the surface reaction is the rate limiting step, smaller particle size enhances the rate of the reaction. It also provides more accessible active sites for the adsorbate and, thus, increases the biosorption capacity.

5) **Agitation speed**

An increase in the agitation speed overcomes the mass transfer resistance and thus increases the biosorption capacity. However, this is only valid up to a certain level.

Increasing the agitation speed further will have a negative effect as it could fragment the biomass.[8]

6) **Mode of operation**

There are two main modes of operation for biosorption, batch and column systems. In most studies so far, the batch system has been efficiently employed. In column dynamics, the column dimensions and the flow rate affect the rate of sorption. Less studies were performed on column systems.

7) **Competition of other co-ions**

The presence of co-ions in the solution can decrease the adsorption capacity due to competition of ions over the active sites. [8, 31, 32]

2.5.2 Biosorption of SA

Fruit peels were utilized as biosorbents for SA. One study reported the adsorption of benzoic acid and SA onto banana peels. The peels were examined using FTIR spectroscopy, scanning electron microscopy (SEM), BET surface area, CHNS analysis and X-ray fluorescence. For the biosorption, several operating factors have been evaluated: temperature, pH, adsorbent dose, initial adsorbate concentration and contact time. A higher adsorbent dose resulted in better adsorption. However, after a certain dosage, a further increase did not yield better results. The optimum pH was 3.68 and 3.3 for benzoic acid and SA, respectively. Applying higher pH values reduced the removal percentage of SA. At very low pH values adsorption occured via hydrogen bonding. When the pH increased and approached the PZC of banana peel (i.e., 5.4), the relative positive charge on the peel decreased and SA became more negative. Thus, the electrostatic force interactions became weaker and as a result the removal percentage decreased In addition, the removal efficiency increased with contact time up till equilibrium was approached and the efficiency became almost constant. As for temperature and initial concentration, their increase resulted in an increase in the equilibrium adsorption capacity. Adsorption equilibrium was best described by Freundlich isotherm model, and kinetics of the adsorption of SA were predicted by the pseudo-first order model. The study concluded that banana peel is a cheap, effective adsorbent for benzoic acid and SA. [11] Another study used pineapple peel to synthesize a magnetic biosorbent to be used for the removal of SA from an aqueous solution. In this work, the pineapple peel was magnetized using a

chemical precipitation method. An increase in the adsorbent dosage resulted in an increase in the removal percentage until reaching a plateau. The optimal operating pH in this study was 3.8 and a further increase in the pH affected the adsorption capacity of the pineapple peel negatively as was the case with the banana peel study discussed earlier. [33]

Activated carbon produced from wastes was successfully employed for SA biosorption. Powdered activated carbon prepared from rice and coffee husk was evaluated for its adsorption capacity to SA and sulfosalicylic acid. The effect of contact time was assessed, and it was observed that the reaction followed the pseudo-second-order model and it occurred in two steps. The first step is a fast one, while the second is a slow step. Furthermore, an increase in the adsorbent quantity led to an increase in the adsorption capacity due to the presence of more active sites. Another factor that influenced adsorption was the pH. When the pH was lower than the pH of point of zero charge, the adsorption capacity was enhanced. At these low pH values, the surface of the adsorbent was positively charged and thus there was a strong affinity towards the adsorbate SA anions.[34] Pine wood biochar was also efficient in adsorbing SA and ibuprofen. The biochar was analyzed by FT-IR, SEM, TEM, point of zero charge and BET surface area analysis. Several factors affected the biosorption; temperature, pH and initial concentration of adsorbate. Adsorption of ibuprofen and SA was better in the acidic media than in the basic one. An increase in temperature resulted in an increase in the adsorbed amount of salicylic acid indicating that the reaction is endothermic. Increasing the adsorbate concentration also had a positive effect on the adsorbed quantity. The reaction followed pseudo- second order kinetics and the biochar was regenerated by methanol with an efficacy of 93% and 88% for the desorption of SA and ibuprofen, respectively.[35]

2.5.3 Biosorption of CA

Activated carbon was prepared using peach stones which have been chemically treated with H_3PO_4. This treatment furnished a mesoporous adsorbent with a high surface area. Additionally, the adsorbent underwent oxidation and gas phase treatments in order to assess the effect of the chemical surface groups (oxygenated groups) on the adsorption process. The prepared activated carbon was used for the biosorption of CA, diclofenac and carbamazepine, and it showed the highest adsorption capacity for carbamazepine compared to the other examined emerging

contaminants. It was concluded that the physiochemical properties of the adsorbent and the adsorbate govern the adsorption rate.[36]

Carbon xerogels were employed in the adsorption of CA and diclofenac. The maximum adsorption capacity of CA reached 182.5 mg/g. Adsorption equilibrium followed Sips isotherm equation, whereas kinetics followed the pseudo-second order model. The adsorption of CA was best achieved when the carbon xerogel was treated with urea solution which enhanced adsorption due to the presence of Lewis bases on the surface of the adsorbent. This increased the affinity of the organic compounds to the surface.[37]

2.5.4 Cape Gooseberry (*Physalis peruviana*) Husk as a biosorbent

Physalis peruviana is a plant species from the genus Physalis and the family Solanaceae. The origin of the plant is Peru. The plant and its natural fruit are more commonly known as cape gooseberry, goldenberry poha and physalis. It is now grown in temperate and tropic zones.[38]

The fruit is round, small and has a sweet-acidic taste. It resembles a small, yellow cherry tomato, with a very smooth outer skin. Its color is green when it is unripe and yellow to orange when it is ripe. It is enclosed by a calyx (husk). This husk grows with the fruit for its protection and it is easily removable. Fig. 2.6 illustrates an image of cape gooseberries.[38]

Figure 2.6 Cape Gooseberries [39]

Cape Gooseberry is rich in Vitamin C and Vitamin A and it is a good source of antioxidants. It is also constituted of thiamin (vitamin B1) and niacin (vitamin B3) but not at high concentrations. The oil from the berry has been analyzed. Linoleic and oleic acid were found to be the main fatty acids present. The oil also included vitamin K and beta-carotene. Additionally, it also contained beta-sistosterol and campesterol as the main phytosterols.

Currently, around 800-1000 MT of cape gooseberry are grown in Egypt, mainly in El Baheira governorate. It is being used for household consumption or in the food and beverage industry. Companies process it to make puree as in the case of Döhler Egypt which produces around 15 MT of puree annually. During processing, the calyx or husk is removed and discarded. So, it is considered as a natural waste and is not of use.[40]

To date, no biosorption studies were conducted on *Physalis peruviana* husk. However, one study was reported on the biosorption of green tomato (tomatillo) husk. Tomatillo and Goldenberry are closely related as they belong to the same genus (*Physalis*) according to the scientific classifications but they are different species. In this study, the tomatillo husk was treated with formaldehyde in order to prevent color leaching. Then, the adsorption of iron (III), manganese (II) and a binary system thereof was studied onto the modified husk. Results showed that the modified tomatillo husk was capable of removing Fe^{3+} from the aqueous solution to about 78.8% of its initial concentration and Mn^{2+} to about 76.6%. Adsorption followed pseudo-second order kinetics and it occurred in two steps, an initial rapid step and a subsequent slow step until equilibrium was reached. Results from the binary system revealed that Fe^{3+} and Mn^{2+} do not compete with one another and their adsorption capacity was similar to that in the single-component system.[41]

Chapter 3
Theoretical Background

3. Theoretical Background

3.1 Ultraviolet-Visible Spectroscopy

The range of wavelength for the ultraviolet-visible region is from 190 nm to 800 nm. Ultraviolet-Visible Spectroscopy is a qualitative and quantitative technique. However, it is mainly used for quantitative analysis. It can give information about the structure of the molecule but has been mainly used for measuring unknown concentrations. [42]

During continuous radiation, atoms and molecules are excited from the ground state to an excited level. Energy is only adsorbed if it matches the energy difference between the ground and the exited state. In the range of ultraviolet radiation, the transitions that take place are between different electronic energy levels. Thus, in UV-Visible Spectroscopy, when a molecule absorbs energy, an electron is excited from the highest occupied molecular orbital (HOMO) to the lowest unoccupied molecular orbital (LUMO). [42]

The difference in energy between the excited and the ground state is reflected in the frequency of the spectral lines. Each transition is specified by its wavelength and the molar absorption coefficient. Fig. 3.1 shows the different electronic excitations which the electrons might undergo. It also shows the difference in energies between these transitions. [42]

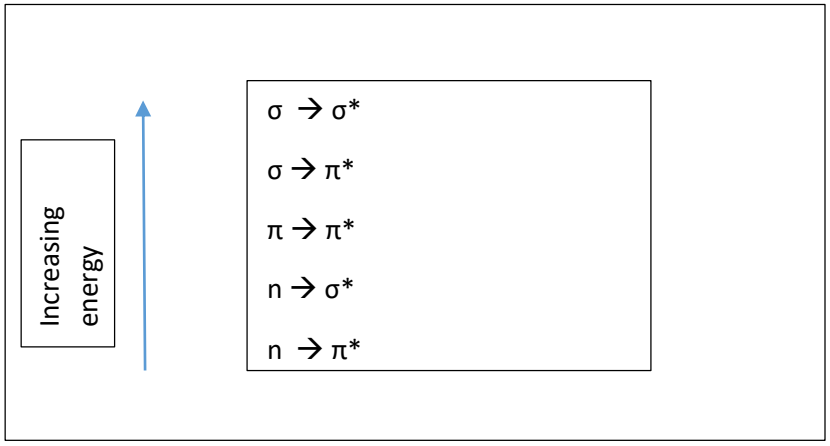

Figure 3.1 Possible transitions. [42]

Beer- Lambert Law is used to correlate absorbance and concentration as given by the equation hereunder:

$$A = abc \qquad \text{Eq. 3.1}$$

where

A = Absorbance

a = molar absorptivity. It is a property of the molecule being excited and is wavelength-dependent. Its units are given by $L.mol^{-1}cm^{-1}$. Additionally, it also varies with temperature and the type of solvent used.

b = path length in cm

c = concentration of the compound/species being studied (mol/L)

In order to be able to determine unknown concentrations, a calibration curve needs to be constructed. The curve is a plot of A vs c. Since absorbance and concentration are directly proportional as given by Beer- Lambert law, a straight line which passes through the origin is obtained. This will allow us to determine any unknown sample concentration using its absorbance. However, Beer- Lambert Law is only valid at low concentrations. At higher concentrations, solute-solute interactions will occur resulting in deviations in the proportionality between absorbance and concentration. [42]

3.2 Fourier Transform Infrared (FTIR) Spectroscopy

Infrared Spectroscopy (IR) is one of the most powerful and used analytical techniques nowadays. Practically, any organic or inorganic compound containing a covalent bond can absorb radiation in the infrared region of the electromagnetic spectrum. The wavelength of this region spans between 400 – 800nm. Choosing the correct sampling technique, allows materials available in different forms, liquids or solids, to be examined. This gives IR an edge over other techniques.[43]

The energies of the electromagnetic radiation corresponding to the IR region are not very high. This energy can be expressed by the following equation:

$$E = h\nu \qquad \text{Eq. 3.2}$$

where h is Planck's constant and ν is the frequency. The frequency is inversely proportional to the wavelength.

The IR spectrum of a molecule could be used as a fingerprint. No two molecules could produce the same spectrum since bonds are different in their frequencies and the environment where this bond is present plays a role as well. In Infrared Spectroscopy, only the vibrational portion is of interest. Like the other absorption techniques, infrared absorption is a quantized process. The molecule can only absorb radiation with very specific frequencies; frequencies corresponding to energy difference between two states. Once the radiation is absorbed, the molecule is excited to a higher energy state. Radiation of this region will result in the stretching and the bending of the covalent bonds. However, not all covalent bonds can absorb radiation in this region. Bonds which do not possess a dipole moment cannot absorb frequencies in this range, for example O_2. Asymmetric bonds, which possess a dipole moment, can absorb IR radiation. This is due to the changes in the electric dipole of the bond which could then couple with the electromagnetic field of the incoming radiation.[42]

The IR region gives information about the chemical structures of organic molecules. Different bonds (N-H, C-H, O-H, C=O and so on) absorb radiation at different regions of the vibrational IR region. For example, absorption in the range of 1715 +/- 100 cm^{-1} is due to a C=O bond. For each bond, there is a specific range as indication by the correlation chart for IR spectroscopy.[42]

FT-IR is a great advance in the world of IR. It produces an interferogram. The interferogram is a complex signal that encompasses all the frequencies. It has a wave- like pattern. Generally, an interferogram is a time-domain spectrum which is a plot of intensity vs. time. A mathematical operation called Fourier transform (FT) is used to translate this spectrum into a frequency- domain spectrum. The interferogram could be obtained in a matter of seconds. Since a lot of interferograms are being collected at the same run, the data obtained is sensitive and reliable. [42]

Fig. 3.2 is a schematic diagram of an FT-IR spectrometer. The radiation from the infrared source passes initially through a beam splitter which has a mirror placed at a 45° angle. The beam splits the incoming radiation into two beams which are perpendicular to one another, one of them is undeflected and the other one at a 90° angle. The beam at a 90° angle goes to a fixed mirror and is

then reflected back to the beam splitter. The undeflected beam goes to the moving mirror and then also back to the beam splitter. The distance that the beam has to traverse depends on the position of the moving mirror. At the beam splitter, both beams recombine again. However, the different wavelengths caused by the moving mirror result in constructive and destructive interferences. The combined beam is called an interferogram. The interferogram then goes through the sample. The sample absorbs all frequencies corresponding to the difference in the energy levels between two states. Then, the interferogram reaches the detector. Afterward, the computer compares the interferogram of the unknown sample to that of a reference sample. This is a time-domain interferogram which is translated by Fourier transform to obtain a frequency-domain spectrum. This spectrum contains peaks that correspond to the vibrational frequencies of the different covalent bonds and hence the compound/molecule could be identified.[42]

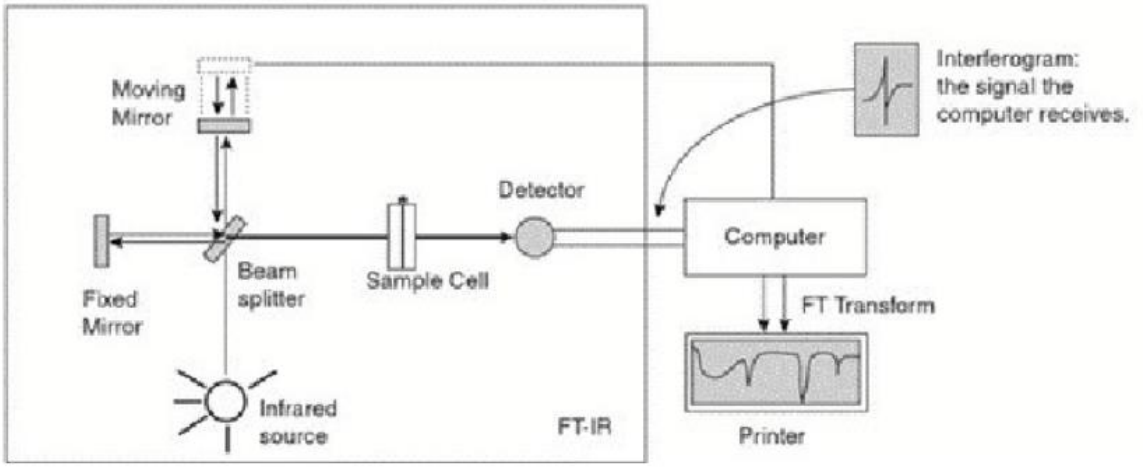

Figure 3.2 Schematic Diagram of a FTIR Spectrometer. [43]

3.3 Scanning Electron Microscopy

Electron Microscopy gives information about the topography (surface), morphology (shape and size of the particles), composition (elements present with their relative amounts) and crystallography (the arrangement of the elements) of the compound. The electron gun (part of any electron microscope) produces a stream of electrons. This stream of electrons is monochromated

and is focused using magnetic lenses and metal apertures. This stream then hits the sample. Interactions occur which are then translated into images.[45, 46]

Two types of scattering could occur as a result of a beam of electrons falling onto the sample; elastic and inelastic. In elastic scattering, only the trajectory changes while the kinetics and the velocity of the electrons remain the same. Examples of inelastic scattering that could occur is portrayed in Fig. 3.3. In inelastic scattering, incident electrons collide with the electrons of the samples causing them to be displaced. For a very short period of time, the sample is in an unstable state. These inelastic interactions are used in electron microscopy to retrieve information about the sample.[46]

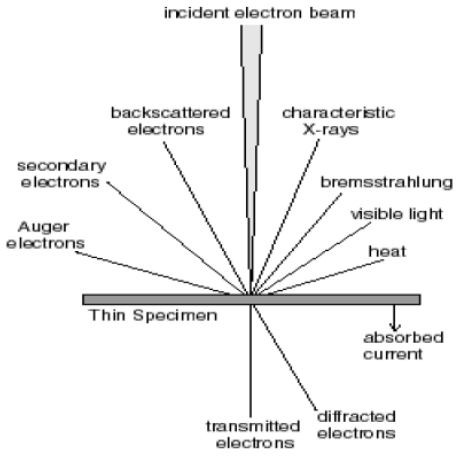

Figure 3.3 Different Inelastic Scattering [46]

Secondary and backscattered electrons play a vital role in the imaging process of the specimen. Secondary electrons (SE) are usually a result of targets with a high atomic number or a high angle of incidence. When an incident electron displaces an electron from its orbital, it loses a lot of energy. The displaced electron tries to move to the surface, however encountering several elastic and inelastic collisions on the way. SE can only leave the surface if they possess sufficient energy. Usually, the energy of these secondary electrons is around 5eV which is very low. Thus, mainly, only electrons near the surface could escape as secondary electrons giving information about the topography of the sample as displayed in Fig.3.4.

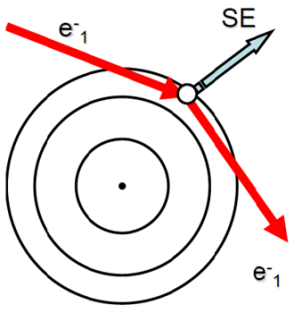

Figure 3.4 Secondary Electron emission. [46]

Backscattered electrons have higher energies than secondary electrons. They are a result of the interaction of the electron beam with the volume of the sample. The rate of production of backscattered electrons is proportional to the atomic number of the specimen. Samples with a high atomic number appear brighter compared to others with a lower atomic number. Excited samples, however, tend to move back to their stable ground state. Thus, a relaxation occurs and as a result energy could be released in one of these forms: Cathodoluminescence, Auger electrons or X-Rays. The relaxation is a fingerprint of each element since it releases very specific energies depending on the irradiated sample.[44, 46]

Fig 3.5 shows two images of Ni/Au heterostructure nanorods where the first one (left panel) is obtained from SE and the second one from BSE (right panel). As can be seen, SE are very useful for topographic examination; while BSE are more helpful for compositional analysis than surface topography. Also, the contrast is much better in the BSE image.[44,47]

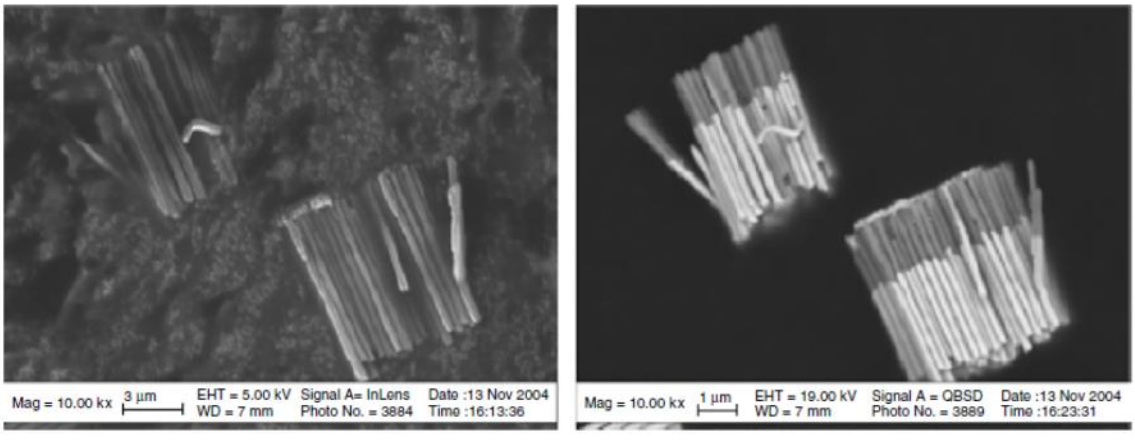

Figure 3.5 Images of Ni/Au heterostructure nanorods, SE (left panel) and BSE (right panel) [44]

The main components of an SEM are given below, and they are assembled as shown in Fig.3.6:

- Electron Source
- Lenses
- Scanning Coil
- Sample Chamber
- Detector
- Computer

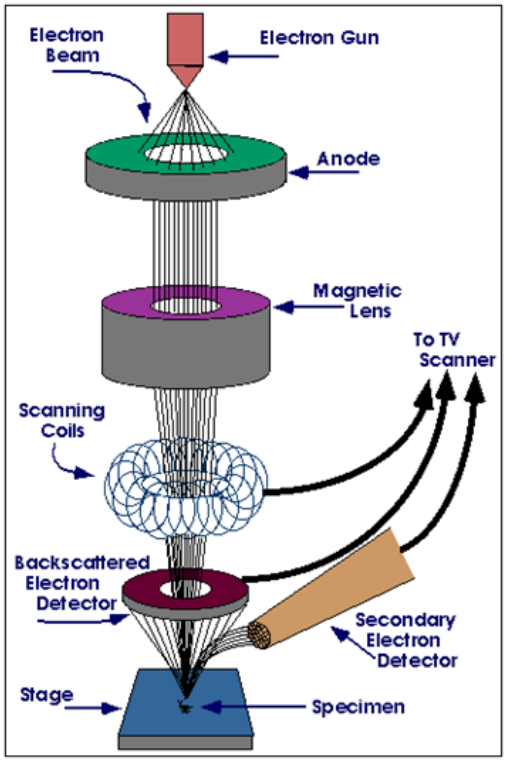

Figure 3.6 SEM Assembly [47]

The Electron gun in all modern SEM should produce an electron beam with high current, minimal dispersive energy, small spot size and adjustable energy. In order to focus the electron beam, either an electrostatic or a magnetic field is applied. Normally, a magnetic field is applied in SEM. Current is applied to coils of wire which act as a magnetic field. These lenses could be used to magnify or de-magnify the electron beam; change the diameter of the electron beam. In SEM, the lenses are mainly for demagnification, in order to have a narrower beam and thus decrease the

"spot size", where the beam hits the specimen. The scanning coils are used to divert the electron beam in all directions in order to scan over the whole sample. The detector then collects the scattered electrons from the specimen. The instrument is attached to a computer which can display the images. SEM must operate under vacuum conditions. This is in order to ensure that scattering of the electron beam and the contamination of the electron gun and the other components is avoided.[46, 47]

3.4 High Performance Liquid Chromatography (HPLC)

HPLC is one of the most powerful separation methods. It can separate molecules that are usually impossible to separate using other techniques.

In liquid chromatography in general, a column is filled with the adsorbent which is called the stationary phase. The sample that needs to be separated is inserted at the top of the column, while the eluting liquid or mobile phase is passed onto the column to move the sample through the column. Depending on the solutes' affinity to the adsorbent, different distances will be travelled along the column. Solutes with a weak affinity will travel longest; will get adsorbed at the end of the column. Solutes with a strong affinity will travel the least and it will get adsorbed strongly. Thus, the different solutes in a solution could be separated depending on their affinity to the adsorbent. This method is called adsorption chromatography. There are also other modes of separation like ion exchange or partitioning. The adsorbent could also be in the liquid or in the solid phase.[48]

HPLC started to come in picture in the 1960s after the development of highly efficient materials. The particle size of the materials of the stationary phase are significantly smaller in HPLC compared to those in normal liquid chromatography. The most commonly stationary phases used today are microparticulate column packing made of uniform, porous silica material. In HPLC, separation occurs depending on how the chemical groups of the solutes bind to the silica particles. Fig. 3.7 shows a schematic diagram of an HPLC. After the solution has passed through the column, the solutes are sensed by a detector. The output of the detector is an electrical signal that is then displayed on a recorder or a screen. Currently, there is no one detector for all solutes. Depending

on the type of solute of interest, the right detector has to be chosen. There is no one detector that is selective for all types of solutes in a mixture. [48]

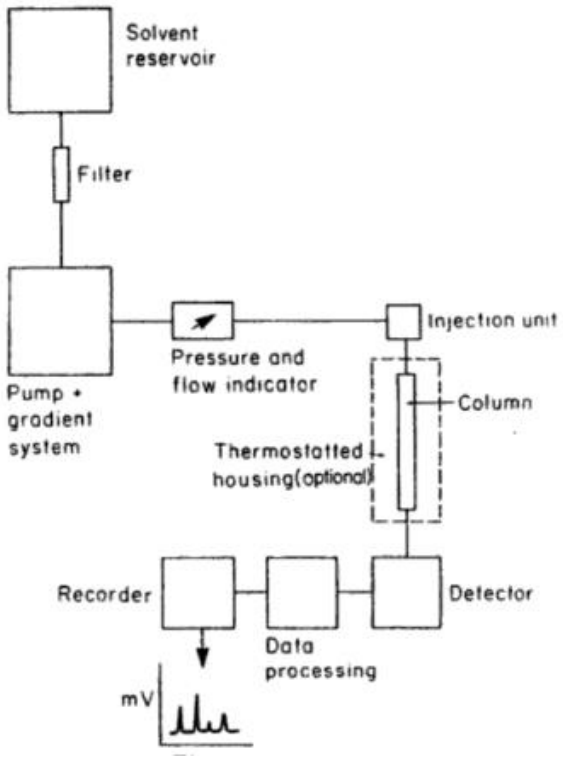

Figure 3.7 Schematic Diagram of an HPLC. [49]

3.5 Adsorption Theory

Adsorption is when the adsorbate in any form; gas, liquid or solid, binds to a surface of a solid (adsorbent). There are two types of adsorption: chemical adsorption (chemisorption) or physical adsorption (physisorption). In chemisorption, the adsorbent and the adsorbate bind strongly to one another. This occurs via electron sharing making the process irreversible. The energy of the chemisorption process is around 800 kJ/mole. In physisorption, the bond between the adsorbent and the adsorbate is very weak; not covalent or ionic. It mainly involves Van der Waals' interactions. The adsorption energy is generally in the range of 80 kJ/mole.[50]

The relationship between the amount adsorbed on the adsorbent and the adsorptive pressure is measured at a constant temperature and is described as the adsorption isotherm. If the adsorbate is a gas, pressure is to be taken into consideration. Concentration is studied in case of liquids. Various mathematical models were developed to describe the adsorption isotherms, the most common of which are the Linear, Langmuir, and Freundlich isotherms which will be discussed in the following lines.[51,52]

3.5.1 The Langmuir Isotherm Model

The Langmuir Model is considered to be one of the simplest adsorption models that are commonly applied. It is based on three plausible assumptions:

1) Adsorption happens only on the surface layer of the adsorbent. It does not form multiple layers.
2) The adsorbent has a uniform surface. Thus, adsorption could occur on any of the active sites. There are no preferences.
3) Interactions between adsorbate molecules do not take place.

The equation for the Langmuir adsorption model is given by the following expression:

$$q_e = \frac{q_m\, bC_e}{1+bC_e} \quad \text{Eq. 3.3}$$

where q_e is the amount adsorbed at equilibrium, C_e is the concentration at equilibrium, q_{max} is the maximum quantity that could be adsorbed and b is the Langmuir constant. [51]

Eq. 3.4 could be re-written to give the linear form

$$\frac{C_e}{q_e} = \frac{1}{bq_{max}} + \frac{C_e}{q_{max}} \qquad \text{Eq. 3.4}$$

3.5.2 Freundlich Model

Unlike Langmuir adsorption isotherm which is theoretical, Freundlich isotherm is more empirical. Freundlich isotherm model is also based on three different assumptions:

1) Not all adsorption sites have the same energy.
2) Energetically, more favorable sites will be occupied first.
3) Enthalpy of adsorption is related to the pressure (concentration) of the adsorbate. The relationship is logarithmic.

The following equation expresses the Freundlich adsorption isotherm model for a solid-liquid system:

$$q_e = K_F C_e^{1/n} \qquad \text{Eq. 3.5}$$

where: q_e is the amount of adsorbed solute, K_F is the Freundlich constant or maximum adsorption capacity, C_e is the concentration of the solution, and 1/n is a measure of intensity. Freundlich equation could also be re-written in the following linear form:

$$\log q_e = \log K_f + (1/n) \log C_e \qquad \text{Eq. 3.6}$$

The limitation of Freundlich adsorption isotherm model is that it cannot measure the adsorption at very high concentration/pressure values when the active sites have been saturated.

3.5.3 The Linear isotherm model

The linear adsorption model is the simplest isotherm model. It could be assumed that it is a special form of the Freundlich Isotherm model where n=1. Accordingly, the equation for the linear isotherm model could be written as:

$$q_e = K_L C_e \qquad \text{Eq. 3.7}$$

where q_e is the amount adsorbed on the adsorbent at equilibrium, K_L is the linear adsorption constant, and C_e is the equilibrium concentration of the adsorbate in the solution.

3.5.4 Dubinin-Radushkevich isotherm

Dubinin- Radushkevich isotherm model gives information about the adsorption mechanism of a system; whether it is chemisorption or physisorption. Here, the Gaussian energy distribution on a heterogeneous surface is expressed. The linear form of the D-R model is given by the following equation:

$$\ln q_e = -ß\varepsilon^2 + \ln q_{max} \qquad \text{Eq. 3.8}$$

where ß is the D-R adsorption isotherm constant, and ε, the Polanyi potential, could be expressed by the following equation

$$\varepsilon = RT \ln [1/C_e] \qquad \text{Eq. 3.9}$$

where R is the universal gas constant, and T is the temperature expressed in Kelvin.

As mentioned before, the D-R adsorption model gives information about the adsorption energy of a system as could be seen in the following equation

$$E = 1/(2ß)^{0.5} \qquad \text{Eq. 3.10}$$

E values lower than 8 kJ/mol indicate that the adsorption is physisorption, while those greater than 8 kJ/mol indicate that the mechanism for adsorption is chemisorption. [54]

3.5.5 BET Isotherm Model

A more elaborate adsorption model than Langmuir and Freundlich is that of Brunauer, Emmett and Teller (BET). It is different from the Langmuir model in the first assumption. In the BET model, the adsorbate could be physically adsorbed on a previous layer of adsorbate. The build-up of multiple layers of adsorbate could occur indefinitely. The BET equation is as follows [53, 56]

$$\frac{V}{Vmon} = \frac{cz}{(1-z)[1-(1-c)z]} \; with \; z = \frac{P}{P0} \qquad \text{Eq. 3.11}$$

where: V_{mon}: Volume of a monolayer of adsorbate

V: Total volume

P: Total pressure

P_0: Vapor pressure above a layer of adsorbate that is more than one molecule thick

c: Constant [56]

As a result of the BET equation, a plot of $P/V(P_0\text{-}P)$ vs P/P_0 is a straight line and V_{mon} could be obtained from the slope and the intercept. The specific surface area (S_{BET}) could be evaluated using the following equation:

$$S_{BET} = n.A_m.N \qquad \text{Eq. 3.12}$$

where $n = V_m/22414$; 22414 cm^3 is the volume occupied by 1 mole of a gas at STP

A_m: molecular cross-sectional area of adsorbate per gram of out-gassed adsorbent

N: Avogadro's number.[56]

Based on the BET theory, five types of adsorption/desorption isotherms have been classified by Brunauer, Demming and Teller and the sixth by Gregg and Sing [58]. The isotherms describe the relation between amount of adsorbed gas and the relative pressure (P/P_0). The six different sorption isotherms are shown below in Fig. 3.8.

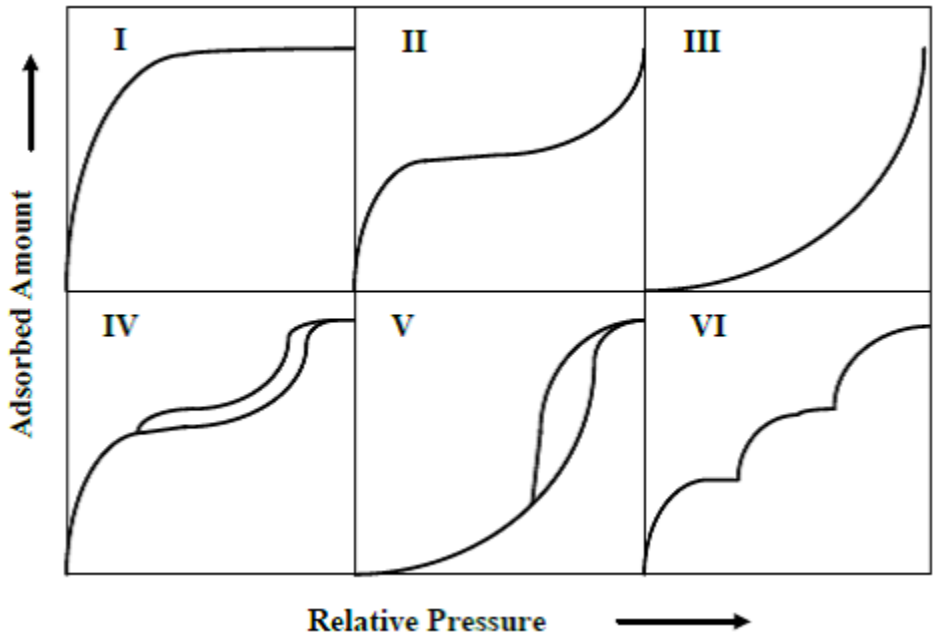

Figure 3.8 The different IUPAC Adsorption Isotherms. [59]

Physical adsorption and desorption isotherms give information about the surface of the adsorbent. Additionally, an analysis about the total surface area of the adsorbent, its total pore volume, the size of the pore volumes, distribution of pore volume and area by pore size and surface energy distribution could be retrieved. There are three distinct pore size classifications: micoropores, mesopores and macropores. Micropores have a width of less than 2 nm; mesopores have a width ranging between 2-50 nm; while macropores have a width larger than 50 nm.[51]

To determine the adsorption isotherm, two methods could be employed: gravimetric or volumetric. In both methods, the temperature is constant. It is kept at a value close to the boiling point of the adsorptive (the gas in equilibrium with the adsorbate). The adsorptive pressure is increased gradually. In a volumetric system, changes in the pressure are correlated to the amount adsorbed by comparing the pressure to a system where there is no adsorbent. In a gravimetric system, the amount adsorbed is measured by determining the mass gain in the adsorbent. The volumetric method is the most commonly used method.[51,52]

3.5.6 International Union of Pure and Applied Chemistry (IUPAC) Adsorption Isotherm Types

According to IUPAC, there are six different types of adsorption isotherms shown in Fig. 3.8 where the amount adsorbed is plotted versus the relative pressure. Type 1 is unique for a chemisorption or physisorption process on a material with micropores. In Type 2, adsorption occurs on a nonporous material or a material with macropores, where adsorption involves strong interactions. Type 3 is the same as Type 2, the only difference is that the adsorbate-adsorbent interactions are very weak and thus the adsorption here requires lower energy. In Type 4, adsorption takes place on a mesoporous material with a high adsorption energy due to strong interactions. As clear from the figure, the isotherm exhibits a hysteresis loop. Hysteresis loop will be explained further in the upcoming section. Type 5 differs from Type 4 in having a low adsorption energy. The last isotherm type could be attributed to several possibilities. Two possible scenarios could be due to a material containing different pore sizes or if the adsorbate is in the solid form and thus forms a structured layer.[58]

3.5.6.1 Hysteresis Loops

Physisorption is a reversible process since it is relatively a weak interaction. The surface of materials with mesopores is not flat and adsorption on the walls of the pores might take place, the process may occur irreversibly in relation to pressure changes. Hysteresis loops are formed due to capillary condensation which is governed by the Kelvin equation

$$\ln(P/P_0) = -2\sigma V/rRT \quad \text{Eq. 3.13}$$

where P = pressure, P_0 = the saturated vapor pressure, σ = surface tension, r = radius of the pore, R = universal gas constant and T = Temperature [58]

Capillary condensation is the change of the physical state of the adsorbate from gas to liquid at the pores of the adsorbent. This change of state of the fluid in the pores occurred at a lower pressure than that of the rest of the adsorbate. Hysteresis loops are very insightful as they give detailed information about the shape of the pores. There are 4 classifications of hysteresis loops according

to IUPAC which are classified as H1-H4 displayed in Fig. 3.9. H1 indicates that the pores are narrow while in H2 the pores are of different sizes. The pores in H3 and H4 are slit-shaped. [57, 58, 59]

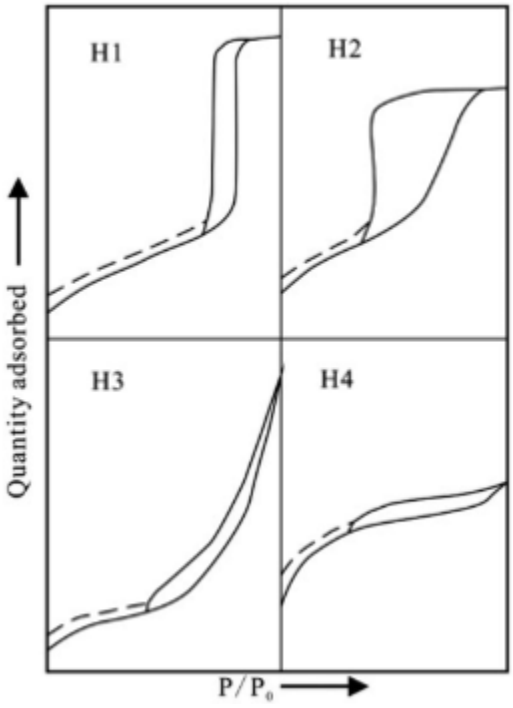

Figure 3.9 Different Types of Hysteresis Loops. [58]

3.6 Kinetics of adsorption

Kinetics is the study of the rate of the reaction. Rate of the reaction is proportional to the concentration of the reactant(s) raised to a certain power, i.e., $v = f([A]^n, [B]^m, \ldots)$. Rate laws are differential equations that could be determined either experimentally or by integration. The overall order of the reaction refers to the sum of the powers to which the concentrations of the individual reactants are raised. A reaction is said to be zero order if the rate of the reaction does not depend on the concentration of the reactant(s). [56]

3.6.1 Pseudo-First Order Reactions

A pseudo-first order reaction is a second-order reaction; mainly containing two reactants. However, it behaves like a first order reaction. This occurs when the concentration of one of the reactants is in excess compared to the other reactant and, thus, it does not change significantly during the reaction. A simplified reaction equation could be written as:

$$A+B \rightarrow C+D$$

Originally, the rate of the reaction should be expressed using the following equation

$$\nu = k_1[A][B] \qquad \text{Eq. 3.14}$$

However, if A is in abundance, then its concentration will not be affected during the reaction and the reaction will be considered as a pseudo-first order reaction with respect to B and, thus, the rate of the reaction can be expressed as:

$$\nu = k_1 [B] \qquad \text{Eq. 3.15}$$

where k_1 is the first order rate constant.

Therefore, the actual order of the reaction is second order, however the reaction behaves like a first-order one; thus it is classified as a pseudo-first order reaction. The integrated rate law of a pseudo-first order reaction is given in Eq.3.15. It implies that a plot of ln ([B]/[B_0]), where [B_0] is the initial concentration of the reactant, vs time is a straight line.

$$\ln (([B]/[B_0]) = kt \qquad \text{Eq. 3.16}$$

It could also be re-written as:

$$\log (q_e - q) = \log q_e - k_1 \qquad \text{Eq. 3.17}$$

The concept of a pseudo-second order reaction is similar to the idea of a pseudo-first order reaction but with three parameters instead of two. The reaction is a third order reaction but it behaves like a second order reaction. For second order reactions, the rate can be expressed by Eq. 3.18. According to the integrated rate law, a plot of 1/[B] vs time yields a straight line as per Eq. 3.19. It could also be written in the form of Eq. 3.20.

$$\nu = k_2 [B]^2 \quad \text{Eq. 3.18}$$

$$1/[B] = k_2 t + 1/[B_0] \quad \text{Eq. 3.19}$$

$$t/q = 1/(k_2 q_e^2) + t/q_e \quad \text{Eq. 3.20}$$

where k_2 is the second order rate constant. [62,65]

3.7 Zeta Potential

The Zeta Potential (ZP) gives an indication of the stability of a colloid. The measurement of the ZP is a key measurement in multiple industries such as medicine, mineral processing and water purification. A colloid is stable if the particles are suspended in the media and do not agglomerate or coagulate. The coagulation of the nanoparticles will result in their sedimentation. The magnitude of the repulsion as well as attraction is measured by the ZP. [60,61]

In a colloid, particles are dispersed in the media. If unstable, they might aggregate together to form flocs. This process is called flocculation and it is a reversible process (flocculation-deflocculation). The flocs might adhere to other particles and form larger size aggregates. This process is called coagulation and it is an irreversible process. Due to gravity, sedimentation will take place. [60,61]

3.7.1 The Electric Double Layer

Particles, possessing a net charge, will affect the alignment of the other ions in the system. Particles/ions with opposite charge will be dense around the surface of the particle due to electrostatic attraction. As a result, a double layer is formed around each particle. The liquid layer around each particle is now composed of two regions; the inner layer (the Stern layer) which is bound strongly to the particle and an outer layer (the diffuse layer), loosely bound to the particle. Between these two regions, there is an imaginary boundary which is known as the slipping plane. The ZP is a measurement of the potential at this boundary as per Fig.3.10. [63,64]

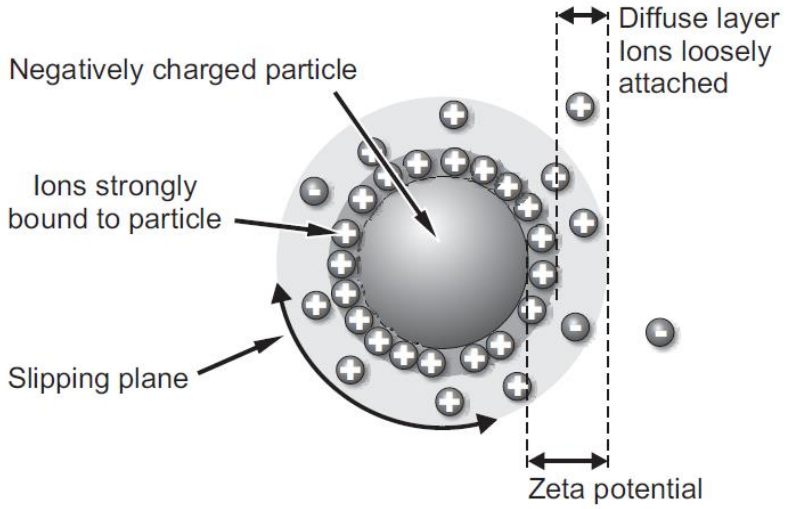

Figure 3.10 Zeta Potential and the electric double layer [63]

The magnitude of the ZP gives an indication of the colloidal stability. If the matrix has large values of ZP, this indicates that the particles mainly possess the same charge and therefore repel each other. This is a stable colloid, and the magnitude of the ZP in this case is greater than 30mV. Colloids of ZP between -30mV and 30mV are usually unstable because the electrostatic repulsion between the particles is not that strong to prevent them from forming aggregates. [60,63]

An important parameter that affects ZP and should be always taken into consideration is the pH of the system. It is important to analyze the environment (pH, ionic strength and presence of any additives) if one ought to understand the ZP. [63]

If a pH vs zeta potential curve is plotted, the point where the ZP is equal to zero is called the isoelectric pH or point of zero charge (PZC). This corresponds to the pH at which the net surface charge is zero. The ZP will be positive at pH values lower than PZC, while it will decrease and move towards a negative potential when the pH increases above PZC. At PZC, the colloidal system is least stable. For example, a graph of ZP and pH of a certain colloid is plotted in Fig. 3.11. This colloid is most stable at pH values below 4 and greater than 8 due to charge abundance. [63]

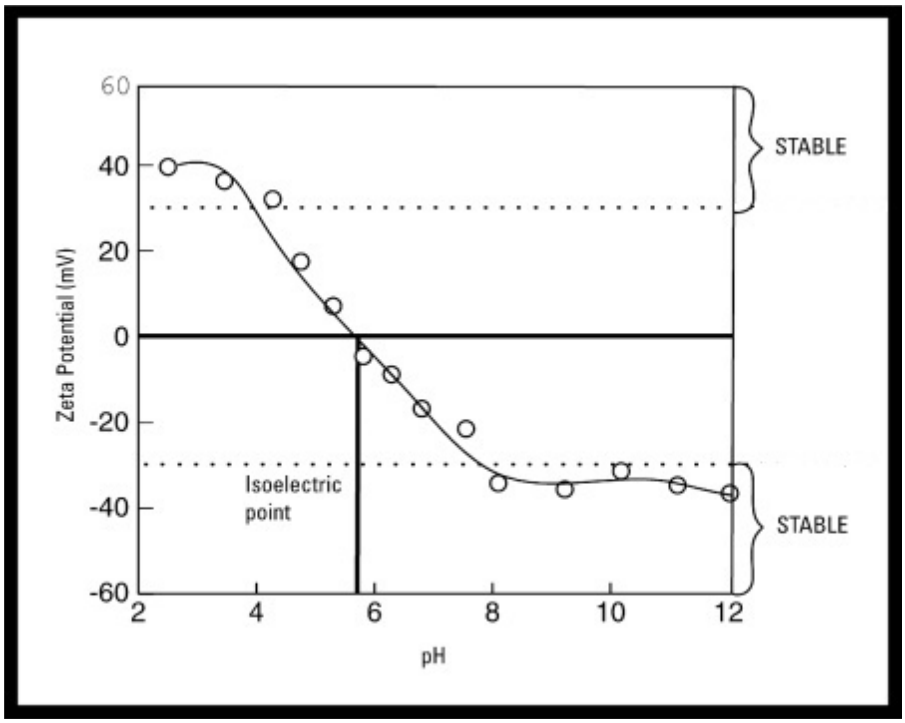

Figure 3.11 A plot of ZP vs pH [65]

Chapter 4
Experimental Work

4.Experimental Work

4.1 Preparation of the Husk

Goldenberry Husk (*Physalis peruviana*) was collected from El Beheira Governorate (Egypt) and rotten husk was excluded. The stem of the husk was removed manually, then the husk was washed with tap water several times and afterwards with distilled water.

After washing the husk, the husk was dried in an oven (HERAtherm, Thermo Scientific) at 50-60°C for approx. 2 h and ground in a blender, then sieved using two sieves (2 mm and 630 μm). Sizes smaller than 630 μm and bigger than 2 mm were discarded. This was done in order to ensure that the used husk samples are of comparable sizes.

4.1.1 Treatment of the Husk

The ground husk was treated with a 0.2% (by vol.) formaldehyde (40 % w/v, CARLO ERBA Reagents, France) solution to bleach its color and remove the pigments.[42] It was left in this solution for 24 h, at pH 4.67 and room temperature. Afterwards, the husk was washed with distilled water followed by deionized water (pH = 5.46) until the pH of the filtrate was close to that of deionized water (pH=5.38 – 5.40). The husk was finally dried in the oven for 2 h at 60°C, and samples were stored in falcon tubes in the fridge at 4 °C. The treated husk will be referred to as un-activated husk or, H, throughout the text.

4.1.2 Activation of the Husk

For the activation of the husk, orthophosphoric acid with 85-85.5% concentration (Brand Chemicals, Egypt) was used. This acid was used due to its strong oxidizing power along with its minimal environmental hazards in comparison to other acids.[67]

The husk was left in H_3PO_4 solution for 24 h, with a ratio of 1:10 (w/v, g/mL) husk to acid. A 120 g sample of the husk was prepared. Afterward, the husk was washed with distilled and deionized

water until the pH of the filtrate was close to that of the deionized water in order to ensure that the H_3PO_4 has been washed off completely (pH: 5.40 – 5.42).

To study the effect of temperature on the characteristics of the husk and its adsorption performance, the husk treated with H_3PO_4 was heated at each of 350°C and 500°C in an oven for two hours to produce the activated husks of H350 and H500, respectively. The activated husks were also stored in different falcon tubes in the fridge at 4^oC.

4.2 Determination of the Point of Zero Charge (PZC)

For all three types of employed husks (H, H350 and H500), the point of zero charge was determined. The pH of the solutions was adjusted using a 1M HCl (Assay 37%, Honeywell, Germany) solution or 0.1 M NaOH (Chem-Lab, Belgium) solution. A plot of initial pH before adsorption versus final pH after adsorption of SA was constructed. Both initial and final pH values equate at the PZC.[33] The concentration of SA that was used in this experiment was 70 mg/L. Six different SA samples were prepared where the pH was adjusted to 2, 4, 6, 8,10 and 12. A mass of 0.1g of each husk was added to 10 mL of each of the prepared solutions. The samples were kept in a shaking waterbath (SHA-C waterbath shaker, China) for 8 h in order to ensure complete adsorption. Afterward, the pH of the samples was measured again.

4.3 Zeta potential measurements

A sample of approx. 50 mg of each of H, H350 and H500 was dispersed in 2 mL of deionized water. The pH of each solution was adjusted to be 3, 5, 6.2, 8 and 10 using a 0.1M NaOH and 1M HCL. The samples were injected in a Zetasizer Nano ZS, Malvern UK. To measure the zeta potential, Laser Doppler Micro-electrophoresis was used, where an electric field was applied to the mixture and accordingly the particles migrated at a certain velocity. In order to measure the velocity of the particles, a M3-PALS (Phase analysis Light Scattering) was used. From the velocity, the electrophoretic mobility could be obtained which, in turn, provides data about the zeta potential and the zeta potential distribution of the sample.

4.4 FTIR for Husk analysis

The FTIR spectra for H, H350 and H500 were determined pre- and after adsorption in order to study the different functional groups present in each type of husk. Thermos Scientific Nicolet 380 FT-IR Spectrometer was used for the analysis and the KBr pellet technique was applied. This model has an EverGlo lamp which provides infrared radiation in the spectral range from 7800 cm^{-1} to 350 cm^{-1}.

4.5 CHNS analysis

The samples (H, H350 and H500) were analyzed using an Elementar, Vario MICRO cube, Germany. The weight of each sample was approximately 50 mg. Oxygen was injected into the active zone and the samples underwent combustion. Quantitatively analyzing the products resulting from combustion gives information about the empirical formula of the matrix, specifically C, H, N, and S quantities in each sample. The detector employed was a thermo-conductivity detector.

4.6 SEM Imaging

Images of the surfaces of the three husk types were taken before and after adsorption at magnifications of 25X, 55X, 1000X, 10KX, and 20KX using the SEM instrument SUPRA 55. SEM imaging was held at an aperture size of 10 Mm and width of 3.5 mm. H, H350 and H500 were coated with a conductive material; a “sputter coater”. Thus, HUMMER 8.0 was used to sputter the husk with gold. This was performed at 15 mA for 3 min.

4.7 BET Analysis

The surface area and porosity of H, H350 and H500 were determined by nitrogen adsorption at 73K in an ASAP 2020-Micromeritics equipment. The amount of sample used ranged between 0.5 – 1.3 g. The samples were heated prior to analysis in order to assure that the samples have been degassed completely. H, H350 and H500 were degassed at 75°C, 120°C and 150°C respectively.

4.8 Preparation of SA Solutions

Salicylic acid (pK_a 2.79) of 98% purity (Oxford, India) was used to prepare serial dilutions of SA solutions of the following concentrations: 18, 35, 70, 105, 140, 175, 210, 262, 280 and 350 mg/ L (ppm). Absorbance of these solutions were measured at 295-298 nm with a UV- spectrophotometer type UV-1650 PC, SHIMADZU, and a calibration curve of SA was constructed to convert the absorbance to concentration (refer to the Appendix, Fig. 8.1).

4.9 Preparation of CA Solutions

Pure Caffeine Anhydrous (pK_a 10.4) 98%, HPLC-grade, was obtained from Loba Chemie, India and was used to prepare the different caffeine solutions. A stock solution was prepared where 0.389 g of pure caffeine was diluted in deionized Millipore water up to 1L. Different concentrations were prepared from the stock solution by serial dilution to obtain 1, 10, 27, 82, 172, 255 and 398 mg/L (ppm). Chromatographic analysis for these solutions was performed on an HPLC (Waters LC 2695- PDA Detector) with a reversed-phase Mediterranea C18 column (250x4.6 mm and a particle size of 5µm). The mobile phase was Acetonitrile and water, containing 0.1% by volume phosphoric acid. The ratio between acetonitrile and water was 60: 40 v/v. The flow rate of the mobile phase was1.0 mL/min. A UV wavelength of 275 nm was used for detection using a Waters 996 photodiode array detector. A calibration curve for CA was constructed as shown in the Appendix, Fig. 8.2 where area under the curve is plotted versus concentration.

4.10 Preparation of a CA/SA Binary Solution

Pure Caffeine Anhydrous 98%, HPLC-grade (Loba Chemie, India) and Salicylic acid of 98% purity (Oxford, India) were used to prepare serial dilutions of 200, 100, 80, 60 and 40 mg/L concentrations. Chromatographic analysis for these solutions was conducted using an HPLC (Waters LC 2695- PDA Detector) with a reversed-phase Mediterranea C18 column (250x4.6 mm and a particle size of 5μm). The analysis followed the same method as the one used for the analysis of CA. The HPLC calibration curves of CA and SA could be found in the Appendix, Fig. 8.2 and Fig. 8.3.

4.11 Biosorption Experiments

4.11.1 Effect of pH

Initial screening experiments were conducted using the three employed husks (H, H350 and H500) in order to determine the optimal pH for the single-component biosorption of SA or CA. This is the pH corresponding to the highest percent removal achieved within the closest proximity to the neutral pH conditions. A solution of SA with a concentration of 70 mg/L and a CA solution with a concentration of 260 mg/L were used. These were the lowest concentrations that showed reasonable differences in adsorption capacities between the three husks in the very first set of preliminary experiments. However, this choice was re-evaluated after conducting the extended studies on the effect of initial concentration. The pH of the solution was adjusted using 0.1 M NaOH or 1 M HCL. The investigated pH range lied between 1.5 and 12. A volume of 15 mL of each solution was added to 0.1 g of each type of husk H, H350 and H500. The solutions were left at room temperature in a shaking waterbath (SHA-C waterbath shaker, China) for 8 h. Afterward, the solutions were filtered using a filter paper (Whatman, 8μm) and the absorbance of the filtrate was measured. For SA, the absorbance was determined using the UV-spectrophotometer (UV-1650 PC, SHIMADZU at a wavelength of 295-298 nm), while an HPLC (Waters LC 2695- PDA Detector) was used for the caffeine filtrates at a wavelength of 275 nm. This experiment monitored

the effect of pH on the % removal and the adsorption capacity of H, H350 and H500 for SA and CA.

4.11.2 Effect of initial concentration

In this set of experiments, a mass of 0.1 g of husk (H, H350 or H500) was added to 15 mL of each of SA and CA solutions. Each mixture was then kept in a shaking water bath (SHA-C waterbath shaker, China) at room temperature (27°C±2) and pH 6.5± 0.2 (optimal pH) for 8 h. Afterward, the mixtures were filtered using a filter paper (Whatman, 8μm). The absorbances of the filtrates were measured using a UV-1650 PC, SHIMADZU spectrophotometer at a wavelength of 295-298 nm for single-component SA solutions and Waters LC 2695- PDA Detector at a wavelength of 275 nm for single-component CA solutions as well as for the binary system. The corresponding concentrations of the solutions were calculated using constructed calibration curves (refer to the Appendix, Fig. 8.1 and 8.2). The equilibrium adsorption capacity was then calculated using the following equation:

$$q_e = (C_0\text{-}C_e).V/w \qquad \text{Eq. 4.1}$$

where,

C_0 is the initial concentration of SA or CA (mg/L), C is the equilibrium concentration of SA or CA in the solution after adsorption (mg/L), V is the volume of SA or CA used (L), and w is the amount of adsorbent used (g).

Additionally, the removal percentage was calculated using the following equation:

$$\%\ \text{removal} = (C_0\text{-}C_e)/C_0*100 \qquad \text{Eq. 4.2}$$

For the binary system, only H350 was tested. H350 was chosen for reasons that will be discussed later in the results and discussion section.

4.11.3 Adsorption isotherm studies

The q_e vs C_e adsorption isotherms obtained from the previous experiments were fitted to different adsorption isotherm models to obtain information about the quantity of adsorbate adsorbed as a function of equilibrium concentration at a constant temperature. These studies indicate how the adsorbate is distributed between the liquid and solid phases at equilibrium and they model the sorption equilibrium parameters. There are several isotherm models that could be used, but the most common ones are the Linear, Langmuir and Freundlich models. The equations for the Langmuir, Freundlich and the Linear isotherm models are given in Eq. 3.3 and 3.5 and 3.7.

4.12 Kinetic modeling of biosorption on un-activated and activated husks

The kinetics of SA and CA adsorption onto H, H350 and H500 in single component systems was studied at different time intervals using the optimal initial concentration of 280 mg/L for SA and 82 mg/L for CA. These two concentrations were chosen based on the removal efficiencies obtained in the previous biosorption experiments as will be discussed later in the results and discussion chapter. The biosorption kinetic profiles of SA and CA onto the husk were obtained experimentally and plotted as q, amount adsorbed at time t, versus the time t. The profiles were then predicted theoretically using two models; pseudo- first and pseudo- second order models. The integrated rate law equations pertaining to these models were given earlier in Eq. 3.17 and 3.20, respectively. The pseudo-second order reactions are usually based on solid phase adsorption where the adsorption process involves three stages of film diffusion, surface reaction, and pore diffusion.

4.13 Regeneration of the Husk

To evaluate if the husk (H350) could be regenerated and reused, a binary system of CA and SA was used. They both had the same concentration of 200 ppm. H350 was left in contact with the solution for a couple of hours in order to assure that complete adsorption has taken place.

Afterward, the husk was dried in an oven (HERAtherm, Thermo Scientific) at 80°C for an hour. The dried husk was then immersed in a 1M HCL solution for a couple of hours. The husk was then washed and dried again for an hour at 80°C. This process was repeated for three times.

4.14 Statistical Analysis

All measurements were performed in triplicate and were expressed as mean ± SD. The two-tailed student's *t*-test was used to examine the significant differences between results at a confidence level of 95%. Linear regression analysis was used to predict the equilibrium and kinetic profiles.

Chapter 5

Results and Discussion

5.Results and Discussion

In this chapter, the three types of employed husks (H, H350 and H500) will be characterized to determine their chemical structure, their composition and their textural and morphological properties. The adsorption of each of SA and CA onto these husks will then be investigated in single component systems to determine the optimum operating conditions. The equilibrium and kinetics of adsorption will also be studied. Based on the adsorption performance of the three husks, one type will be selected as the optimal husk. Afterward, the simultaneous adsorption of SA and CA onto the selected husk will be investigated in binary systems, alongside with the desorption and regeneration of the husk.

5.1 Characterization of the husk

5.1.1 Determination of Point-of-Zero Charge and Zeta Potential

The isoelectric pH or also known as the point-of-zero charge (PZC) of the adsorbent, is the pH at which the net surface charge of the adsorbent is equal to zero. It is important to determine the PZC of the employed husk in all its different forms in order to get more insight into the binding mechanism by which each husk adsorbs SA and CA. Thus, a plot of initial pH of the solution vs the final pH of the solution has been constructed. The pH at which both equate is equal to the PZC. For all three types of husks (H, H350 and H500), it can be observed that PZC is 2.0 as shown in Fig. 5.1. This means that the husk is positively charged at pH values lower than 2.0 and is negatively charged at pH values greater than 2.0.

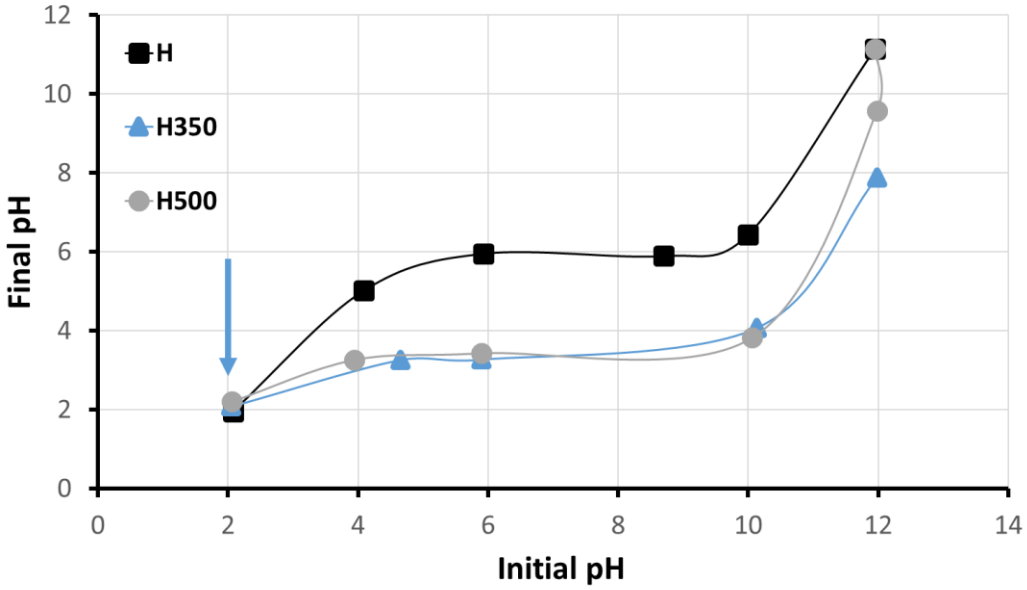

Figure 5.1 Determination of Point-of-Zero Charge (PZC) for H, H350 and H500.

To determine the charge on each husk, its zeta potential was measured at different pHs as depicted in Fig. 5.2. For all three types of husk, it can be seen that the zeta potential is negative. As the solution pH increased, the zeta potential for H, H350 and H500 became more negative. At approximately pH 6.5, the zeta potential for H350 dropped to -30 mV. It then further decreased with increasing the pH. H500, on the other hand, possessed a zeta potential below -30 mV at pH 8. A zeta potential of -30 mV and below indicates a stable colloid. [60] The zeta potential results are in accordance to the results obtained from the PZC measurements given above, where it was indicated that the husk will be negatively charged at pH values greater than 2. At pH 6.5, which is the pH that will be chosen later for adsorption studies, H350 had the most negative ZP, followed by H500 then H which had the least negative ZP at this pH.

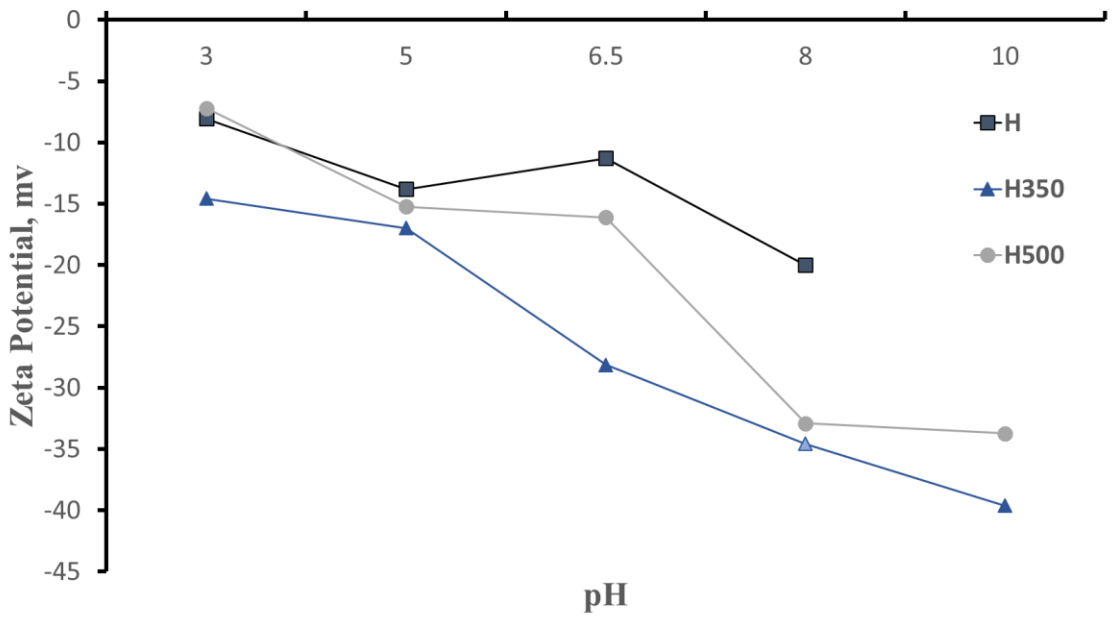

Figure 5.2 Zeta Potential of H, H350 and H500 at different pH values.

5.2 FT-IR Spectroscopic Analysis

The FT-IR spectra of the three investigated husks (Fig. 8.4-8.6, Appendix) were analyzed to determine the main functional groups present on each husk which are compiled in Table 5.1. All three types of husk (H, H350 and H500) showed a band at 3434 cm^{-1} indicating the presence of a hydroxyl group or an N-H group. This band is also present in Tomatillo husk as has been previously reported. [41] H showed a band at 1053 cm^{-1} which is possibly due to the stretching of C-OH bond. This band was weakened in H350 and shifted to 1093 cm^{-1} in H500 due to husk activation. Another band appeared in the spectrum of H at 2922 cm^{-1} which could be ascribed to the C-H stretch, present also in Tomatillo husk [41], however it vanished completely in H350 and H500 due to the carbonization and activation of the husk. The changes that occurred in the C-OH and C-H bands could be attributed to the breakage of the C-OH and C-H bonds and loss of water after activation. In addition, the presence of a band at 1722-1732 cm^{-1} in the spectrum of H indicates the presence of a C=O. However, this band weakened in the spectrum of H350 and disappeared in the spectrum of H500 probably as a result of the carbonization and release of CO_2

during the activation process. The bands at 1610-1650 cm^{-1} in the three husks correspond to the water adsorbed in the pores of the adsorbent, while the bands at 2300 cm^{-1} along with the bands at 650 cm^{-1} in H350 and H500 could be assigned to the adsorbed CO_2. [67] It can also be observed that the intensity of the CO_2 bands in the spectrum of H350 is higher than their counterparts in the H500 spectrum. The CO_2 entrapped inside the pores of H350 could have escaped as a result of the higher temperature treatment at 500^0C. In addition, the N-O band appearing at 1513 cm^{-1} in H disappeared in H350 and H500 due to carbonization of the husk. In the spectrum of H, the bands at 1251 cm^{-1} and at 1372 cm^{-1} could be ascribed to the ester sulfate groups and the S=O group of sulfate, respectively. These groups probably belong to the polysaccharides present in the husk. The presence of polysaccharides can be also confirmed by the band shown in the H spectrum at 1053 cm^{-1}.[67,68] These bands disappeared in H350 and H500 due to the carbonization. Clearly, the activated husks exhibit less FTIR peaks relative to the non-activated husk since activation involves breaking down and carbonization of the husk material.

Table 5.1 Main Functional groups present in H, H350 and H500 as retrieved from the IR spectra.

Functional Group	Wavelength cm^{-1}	H	H350	H500
Ester sulfate group	1260-1258	√		
Polysaccharides	1088-1012	√		
C-OH	1050-1300	√	√	√
N-O	1500-1550	√		
C=O	1670-1820	√	√	
C- H	2850-3000	√		
O-H/ N-H	3300-3500	√	√	√

5.3 CHNS Analysis

CHNS analysis provides information on the elemental analysis of the husk by determining the total amount of carbon, hydrogen, nitrogen and sulfur present in the husk. Table 5.2 represents the CHNS analysis for all three types of husk, H, H350 and H500. The CHNS analysis could be used

to complement the data found by the FT-IR analysis. According to the CHNS analysis, the % H is highest in H and lowest in H500. This is in accordance to the data found in the FT-IR analysis, which indicates that the C-H bond disappeared in H350 and H500 possibly due to the loss of hydrogen in the form of water. However, there is still a certain percentage of hydrogen that remained bound in the form of N-H or O-H bonds. Among the three investigated husks, the percentage of C in H350 is the highest and this could be attributed to the carbonization of the husk as well as the formation of CO_2 which got adsorbed into the H350 pores during the activation of the husk. H500, on the other hand, constitutes the lowest percentage of C among the three husks, possibly due to the escape of CO_2 from the pores when the higher temperature was applied as discussed in the FTIR section. The three husks contain nitrogen and its percentage ranges between 1-3%. The presence of nitrogen was confirmed by the FTIR spectra of the three husks which exhibited N-H bonds and by the N-O band present in H. The presence of sulfur can be also confirmed by the presence of ester sulfate bands in H.

Table 5.2 Textural Properties and CHNS analysis of H, H350 and H500.

Adsorbent	N%	C%	H%	S%	C/N %	C/H%
H	0.9	48.4	7.3	0.7	55.6	6.6
H350	3.0	60.4	2.6	0.4	20.1	23.0
H500	2.1	9.7	0.5	1.4	4.5	21.7

5.4 SEM morphology

SEM images of H, H350 and H500 are shown in Fig. 5.3a, b and c, respectively. All images were taken at a magnification of 1000X. Clearly, the surface of the husk became smoother with activation as a result of the chemical and thermal treatment of the husk which leads to dehydration, de-polymerization and carbonization of the husk.

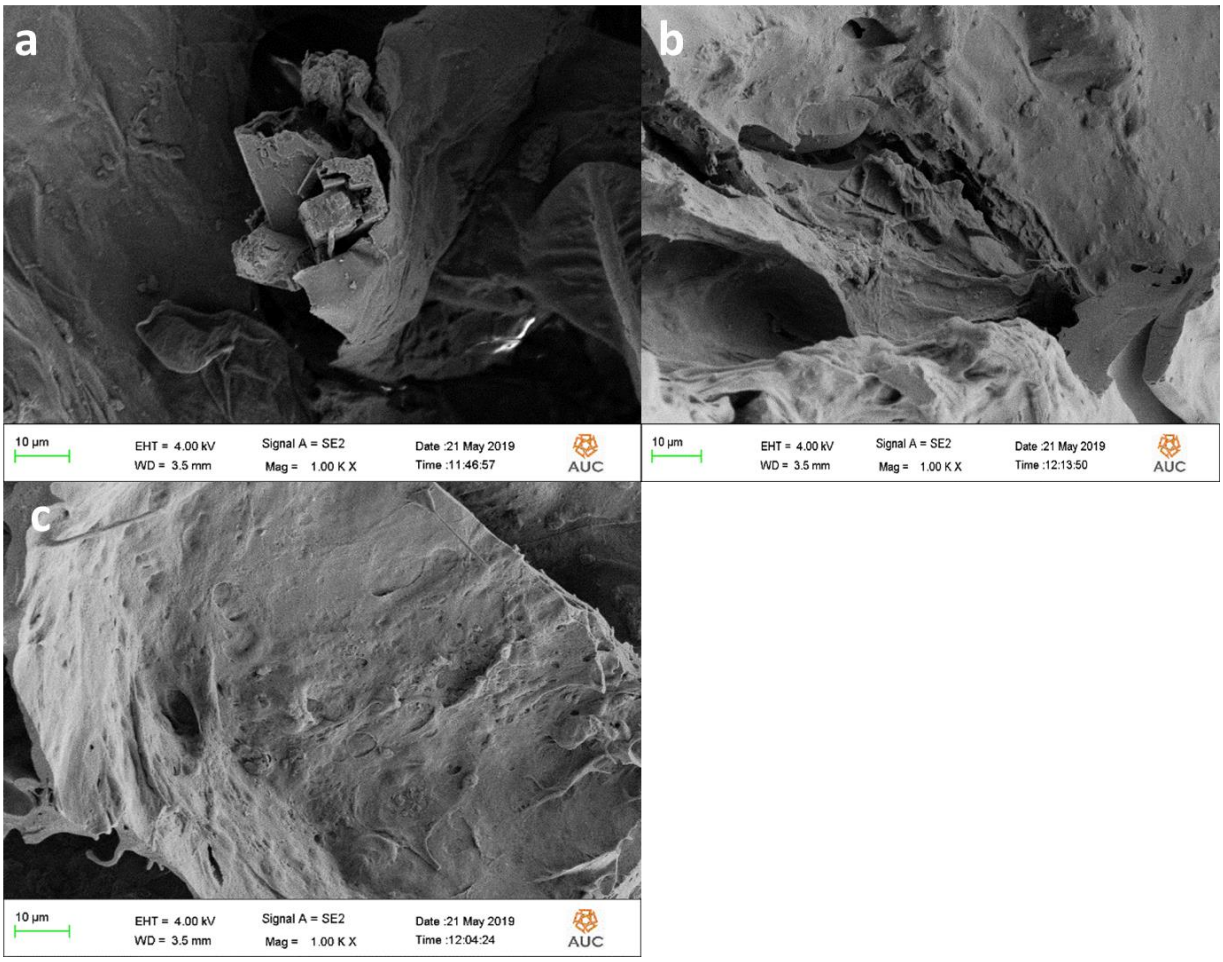

Figure 5.3 SEM images of H (a), H350 (b) and H500 (c).

5.5 Textural properties

Fig. 5.4a, b and c show the N_2 adsorption/desorption isotherms of H, H350 and H500, respectively. All husks exhibit Type IV isotherms with a small hysteresis loop. This indicates a primarily mesoporous adsorbent which interacts strongly with the adsorbate. The hysteresis loop is Type 3, which represents slit-shaped pores. The pore size distribution plots pertaining to H, H350 and H500 are shown in Fig. 5.5a, b and c, respectively. From these plots, it can be inferred that all husk types are primarily composed of mesopores which range between 2-50 nm in size, along with some macropores that are larger than 50 nm. The pore volume plot in Fig. 5.6 shows that H500 possesses the largest pore volume, followed by H350 and then H. It also confirms that the majority of pores in the three husks are mesopores. By comparing the BET and Langmuir surface areas as well as the pore volumes of the three husks as presented in Table 5.3, it can be deduced that H500 has the

largest BET surface area, which is about 12 times larger than H350 and 34 times larger than H. H500 has also the largest Langmuir surface area among the three husks. The pore volume of H500, on the other hand, exceeds that of H and H350 by 88 and 71 fold, respectively. The BET surface area of H350 is larger than H by 2.8 times, while its pore volume is comparable to that of H. It can be, thus, concluded that the activation of the husk increased its surface area and pore volume and this may enhance its adsorption capacity. It is notable, however, that surface area and pore volume are not the sole factors that influence the adsorption capacity of the husk since not all pores are necessarily active sites for adsorption. In addition, the average pore size of H500 (Table 5.3) is larger than that of H and H350.

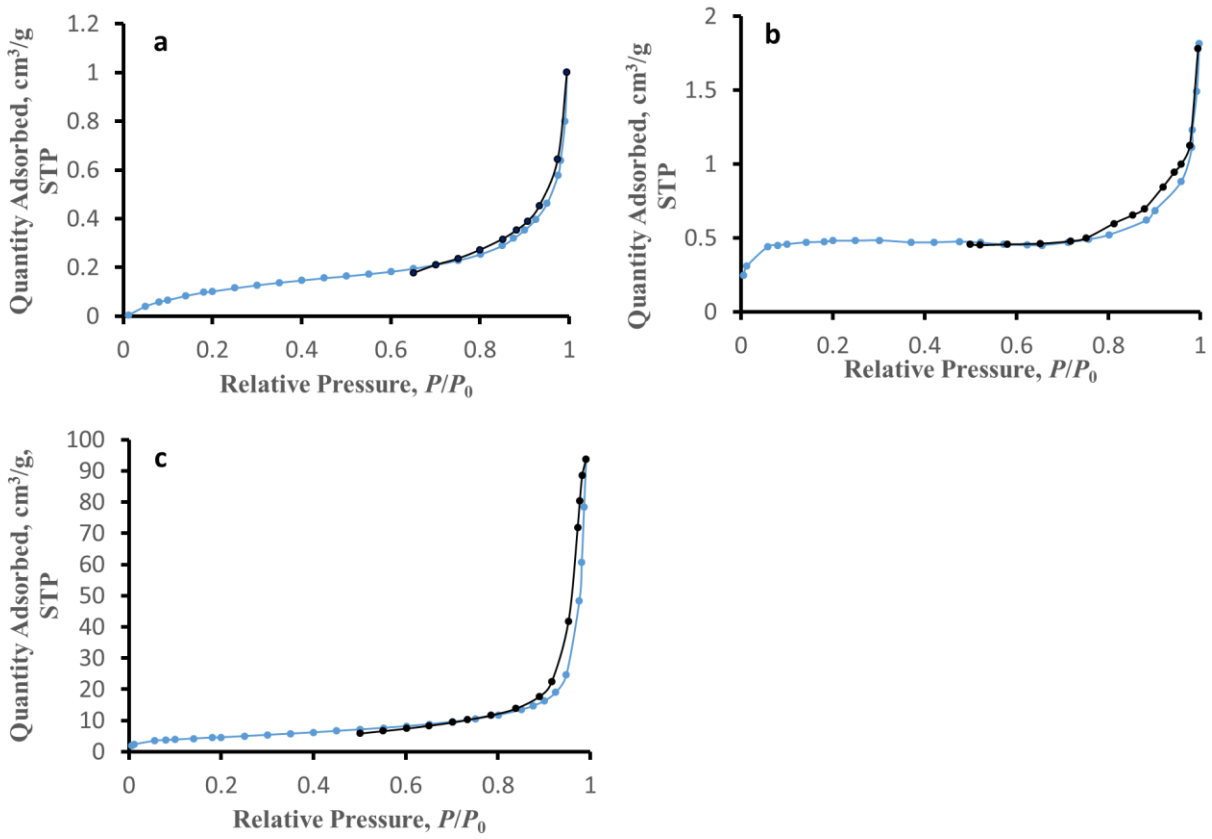

Figure 5.4 BET Isotherm for H (a), H350 (b) and H500 (c).

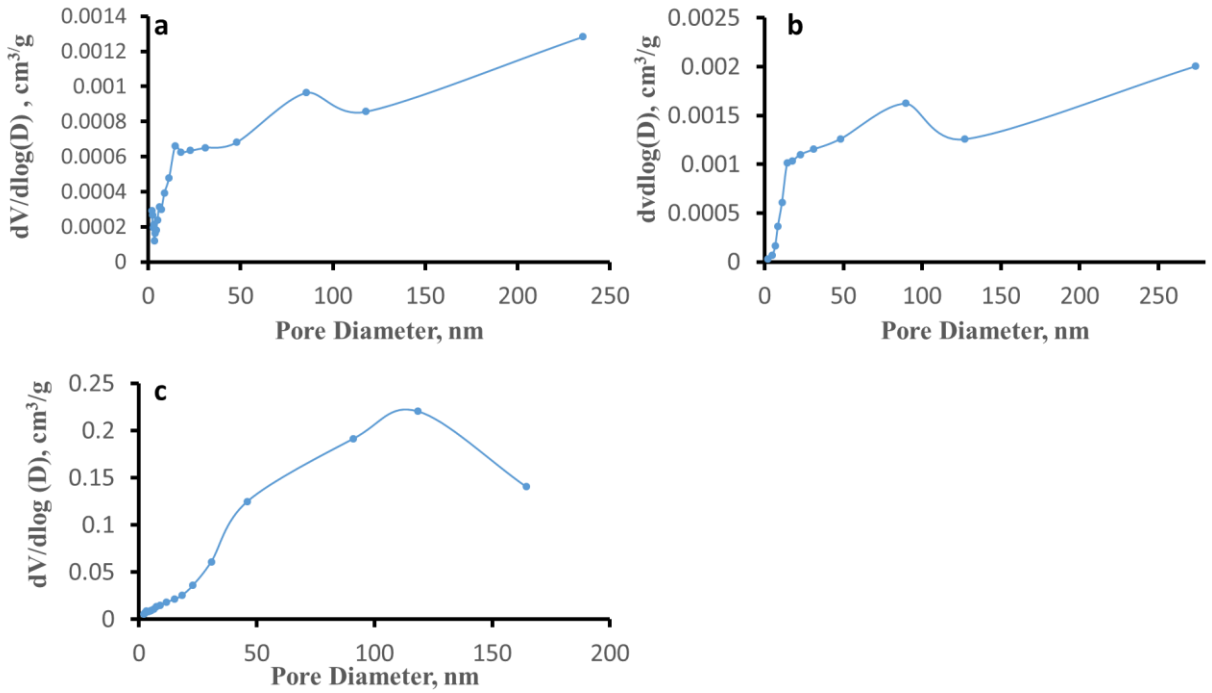

Figure 5.5 BJH Pore Size Distribution for H (a), H350 (b) and H500 (c).

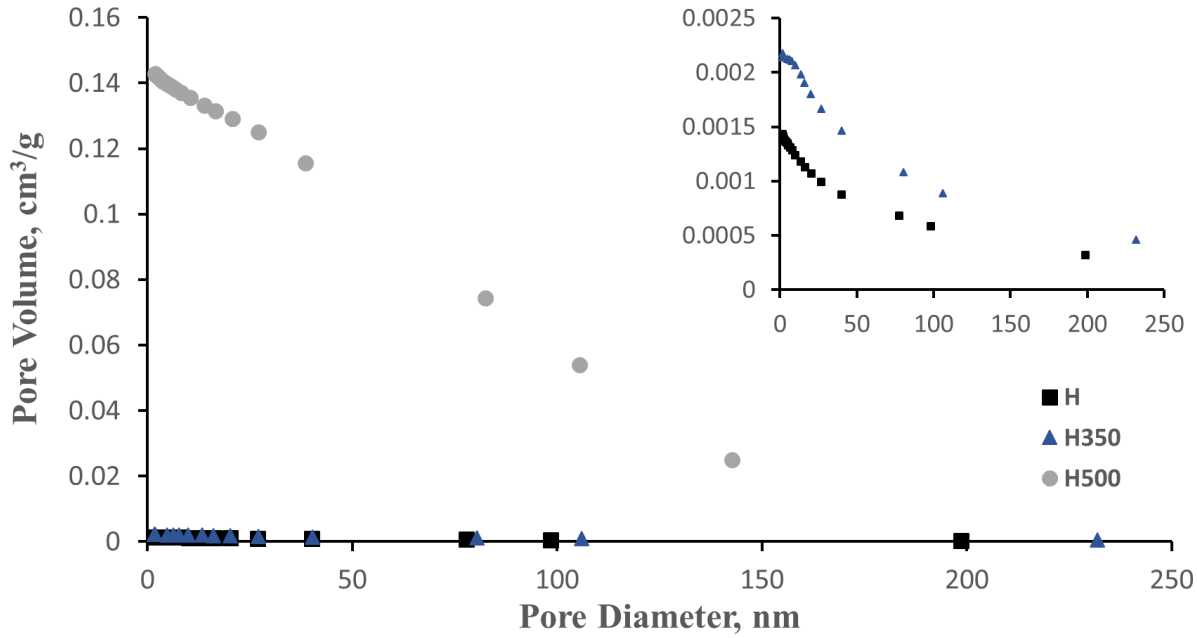

Figure 5.6 Pore Volume Distribution per Pore Diameter.

Table 5.3 Surface Areas and Pore Volumes of H, H350 and H500

Adsorbent	BET Surface Area, m^2/g	Langmuir Surface Area, m^2/g	BJH Pore Volume, cm^3/g	Average Pore size, nm
H	0.5	0.92	0.0016	18.8
H350	1.4	2.2	0.002	26.8
H500	16.9	24.1	0.142	34.9

5.6 Equilibrium Studies

5.6.1 Effect of pH on % Removal and Adsorption Capacity

As explained before, the pH is one of the key parameters that affects the adsorption process since it affects the surface charge of the adsorbent as well as the degree of ionization of the adsorbate. The effect of pH on the adsorption of SA was investigated at an initial SA concentration of 70 mg/L and different pHs ranging from 2 -12. Fig. 5.7 and 5.8 show the respective % removal and adsorption capacity of SA onto the three employed husks at different pHs. Clearly for all three types of husk, both the removal and adsorption capacity decrease with increasing the pH above the neutral pH. In the acidic region, no significant differences, according to the student's *t*-test, can be observed. The percent removal in this region reaches up to 70% onto H500, exceeding the removal onto H and H350 by only 20%. In a study on the adsorption of SA onto pine wood biochar, the percent removal was 85% at an initial concentration of 50 mg/L, 2 g/L and an initial pH of 2. [35] As the pH increases above the PZC of the husk (i.e., pH = 2) and the pK_a of SA (i.e., 2.79), both SA and the husk become negatively-charged. With further increase in pH, the negativity of each of SA and the husk increases resulting in electrostatic repulsion that, in turn, leads to a decline in the adsorption capacity and the percent removal. A similar behavior was observed in a previous study on the adsorption of SA on polar-modified post-cross-linked polystyrene .[26] Additionally, in the study of adsorption of SA onto powdered AC prepared from rice and coffee husk, the amount adsorbed per each gram of adsorbent, q_e, decreased with an increase in the pH.[34] At the employed pH range, both SA and the husk are negatively charged and, yet, significant removal took place. This implies that the interaction between SA and the husk is unlikely to be electrostatic.

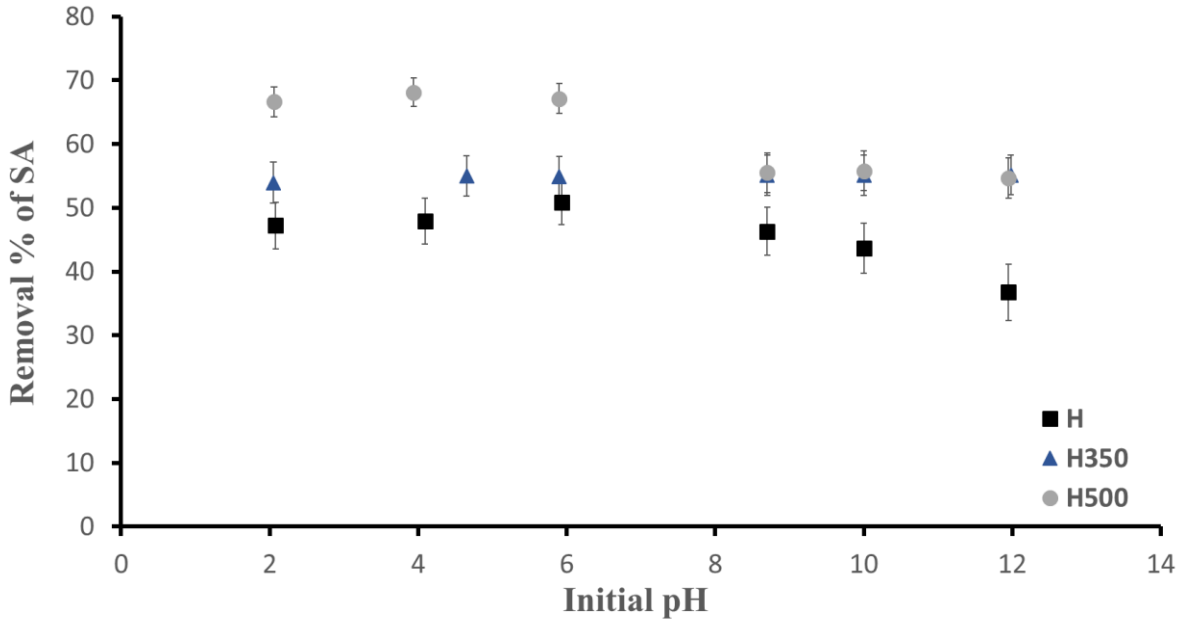

Figure 5.7 Removal of SA (70 ppm) onto H, H350 and H500 as a function of initial pH. Values are mean ± SD (n = 3)

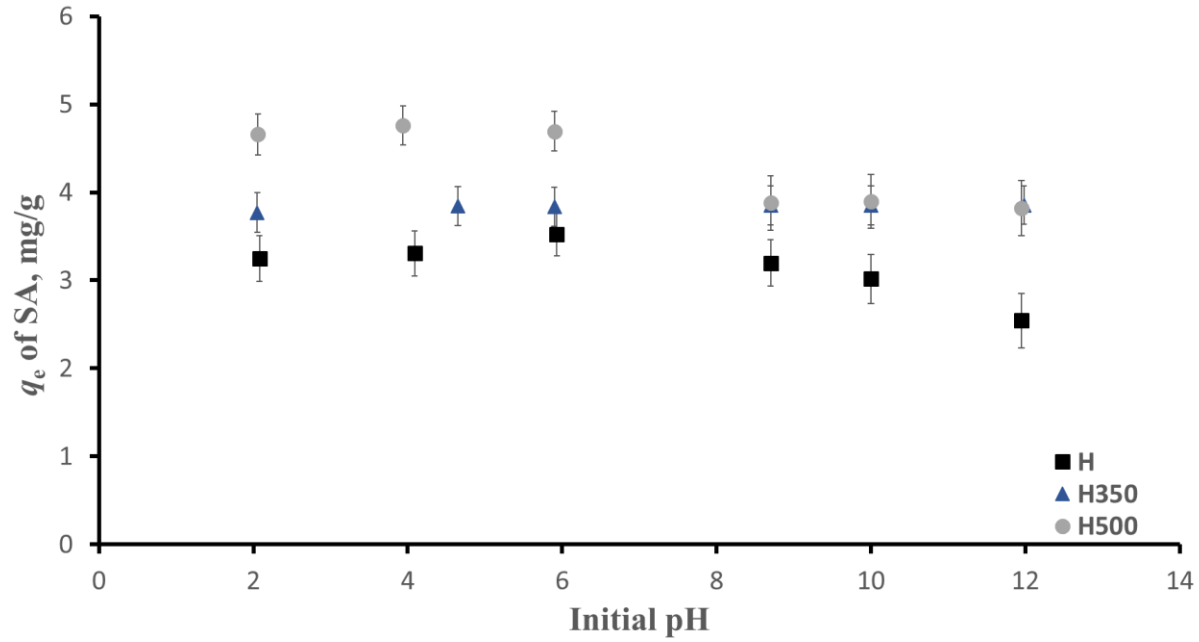

Figure 5.8 Equilibrium adsorbed quantity of SA (70 ppm) onto H, H350 and H500 as a function of initial pH. Values are mean ± SD (*n* = 3)

Similarly, Fig. 5.9 and 5.10 depict the effect of pH on the % removal and adsorption capacity of CA, respectively. For the three husks, both the removal and the capacity decreased with increasing the pH up till 10.4, the pK_a of CA, in the alkaline region. As the pH approaches 10.4, CA becomes less positively charged. Hence, the electrostatic interaction weakens between CA and the negatively charged husk. It can also be observed that the removal efficiencies and adsorption capacities of the three husks are comparable at the different employed pHs.

In view of the above results, pH 6.5 was chosen as the optimal pH since it provides the optimum percent removal for both SA and CA under almost neutral conditions which are favorable for operation. Hence, this pH will be the working pH in the following studies.

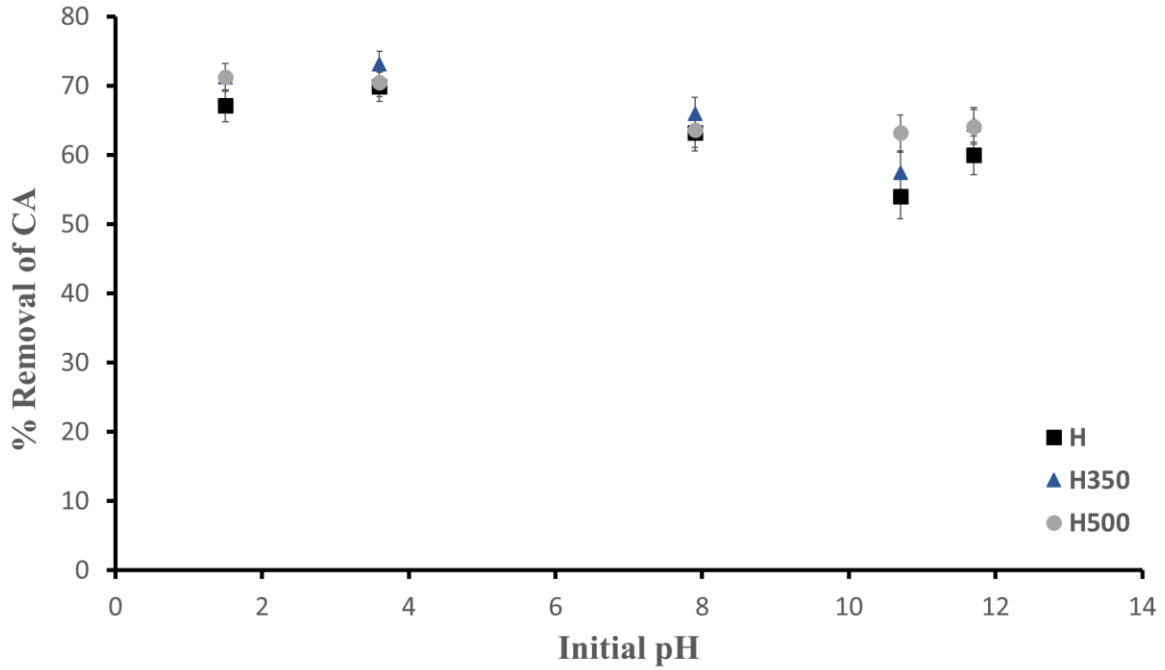

Figure 5.9 % Removal of CA (255 ppm) onto H, H350 and H500 as a function of initial pH. Values are mean ± SD (n = 3)

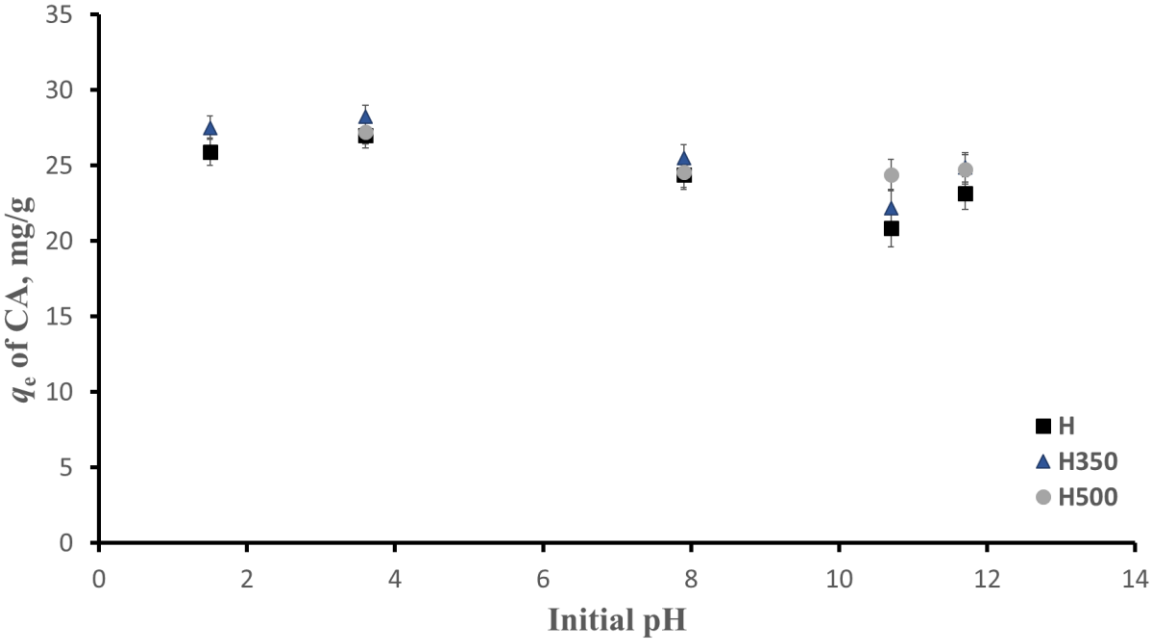

Figure 5.10 Equilibrium adsorbed quantity of CA (255 ppm) onto H, H360 and H500 as a function of initial pH. Values are mean ± SD (n = 3)

5.6.2 Effect of Initial Concentration on Removal Percentage

The effect of initial concentration on the percentage removal of SA by the three husks was evaluated in the concentration range of 18 – 280 mg/L at pH 6.5± 0.2 as depicted in Fig. 5.11. At all employed concentrations, the activated husks H350 and H500 exhibited higher removal efficiencies than H. This could be attributed to their higher surface areas and pore volumes relative to H. At the low concentrations (up to about 35 mg/L), H350 and H500 removed SA by up to 85% exceeding that of H by 1.4 times. However at higher concentrations, the percent removal dropped and remained almost constant at about 65, 55 and 50% for H500, H350 and H, respectively, indicating that the active sites have been almost saturated. Thus, the activation of the husk enhanced the removal of SA. In a previous study on the adsorption of SA onto banana peel, the removal percentage was 70% at an initial concentration of 50 mg/L and at a pH of 3.3. An increase in the initial concentration decreased the removal percentage which remained constant at almost 52%.[11] In our study, the average removal efficiency obtained by all husks at the different

concentrations in the range of 70-280 ppm is 55%. Higher and lower values fluctuate around this average that is indicated by the solid horizontal line in Fig. 5.11.

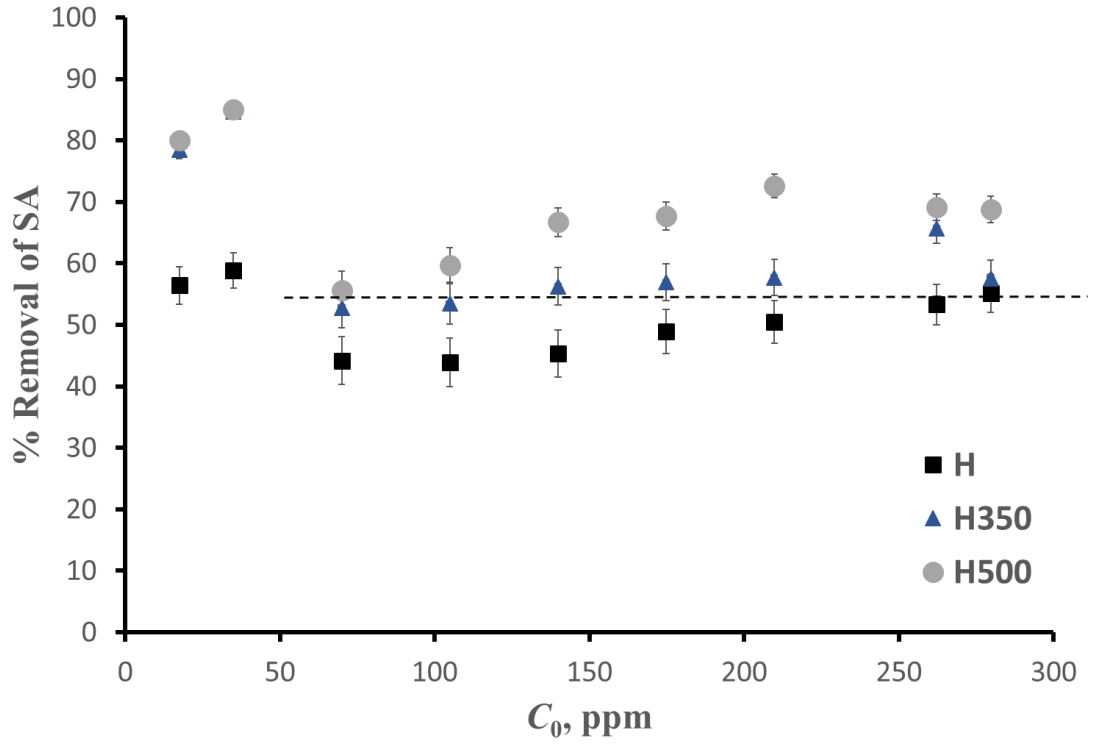

Figure 5.11 % Removal of SA onto H, H350 and H500 as a function of its initial concentration at pH 6.5 ± 0.2. The horizontal dotted line indicates the % average removal for all husks at the concentration range of 70-280 ppm. Values are mean ± SD (n = 3)

The same study was conducted for CA using the initial concentration range of 1.5 – 400 mg/L at pH 6.5± 0.2 as illustrated in Fig. 5.12. Investigating the removal percent of CA on H, low removal can be observed in the low initial concentration range up till about 82 mg/L, after which the removal increases but remains almost constant independent of concentration at about 55%, as indicated by the dotted horizontal line in Fig. 5.12, probably due to saturation of active sites.[32] The activated husks H350 and H500 exhibited higher removal efficiencies than the non-activated husk H only at the lower concentrations (i.e., up to 25 mg/L) recording values of slightly higher than 60%. At higher concentrations, H350 and H500 showed comparable removal efficiencies to those of H. At the employed pH, the husk is negatively charged, as mentioned in the PZC subsection,

while CA (pK_a = 10.4) is positively charged. Thus, electrostatic interaction has most likely occurred between CA and the husk. Interestingly, H350 is more negatively charged than H500, yet it showed comparable removal to that of H500. The effect of charge, however, could have been counteracted by the effect of surface area, since H350 has less surface area than H500.

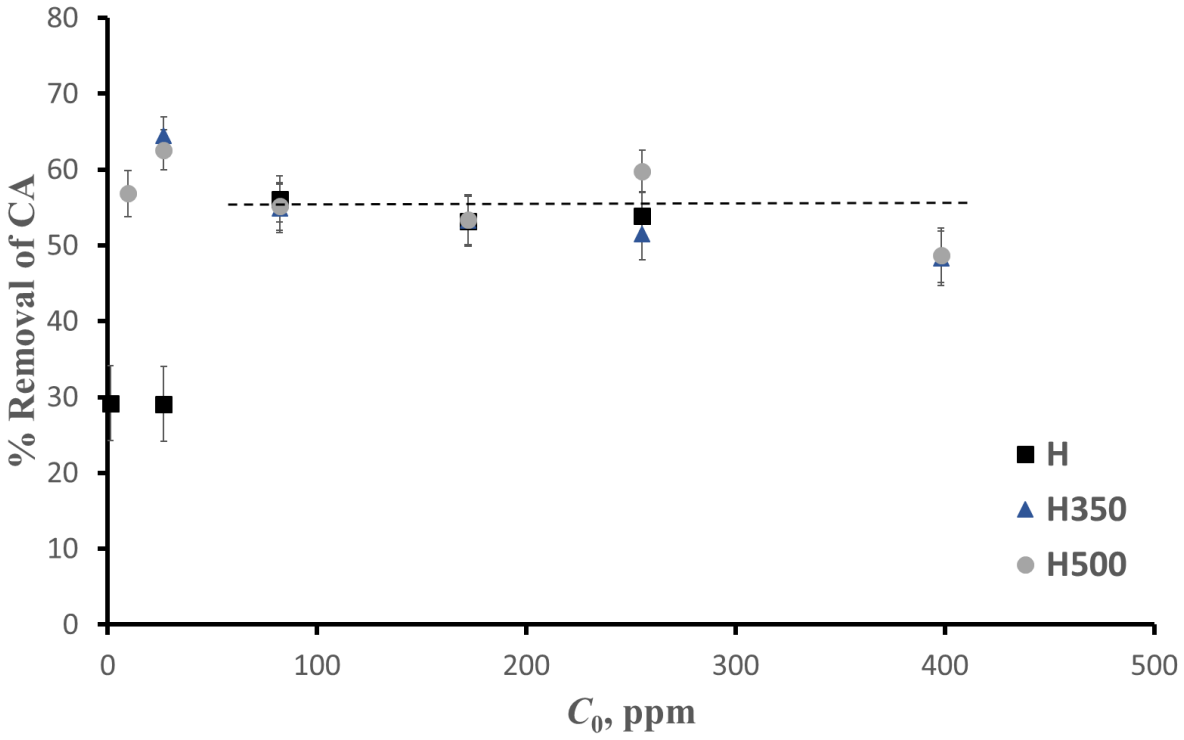

Figure 5.12 % Removal of CA onto H, H350 and H500 as a function of its initial concentration at pH 6.5± 0.2. The horizontal dotted line indicates the % average removal for all husks at the concentration range of 82-400 ppm. Values are mean ± SD (n = 3)

From the above study, it can be concluded that an average percentage removal of about 55% at most of the employed range of concentrations was obtained for each of SA and CA onto the three husks. The activated husks, however, showed higher removal percentages, particularly for SA, than their un-activated counterpart. This could be attributed to the higher charge as well as the larger surface area and pore volume of the activated husks relative to the un-activated one. Since CA and the husk have opposite charges under the investigated operating conditions, electrostatic interaction has most likely occurred. For SA adsorption on to the husk, binding took place despite the like charges possibly due to physical interaction via H-bonding and van der Waal's. Thus, it is

expected that the CA-husk interaction, being electrostatic, would be stronger than the SA-husk interaction.

5.6.3 Effect of Initial Concentration on Adsorption Capacity

The effect of initial concentration on the adsorption capacity was also investigated under the same conditions adopted in the removal study. As shown in Fig. 5.13, the adsorption capacity of all husks increases linearly with increasing the initial concentration of SA probably as a result of the higher concentration gradient which increases the mass transfer driving force.[31] The linear relationship is confirmed by the high correlation factors (R^2) estimated for the linear plots, as presented in Fig. 5.13. The three husks followed the same behavior, however, the adsorption capacity was best for H500, followed by H350 and then H. For the highest concentration of SA (280 mg/L), the uptake was 28.7 mg/g, 23.6 mg/g and 19.2 mg/g for H500, H350 and H, respectively. This indicates that the activation of the husk improved its adsorption capacity for SA as was the case for the removal. The same behavior was observed in previous literature that studied the adsorption of SA on granular activated carbon, where the amount adsorbed increased proportionally with the initial concentration.[69]

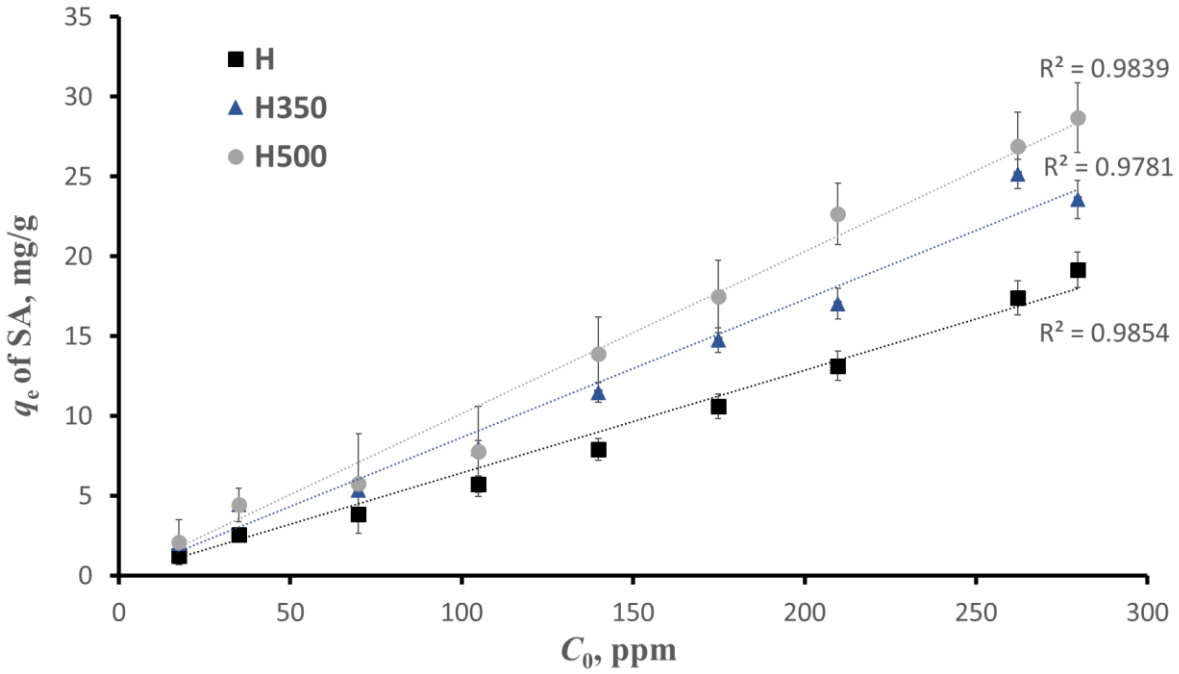

Figure 5.13 The equilibrium adsorbed quantity of SA onto H, H350 and H500 as a function of its initial concentration at pH 6.5±0.2. Values are mean ± SD (n = 3)

Similarly for the adsorption of CA (Fig. 5.14), the adsorption capacity increased linearly with increasing the initial concentration of CA. Again, the linear relationship is evident from the high correlation factors (R^2) pertaining to the linear plots. The three husks showed comparable adsorption capacities as was mostly the case with the removal.

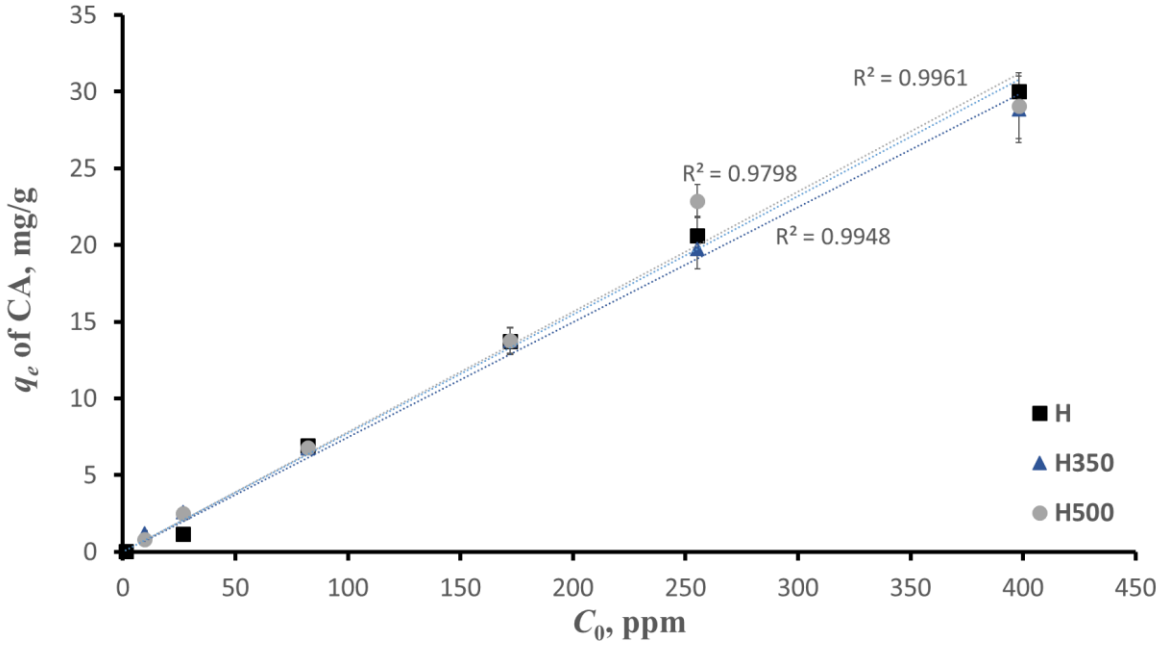

Figure 5.14 The equilibrium adsorbed quantity of CA onto H, H350 and H500 as a function of its initial concentration at pH 6.5±0.2. Values are mean ± SD (n = 3)

5.7 Kinetic Study

In this section, the effect of time on the adsorption of SA and CA in single component systems will be examined. This will give insight on the adsorption kinetics and the time needed for the adsorption process to reach equilibrium. The kinetic study will be conducted at the optimal pH of 6.5± 0.2 and initial concentrations of 280 mg/L for SA and 80 mg/L for CA. These concentrations were chosen as representative concentrations at which the average % removal (55%) was achieved by all husks at most of the employed concentrations. The high concentration was chosen for SA,

while the low concentration for CA since the interaction between the husk and SA is expected to be weaker than its interaction with CA.

5.7.1 Effect of Time on the Adsorption Capacity

Fig. 5.15 shows the kinetic uptake profiles for the adsorption of SA onto the three husks. Clearly, the adsorption process by all husks occurred very rapidly since equilibrium was approached in almost 5 min of contact time. After that, the adsorption capacity remained almost constant. This indicates a very fast process. H500 showed the highest adsorption capacity. The adsorption capacities were 29.28 mg/g, 24.49 mg/g and 19.2 mg/g for H500, H350 and H, respectively.

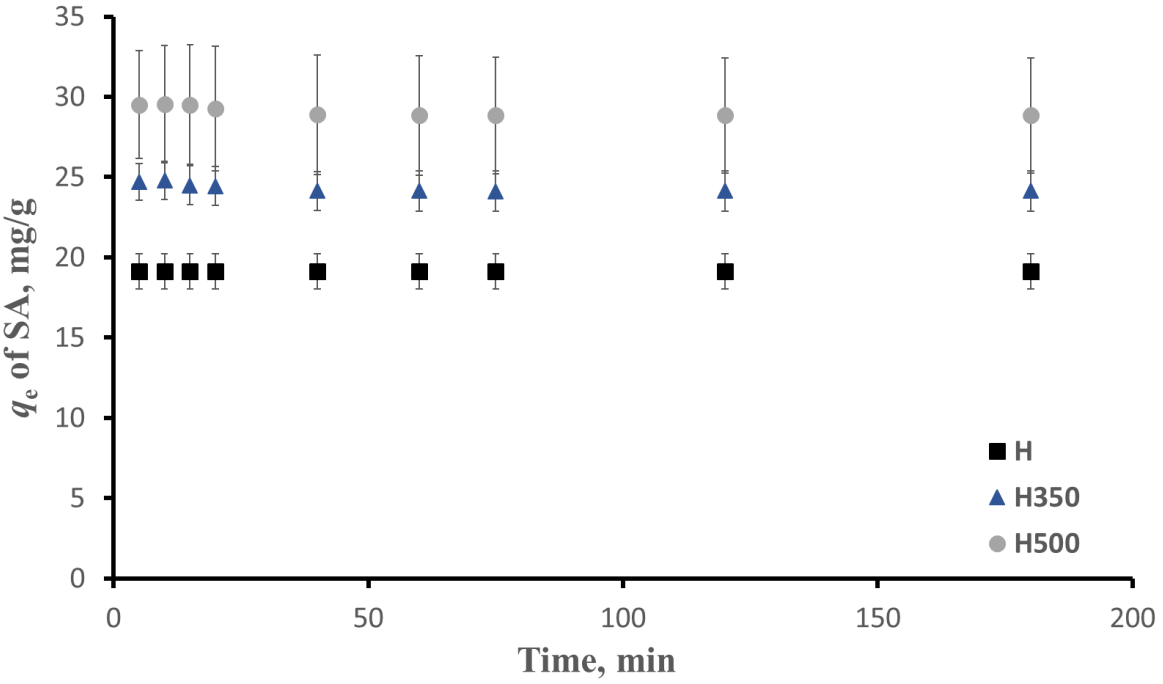

Figure 5.15 Effect of time on the adsorption capacity of SA (280 ppm) onto H, H350 and H500 at pH 6.5±0.2. Values are mean ± SD (n = 3)

The same experiment was repeated for CA. The initial concentration for H, H350 and H500 was 82 mg/L. As with SA, the reaction was very rapid and saturation was almost attained in the first 5 min as clear from Fig. 5.16. In this experiment, the adsorbed quantities for H, H350 and H500 were comparable and recorded 7.0, 7.4 and 7.3 mg/g respectively.

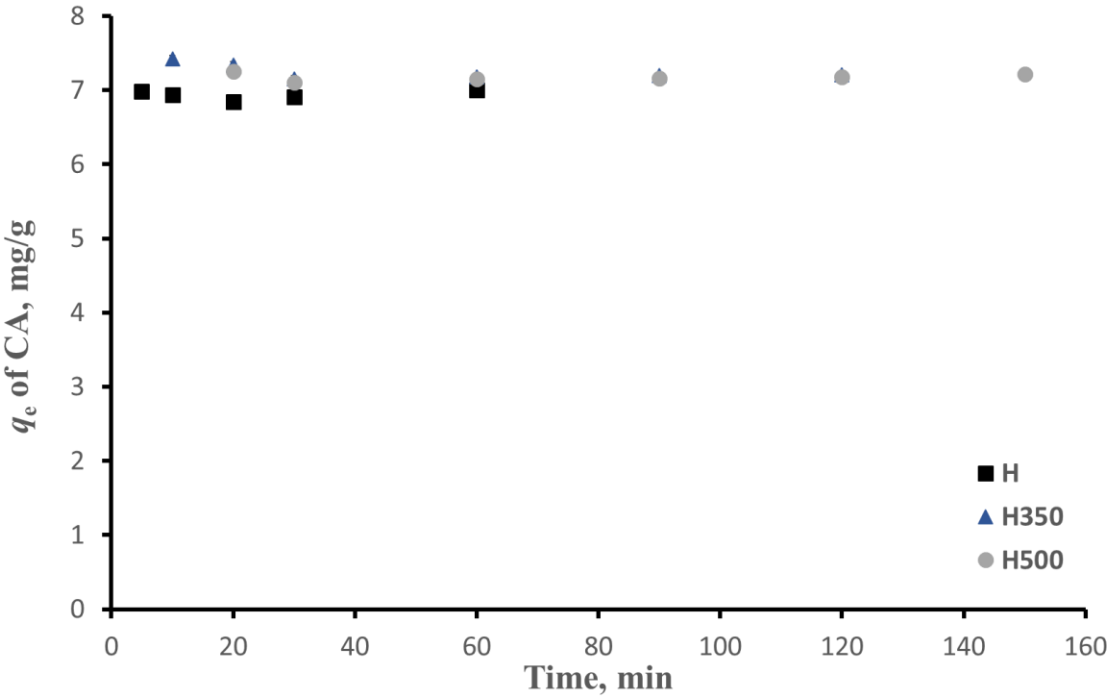

Figure 5.16 Effect of time on the adsorption capacity of CA (82 ppm) onto H, H350 and H500 at pH 6.5±0.2. Values are mean ± SD (n = 3)

5.7.2 Kinetic Modeling

To predict the kinetic profiles for the adsorption of SA onto the three husks, the experimental profiles obtained earlier were fitted to the pseudo-first order and pseudo-second order kinetic models as shown in Fig. 5.17 and Fig. 5.18, respectively. By inspecting the two figures, it can be inferred that the kinetic profiles can be best described by the pseudo-second order kinetic model, as evident from the higher R^2 values relative to their pseudo-first order counterparts. In the studies conducted by Fu et al. and Raoul et al, the adsorption of SA onto the different adsorbents were also well described by the pseudo-second order reactions.[17, 35]

The kinetic rate constants for the pseudo-first order (k_1) and pseudo-second order (k_2) models were determined from the slopes and the intercepts of the linear plots and are tabulated in Table 5.4. By comparing the pseudo-second order kinetic rate constants, it can be deduced that the rate of adsorption of SA onto H is comparable to its adsorption onto H350, however much higher

than its rate of adsorption onto H500. This could be owed to the larger pore volume and larger average pore size of H500 relative to H and H350. As a result, the adsorption onto H500 is more likely governed by slow pore diffusion kinetics rather than fast surface reaction kinetics.

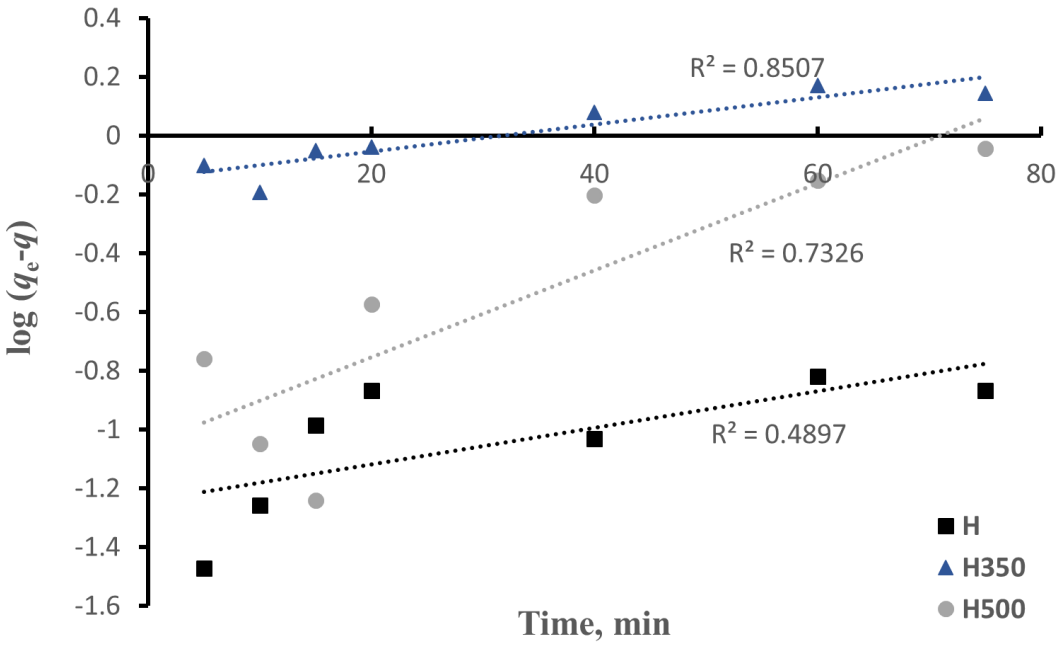

Figure 5.17 Pseudo-first order kinetic plots for the adsorption of SA (280 ppm) onto H, H350 and H500.

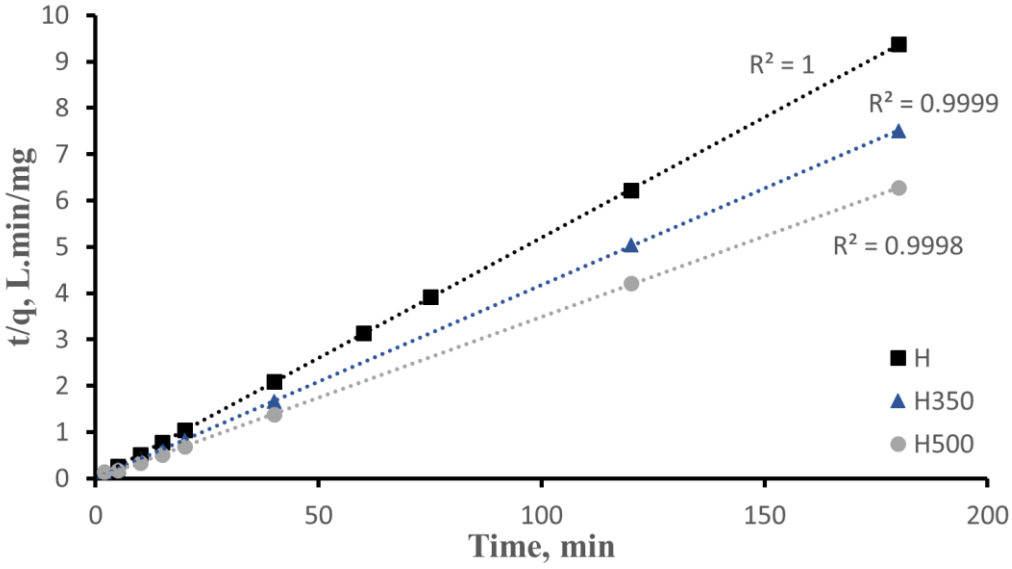

Figure 5.18 Pseudo-second order kinetic plots for the adsorption of SA (280 ppm) onto H, H350 and H500.

Table 5.4 Kinetic rate constants (k_1 and k_2) for the adsorption of SA (280 ppm) onto H, H350 and H500.

	k_1(min^{-1})	k_2 (g/mg*min)
H	5*10^{-3}	13.7
H350	0.03	11.3
H500	0.01	4.1

The kinetic profiles for the adsorption of CA onto H, H350 and H500 were also fitted to the pseudo-first order and pseudo-second order kinetic models as shown in Fig. 5.19 and Fig. 5.20, respectively. The relevant k_1 and k_2 values are presented in Table 5.5. The profiles were better predicted by the pseudo-second order kinetic models, with correlation factors (R^2) of almost 1. According to a previous study conducted on the adsorption of CA onto carbon xerogels, the kinetic profiles were also best fitted to the pseudo-second-order model.[37] As evident from the k_2 values in Table 5.5, the rate of adsorption of CA onto H350 exceeds its rate of adsorption onto H500 and H by about 2 and 4 times, respectively. This could be explained in view of the lower surface charge of H350 relative to H and H500, since the interaction is anticipated to be electrostatic.

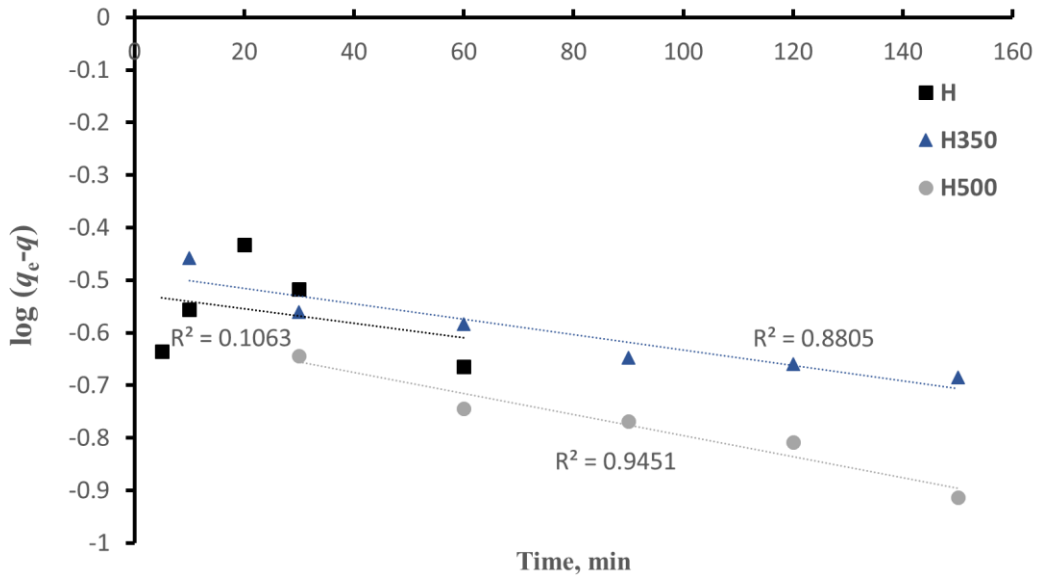

Figure 5.19 Pseudo-first order kinetic plots for the adsorption of CA (82 ppm) onto H, H350 and H500.

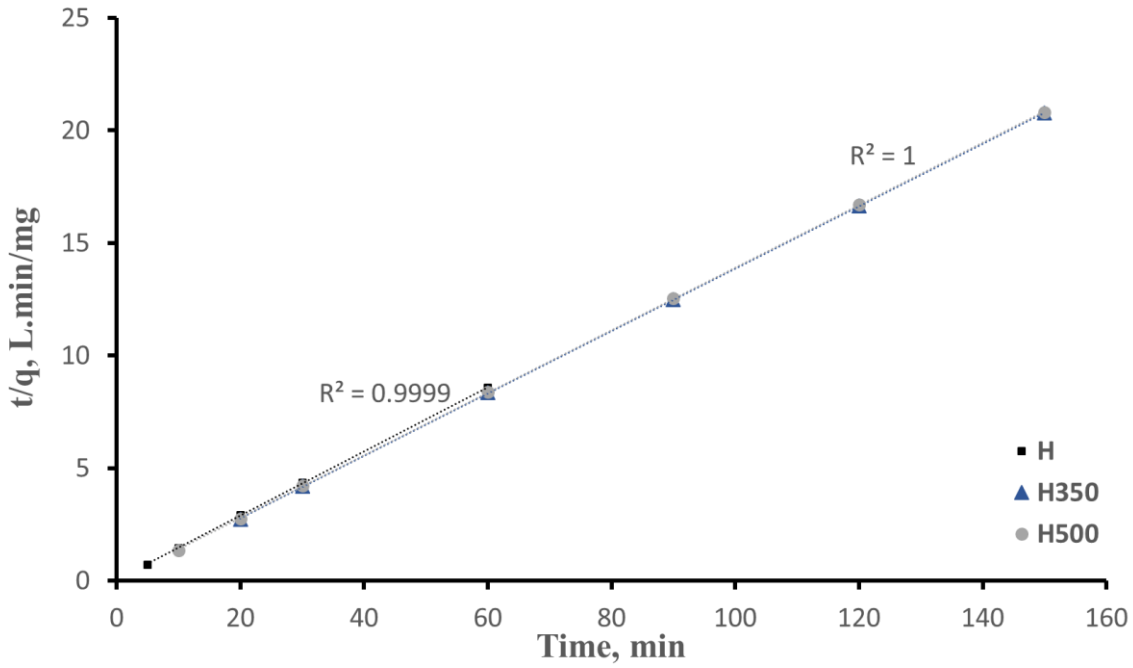

Figure 5.20 Pseudo-second order plots for the kinetics of the adsorption of CA (82 ppm) onto H, H350 and H500.

Table 5.5 Kinetic rate constants (k1 and k2) for the adsorption of CA (82 ppm) onto H, H350 and H500

	k_1 (min^{-1})	k_2 (g/mg*min)
H	$2.7*10^{-3}$	4.7
H350	$3.1*10^{-3}$	18.7
H500	$3.4*10^{-3}$	8.6

5.8 Adsorption Isotherm study

The equilibrium adsorption isotherms for the binding of SA onto the three husks is shown in Fig. 5.21, where a linear relationship can be observed between the equilibrium adsorption capacity and the corresponding equilibrium SA concentration. The linearity is confirmed by the moderately high correlation factors shown in Fig. 5.21 and Table 5.6. The linear isotherms indicate that the active sites on the adsorbent surface were not completely saturated with SA under the employed range of initial concentrations. Much higher initial concentrations might saturate the adsorbent surface, however they cannot be practically applied. This was also confirmed by fitting the isotherms to the Langmuir model which yielded very low R^2 values (data not shown).

The isotherm parameter for the Linear isotherm, K_L, was estimated from the slope of the linear plot and the corresponding dimensionless equilibrium constant, K_a, was calculated by multiplying K_L × (volume of the solution/mass of the adsorbent). The K_L and K_a for the adsorption of SA onto the three husks are compiled in Table 5.6. The K_a values for the adsorption onto the activated husks are greater than one indicating favorable adsorption, as opposed to a slightly less favorable adsorption onto H (K_a < 1). Further, having n > 1 for the Freundlich isotherms pertaining to the adsorption of SA onto H350 and H500 confirms the favorable adsorption.

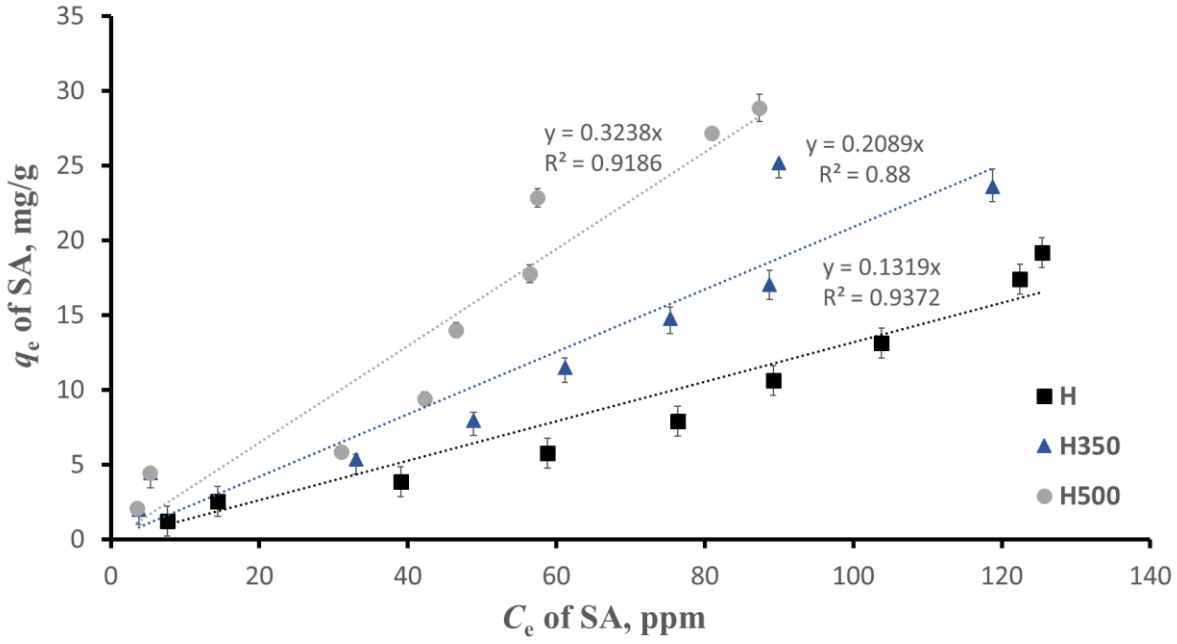

Figure 5.21 Equilibrium Adsorption Isotherms of SA onto H, H350 and H500 at pH 6.5± 0.2 and 27°C±2. Values are mean ± SD (n = 3)

Table 5.6 Isotherm parameters and correlation factors for the Linear adsorption isotherm and Freundlich Isotherm for SA adsorption onto the three husks

	K_L(L/g)	K_a	R^2 (Linear Isotherm Model)	K_F ($mg^{1-(1/n)}.g^{-1}L^{1/n}$)	n	R^2 (Freundlich Isotherm Model)
H	0.132	0.88	0.937	-	-	-
H350	0.209	1.39	0.880	1.119	1.602	0.935
H500	0.324	2.16	0.919	1.457	1.543	0.960

In addition to the Linear and Langmuir models, the isotherms were also fitted to the Freundlich model. Fig. 5.22 shows that the equilibrium isotherms for the adsorption of SA onto all husks could be fitted to the Freundlich isotherm model except for H which yielded a negative intercept. Hence, H can only be described by the Linear isotherm model. For the adsorption of SA onto H350 and H500, it is evident that the Freundlich isotherm model is a better fit as indicated by the higher R^2 values pertaining to this model relative to the Linear model (Table 5.6).

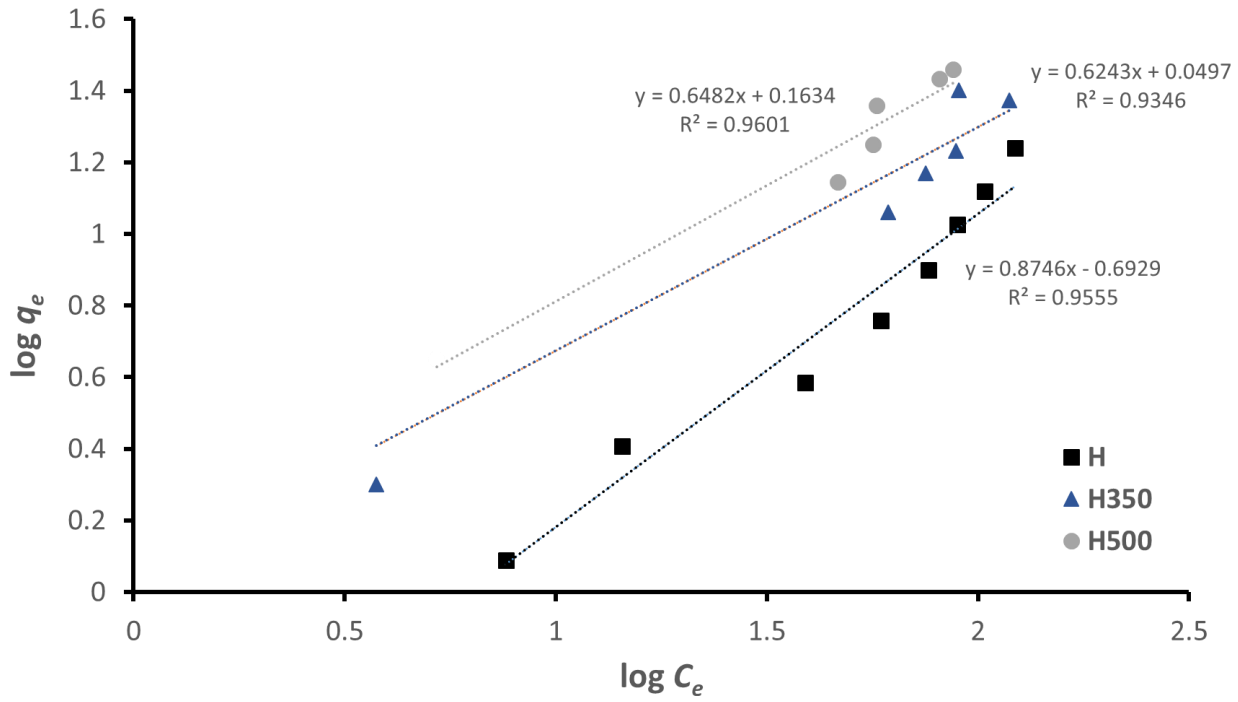

Figure 5.22 Freundlich Isotherm linear plots for the adsorption of SA onto H, H350 and H500 at pH 6.5 ± 0.2 and 27°C±2.

Similarly, the isotherms pertaining to the adsorption of CA onto the three husks are linear as evident from the high correlation factors shown in Fig. 5.23 and Table 5.7.

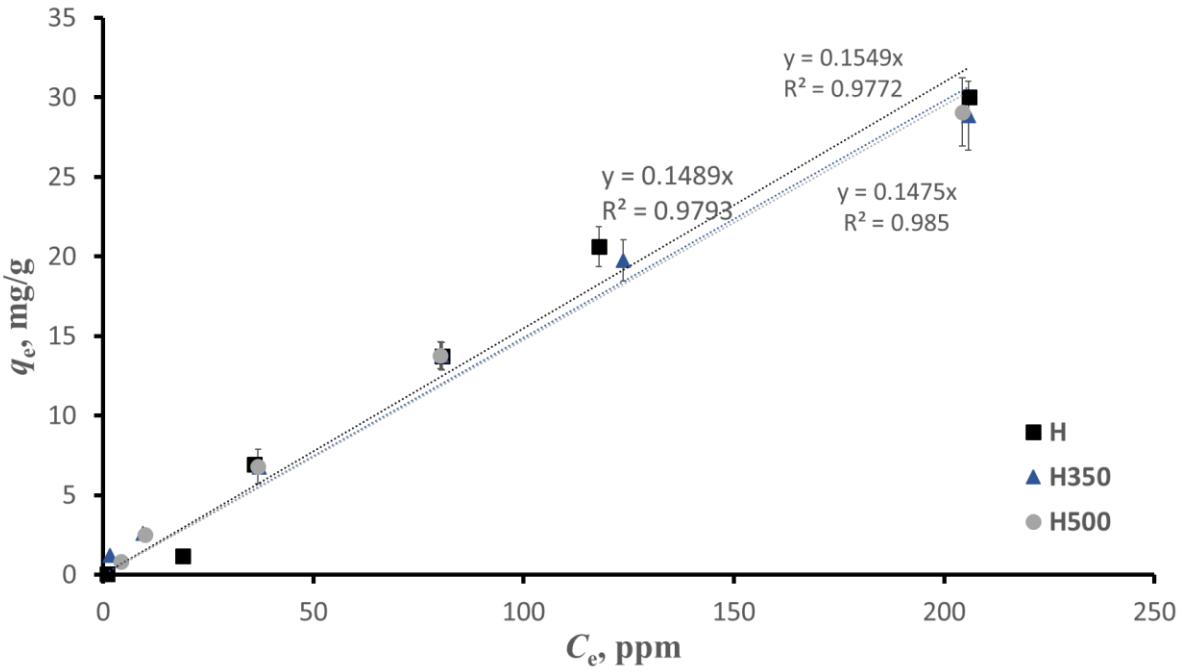

Figure 5.23 Equilibrium Adsorption Isotherms of CA onto H, H350 and H500 at pH 6.5 ± 0.2 and 27°C±2. Values are mean ± SD (n = 3)

Table 5.7 Isotherm parameters and correlation factors for the Linear adsorption isotherm for CA adsorption onto the three husks

	K_L(L/g)	K_a	R^2
H	0.155	1.03	0.977
H350	0.149	0.99	0.979
H500	0.148	0.99	0.985

The above isotherms for the adsorption of CA onto the three husks were also fitted to the Freundlich model as shown in Fig. 5.24. However, they yielded negative intercepts. Thus, it can be inferred that the adsorption of CA onto all three different types of husks could not be fitted to the Freundlich isotherm model. However, the adsorption can be well described by the Linear model. This contradicts the results of a previous study which reported that the adsorption isotherm of caffeine onto activated carbon can be best described by Freundlich isotherm.[29] However, this can be owed to the use of a different adsorbent.

By inspecting the equilibrium constants for the adsorption of CA onto each husk (Table 5.7), it is clear that they are comparable. This is consistent with the previously obtained adsorption capacities that were, as well, comparable for the three husks.

Only the K_a values for the adsorption of SA and CA onto H could be compared since their adsorption isotherms follow the same model; the Linear isotherm. As clear from Table 5.6 and Table 5.7, the adsorption of CA onto H possesses a larger equilibrium constant than its SA counterpart implying stronger binding probably due to the electrostatic interaction.

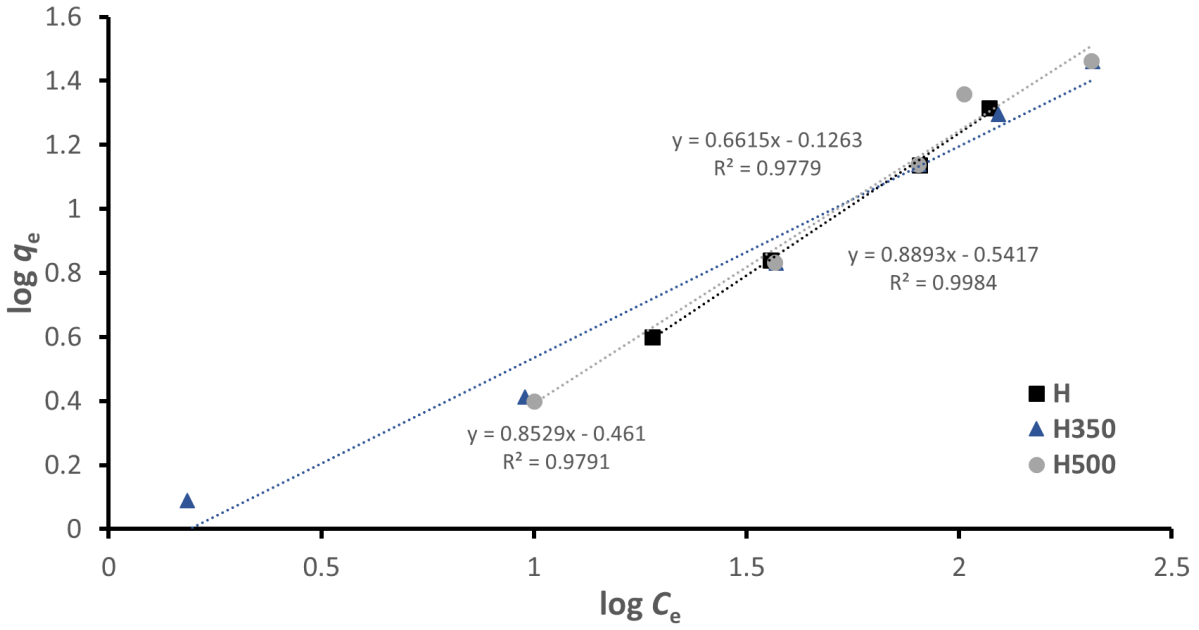

Figure 5.24 Freundlich Isotherm linear plots for the adsorption of CA onto H, H350 and H500 at pH 6.5 ± 0.2 and 27°C±2.

To gain more insight into the mechanism of sorption as to whether it is a chemical or physical one, the adsorption isotherms of SA and CA onto the three husks were fitted to the D-R model as presented in Fig. 5.25 and Fig. 5.26, respectively. The relevant adsorption energies were calculated using Eq.3.10, and values thereof were compiled in Table 5.8. Clearly, all energies of adsorption are below 8 kJ/mol.[67] This suggests physisorption of SA and CA onto all three husks. Further, the energies for the adsorption of CA onto H, H350 and H500 are higher than their corresponding

values for the adsorption of SA. This supports the findings obtained from the equilibrium and kinetic studies which suggested that CA binds more strongly to the husk than SA.

The K_L values for the adsorption of CA onto H350 and H500 are also in accordance with the D-R isotherm values since they both showed almost the same values K_L=0.99 and E (kJ/mol) = 0.04.

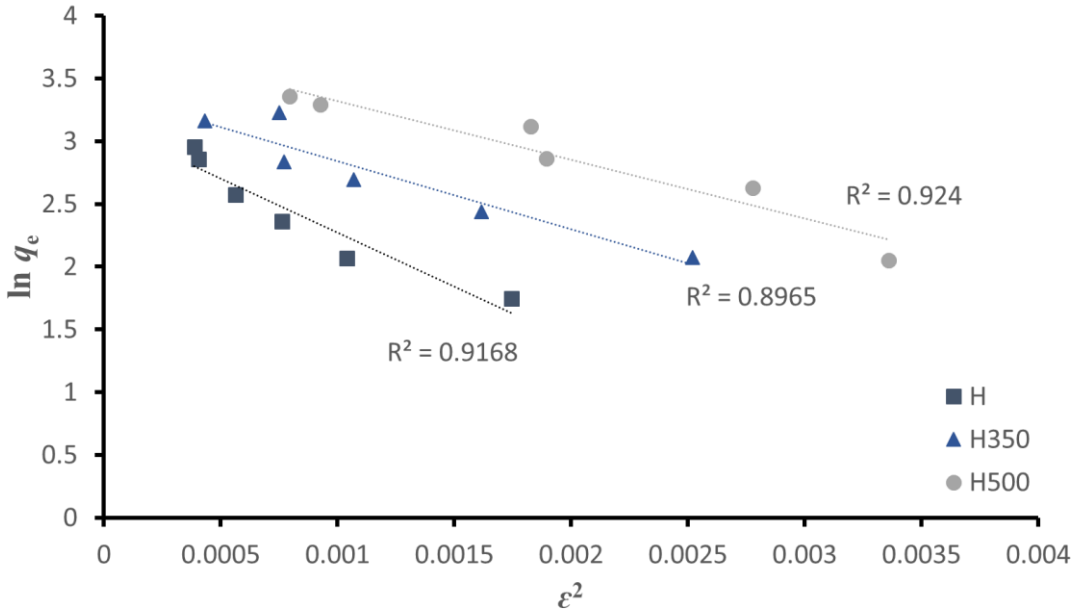

Figure 5.25 D-R isotherm model for the adsorption of SA onto the three husks.

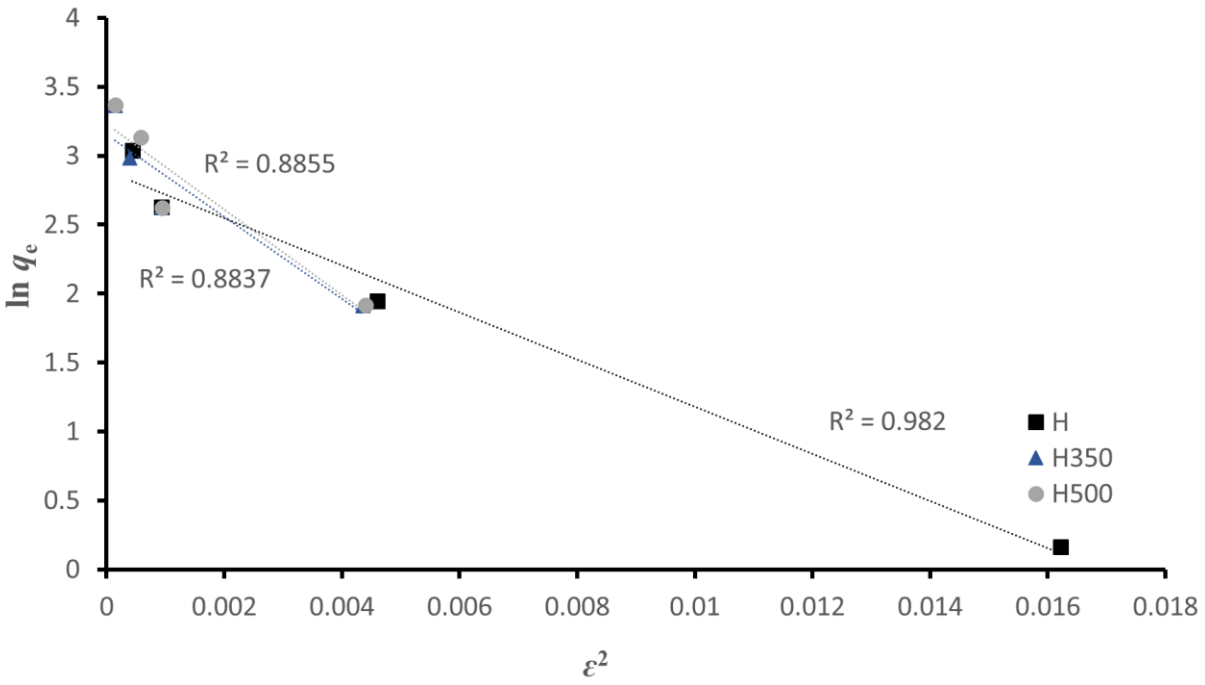

Figure 5.26 D- R isotherm model for the adsorption of CA onto the three husks.

Table 5.8 E(kJ/mol) values, as estimated from the D-R model, for the adsorption of SA and CA onto H, H350 and H500

	CA	SA
H	0.05	0.02
H350	0.04	0.03
H500	0.04	0.03

5.9 Binary Adsorption Studies

The adsorption of SA and CA onto H350 was studied in binary systems of both adsorbates applied at equal initial concentrations. H350 was chosen for this study because it provided the highest adsorption rates for both SA and CA. The removal percentages, as well, of each of SA and CA onto H350 and H500 were very comparable. Fig. 5.27 and 5.28 show the % removal and adsorption capacity of SA and CA onto H350 in the binary system. Clearly, the husk has much higher affinity for CA than for SA and hence is selective for CA. CA is highly competitive due to its ability to

bind electrostatically to the husk, while SA only adsorbs by weak physical interactions. The removal of CA in the binary system is comparable to its removal in the single system which confirms that it faced almost no competition from SA over the adsorption sites. The same reasoning can be applied for the adsorption capacity as shown in Fig.5.28. The adsorption capacity of CA in both the binary and single component systems increases linearly with initial concentration showing comparable capacities in both systems.

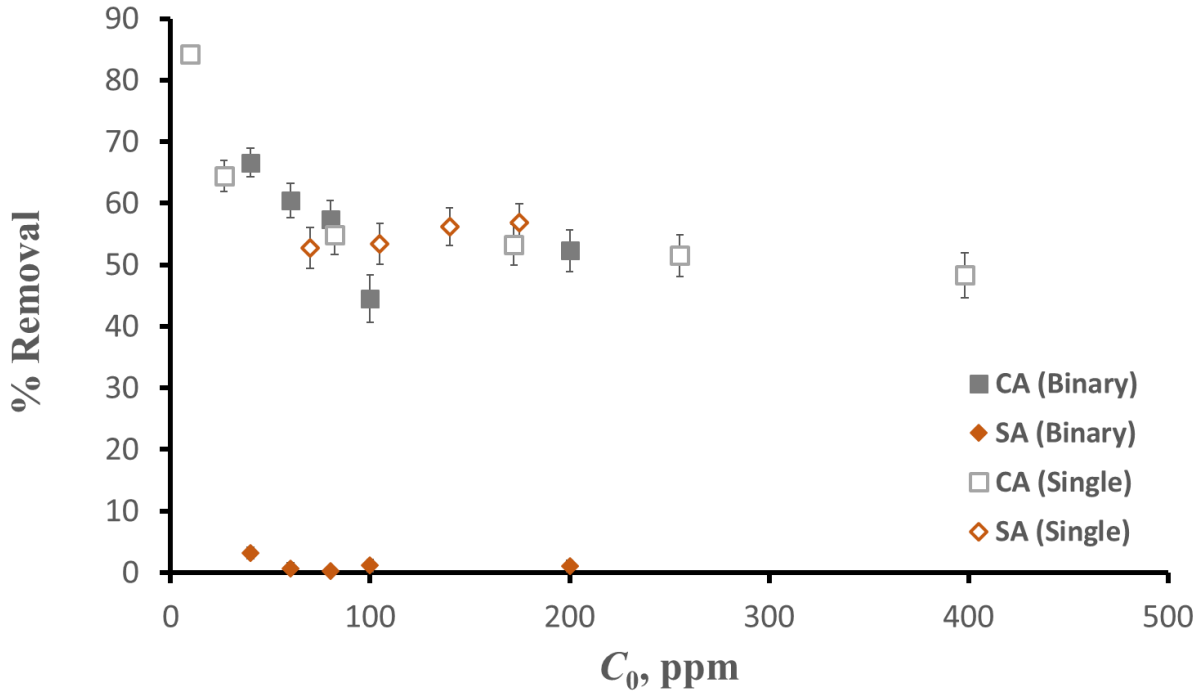

Figure 5.27 % Removal of CA and SA in a binary system as a function of initial concentration. Values are mean ± SD (n = 3)

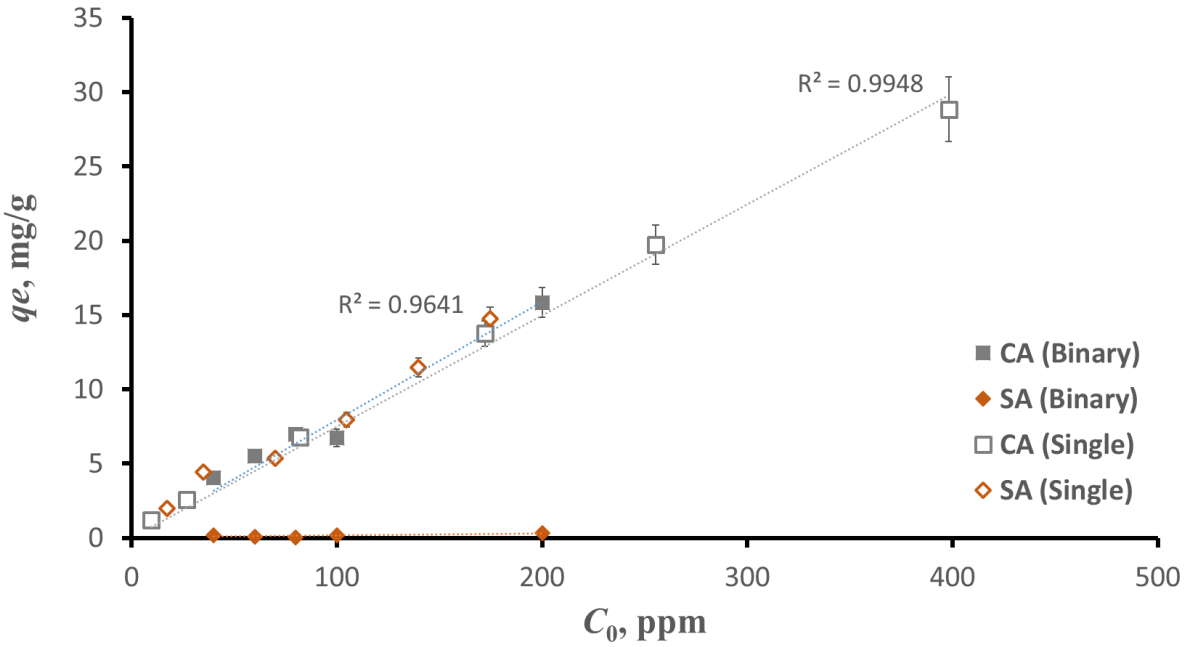

Figure 5.28 Adsorbed quantity of CA and SA in a binary system as a function of initial concentration. Values are mean ± SD (n = 3)

5.10 Regeneration of the husk

In order to test the regenerability of the chosen husk (H350), the husk regenerated with 1.0 M HCL solution for 2 h. Both SA and CA were first adsorbed then desorbed for 4 consecutive cycles. The adsorption capacity and percent removal were calculated after each cycle as given in Fig. 5.29 and 5.30, respectively. Obviously, the husk can be efficiently reused for up to 4 cycles, without impacting its adsorption performance.

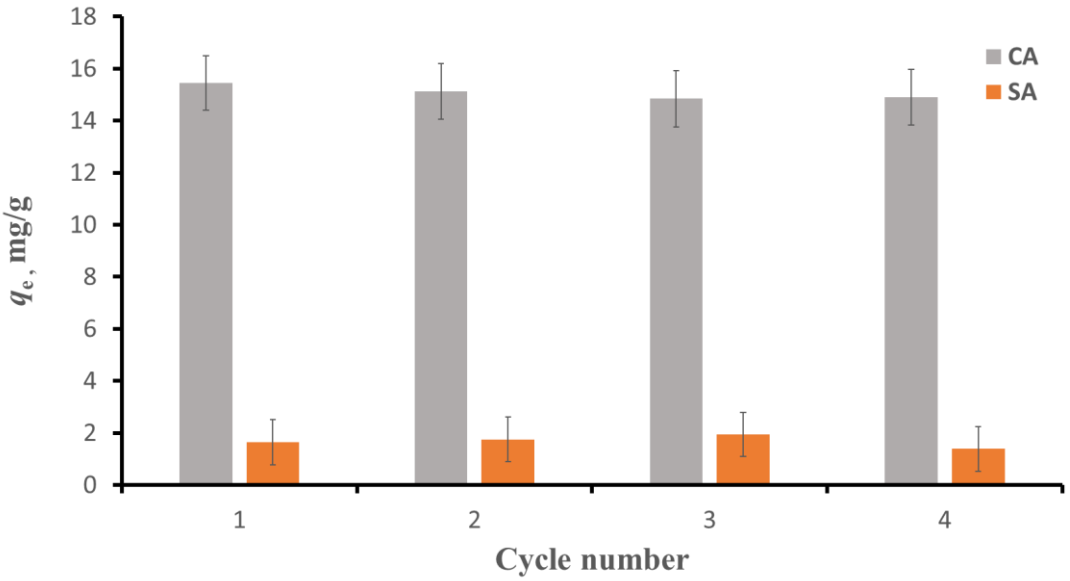

Figure 5.29 Adsorption capacity of H350 after regeneration for four cycles. Values are mean ± SD (n = 3)

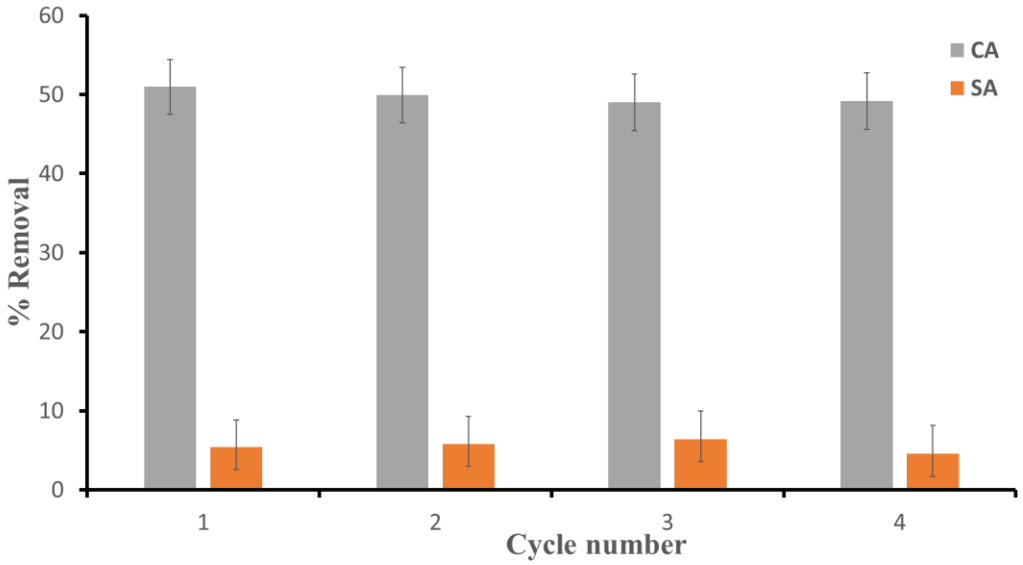

Figure 5.30 % Removal of H350 after regeneration for four cycles. Values are mean ± SD (n = 3)

Chapter 6
Conclusion

6. Conclusion

In this study, cape gooseberry husk was investigated as an alternative biosorbent for the safe removal of SA and CA from wastewater. Three different forms of husk (H, H350, H500) were employed. H is the un-activated husk, H350 and H500 are chemically activated forms of the husk that were prepared by acid treatment followed by heating at 350 ^{o}C and 500 ^{o}C, respectively. The husks were first characterized using different techniques: SEM, FT-IR, BET, ZP, and CHNS analysis. FT-IR results revealed the disappearance and weakening of different bands after husk activation, which confirmed the carbonization of the husk. ZP measurements indicated that the husks were all negatively-charged with H350 showing the highest negativity among the three husks. H350 recorded a ZP of -30 mV at pH 6.5, indicating its colloidal stability at this pH. BET results revealed that the three husks were primarily mesoporous. H500 exhibited the largest surface area and pore volume as well as the highest average pore size.

The husks were then investigated for their adsorption performance with regard to SA and CA in single-component and binary systems. Adsorption of each of SA and CA was conducted onto the three husks at different pHs. The maximum removal efficiency was obtained in the highly acidic pH of 2 for SA and 3.6 for CA. Higher pH conditions resulted in a slight decrease in the removal percentage. Thus, the optimal pH was chosen to be pH 6.5 for operability reasons.

Afterward, adsorption was investigated at different initial concentrations of SA and CA. The maximum removal efficiencies of 59%, 85%, 85% were achieved at an initial concentration of 35 mg/L. However, the percent removal averaged around 55% in most of the employed range of concentrations (70-280 mg/L). The equilibrium adsorption capacity, on the other hand, increased with increasing the initial concentration, and maximum equilibrium adsorbed quantities of SA were 19 mg/g, 25 mg/g and 27 mg/g for H, H350 and H500, respectively at an initial concentration of 280 mg/L. For CA, maximum removal efficiencies of about 56%, 65% and 63% were obtained for H, H350, and H500, respectively below initial concentrations of 85 mg/L. However, they averaged around 55% similar to SA adsorption, in most of the employed range of concentrations (82-400 mg/L). The maximum adsorption capacity for CA onto H, H350 and H500 were comparable amounting to about 29 mg/g. Thus from the above, it was concluded that H350 and H500 showed very comparable results in terms of their removal for SA and CA.

Kinetics of the adsorption of SA and CA onto all three husks was studied and it followed pseudo-second order kinetics. The rates of adsorption of SA onto H and H350 were comparable but higher than H500 by 3 times. For CA, H350 showed the highest rate of adsorption, exceeding that of H500 by almost 2 times. The equilibrium adsorption isotherm for SA onto H followed the Linear adsorption isotherm, while the isotherms for its adsorption onto H350 and H500 were better described by the Freundlich model. The adsorption of CA onto all three husks followed the Linear adsorption isotherm. The values of the estimated isotherm parameters indicated that adsorption was more favorable onto the activated husks. In addition, the D-R isotherm model suggested physisorption of SA and CA onto all three husks. Further, the energies for the adsorption of CA onto H, H350 and H500 surpassed their corresponding values for the adsorption of SA. This implies that CA was more strongly bound to the husk, probably due to electrostatic interaction between the oppositely charged CA and the husk. Despite the like charges of SA and the husk, interaction still occurred due to physical interaction, possibly via H-bonding or van der Waals'. A proposed mechanism is shown in Fig.6.1.

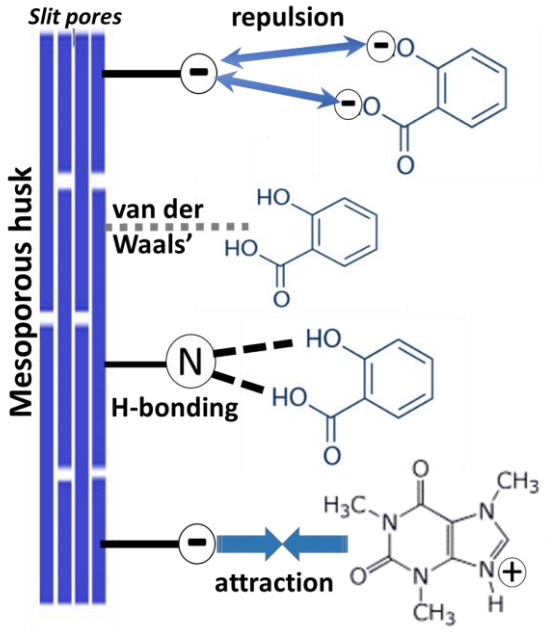

Figure 6.1 Proposed mechanism for the adsorption of SA and CA onto the husk at pH 6.5.

Since both H500 and H350 showed comparable removal for SA and CA, while H350 showed higher rate of adsorption towards both adsorbates, H350 was chosen as the optimal husk for the binary system study. In the binary system, adsorption of CA was favored over that of SA due to

the electrostatic interactions between positively charged CA and the negatively charged husk. SA hardly showed any competition and CA behaved almost the same as in single-component systems. Additionally, it was observed that H350 could be regenerated for at least three times without losing its adsorption efficiency.

In view of the above, cape gooseberry husk can be regarded as an efficient adsorbent for CA and SA, particularly its H350 activated form. Therefore, H350 could be used in WWTPs for the removal of CA and SA. Since H350 has a high selectivity for CA, it can be deployed in a two-unit batch or column treatment system. In the first unit, CA will be removed with high efficiency. Then the effluent from this unit will pass to the second unit, where fresh or regenerated husk is used for the removal of SA. We recommend to run this system under almost neutral conditions, pH 6.5. Despite the possibility of obtaining better removal efficiencies by decreasing the pH of the husk, we believe that the enhancement in removal does not suffice working at highly acidic pHs since this would require an additional treatment step involving a neutralization tank.

Future studies could be performed on the following:

- Investigating other adsorption parameters for the adsorption of both adsorbates onto all three husks, such as agitation speed, temperature and adsorbent dose.
- Scaling-up the proposed treatment method.
- Applying the proposed treatment method on real wastewater effluents.
- Extending the already, existing study to remove other contaminants of emerging concern.

7. References

1) M. Raghav, S. Eden, K. Mitchell, B. Witte Contaminants of Emerging Concern in Water Arroyo 2013 *Water Resources Research Center*, College of Agriculture and Life Sciences, University of Arizona, Tucson, AZ (2013)
2) Deblonde, T., Cossu-Leguille, C., & Hartemann, P. (2011). Emerging pollutants in wastewater: A review of the literature. *International Journal of Hygiene and Environmental Health*, 214(6), 442-448. doi:10.1016/j.ijheh.2011.08.002
3) Ayyash, Fatima and Kamis, Mustafa and Khalaf, Samer and Thawabteh, Amin and Karaman, Rafik, Removal of Aspirin, Salicylic Acid, Paracetamol and p-Aminophenol by Advanced Membrane technology Activated Charcoal and Clay Micelles Complex. (May 2015). Case Studies Journal ISSN (2305-509X) – Volume 4, Issue 5 – May-2015, Available at SSRN: https://ssrn.com/abstract=3402299
4) Sim, W., Lee, J., Lee, E., Shin, S., Hwang, S., & Oh, J. (2011). Occurrence and distribution of pharmaceuticals in wastewater from households, livestock farms, hospitals and pharmaceutical manufactures. *Chemosphere, 82*(2), 179-186. doi:10.1016/j.chemosphere.2010.10.026
5) Pharmaceuticals in Drinking-Water, World Health Organization (WHO). Retrieved December05,2020,from https://www.who.int/water_sanitation_health/publications/2012/pharmaceuticals/en/
6) Odize, V., Rahman, A., Jones, K., Khunjar, W., & Murthy, S. (2017). Removal of 17α-ethinylestradiol, salicylic acid, trimethoprim, carbamazepine and nonylphenol through biological carbon and nitrogen removal processes: Removal of 17α-ethinylestradiol. *Water and Environment Journal, 31*(3), 440-449. doi:10.1111/wej.12262
7) Lee, X; Chemmangattuvalappil, N.; Lee, L. Adsorptive Removal of Salicylic Acid from Aqueous Solutions using New Graphene-Based Nanosorbents. *Chemical Engineering Transactions*. 2015, 45, 1387-1392
8) El-Sayed, H. E. M., & El-Sayed, M. M. H. (2014). Assessment of food processing and pharmaceutical industrial wastes as potential biosorbents: A review. *BioMed Research International, 2014*, 146769-24. doi:10.1155/2014/146769
9) Mallek, M., Chtourou, M., Portillo, M., Monclús, H., Walha, K., Salah, A. b., & Salvadó, V. (2018). Granulated cork as biosorbent for the removal of phenol derivatives and emerging contaminants. *Journal of Environmental Management*, 223, 576-585. doi:10.1016/j.jenvman.2018.06.069
10) Bernardo, M. M. S., Madeira, C. A. C., dos Santos Nunes, Nuno Carlos Lapa, Dias, Diogo André Costa Messias, Godinho, D. M. B., de Jesus Pinto, Maria Filomena, . . . de Figueiredo Ligeiro Fonseca, Isabel Maria. (2017). Study of the removal mechanism of aquatic emergent pollutants by new bio-based chars. *Environmental Science and Pollution Research*, 24(28), 22698-22708. doi:10.1007/s11356-017-9938-9

11) Pathak, Pranav & Mandavgane, Sachin & Kulkarni, Bhaskar. (2015). Utilization of banana peel for the removal of benzoic and salicylic acid from aqueous solutions and its potential reuse. Desalination and water treatment. 57. 10.1080/19443994.2015.1051589.
12) Ayyash, Fatima and Kamis, Mustafa and Khalaf, Samer and Thawabteh, Amin and Karaman, Rafik, Removal of Aspirin, Salicylic Acid, Paracetamol and p-Aminophenol by Advanced Membrane technology Activated Charcoal and Clay Micelles Complex. (May 2015). Case Studies Journal ISSN (2305-509X) – Volume 4, Issue 5 – May-2015, Available at SSRN: https://ssrn.com/abstract=3402299
13) Ali A, Singh BP. Studies on production potential of cape gooseberry (Physalis peruviana L.) in sodic soil under varying agronomic manipulations. *Journal of Applied and Natural Science*. 2016; 8:368-374
14) Ahmed, Lamiaa. (2014). Renoprotective Effect of Egyptian Cape Gooseberry Fruit (Physalis peruviana L.) against Acute Renal Injury in Rats. *TheScientificWorldJournal*. 2014. 273870. 10.1155/2014/273870.
15) Ncibi, M. C., Mahjoub, B., Mahjoub, O., & Sillanpää, M. (2017). Remediation of emerging pollutants in contaminated wastewater and aquatic environments: Biomass-based technologies: Water. *CLEAN- Soil,Air,Water*, 45(5), 1700101. doi:10.1002/clen.201700101
16) Otero M, Grande C and Rodrigues A. "Adsorption of salicylic acid onto polymeric adsorbents and activated charcoal." *Reactive & Functional Polymers*. (2003) 60: 203-213.
17) Fu, Z., Li, H., Yang, L., Yuan, H., Jiao, Z., Chen, L.,. Liu, Y. (2015). Magnetic polar post-cross-linked resin and its adsorption towards salicylic acid from aqueous solution. *Chemical Engineering Journal, 273*, 240-246. doi:10.1016/j.cej.2015.03.005
18) Rao, A. N., Sivasankar, B., & Sadasivam, V. (2009). Kinetic study on the photocatalytic degradation of salicylic acid using ZnO catalyst. Journal of Hazardous Materials, 166(2), 1357–1361. https://doi.org/10.1016/j.jhazmat.2008.12.051
19) Ahmad Bhawani S, Fong SS, Mohamad Ibrahim MN. Spectrophotometric Analysis of Caffeine. *Int J Anal Chem*. 2015;2015:170239. doi: 10.1155/2015/170239. Epub 2015 Oct 29. PMID: 26604926; PMCID: PMC4641934
20) Case Study: Removing caffeine from Coffee. (2013, October 2). Chemistry LibreTexts.https://chem.libretexts.org/Bookshelves/Physical_and_Theoretical_Chemistry_Textbook_Maps/Supplemental_Modules_(Physical_and_Theoretical_Chemistry)/Physical_Properties_of_Matter/States_of_Matter/Supercritical_Fluids/Case_Study%3A_Removing_caffeine_from_Coffee
21) Hopcroft, F. J. (2015;2014;). Wastewater treatment concepts and practices (1st ed.). New York, [New York] (222 East 46th Street, New York, NY 10017): Momentum Press.
22) Yang, P. Y., and Zhi-Qin Zhang. “Nitrification and Denitrification in the Wastewater Treatment System.” *Eubios Ethics Institute.* www.eubios.info/TTEC/TTECPY.htm.

23) Das, S., Ray, N. M., Wan, J., Khan, A., Chakraborty, T., & Ray, M. B. (2017). Micropollutants in wastewater: fate and removal processes. *In Physico-Chemical Wastewater Treatment and Resource Recovery*. IntechOpen.
24) AbuZeid,K.,Elrawady,M., CEDARE (2014), 2030 Strategic Vision for Treated Wastewater Reuse in Egypt, Water Resource Mangaement Program- CEDARE
25) Ling, X., Li, H., Zha, H., He, C., & Huang, J. (2016). Polar-modified post-cross-linked polystyrene and its adsorption towards salicylic acid from aqueous solution. *Chemical Engineering Journal, 286*, 400-407. doi:10.1016/j.cej.2015.11.014
26) Combarros, R. G., Rosas, I., Lavín, A. G., Rendueles, M., & Díaz, M. (2014). Influence of biofilm on activated carbon on the adsorption and biodegradation of salicylic acid in wastewater. *Water, Air, & Soil Pollution, 225*(2), 1-12. doi:10.1007/s11270-013-1858-9
27) R.N. Coimbra, V. Calisto, C.I.A. Ferreira, V.I. Esteves, M. Otero, Removal of pharmaceuticals from municipal wastewater by adsorption onto pyrolyzed pulp mill sludge, *Arabian Journal of Chemistry*, Volume 12, Issue 8, 2019,Pages 3611-3620, ISSN 1878-5352,https://doi.org/10.1016/j.arabjc.2015.12.001.
28) Sotelo, J. L., Ovejero, G., Rodríguez, A., Álvarez, S., Galán, J., & García, J. (2014). Competitive adsorption studies of caffeine and diclofenac aqueous solutions by activated carbon. *Chemical Engineering Journal*, 240, 443-453. doi:10.1016/j.cej.2013.11.094
29) Michalis K. Arfanis, Panagiota Adamou, Nikolaos G. Moustakas, Theodoros M. Triantis, Athanassios G. Kontos, Polycarpos Falaras, Photocatalytic degradation of salicylic acid and caffeine emerging contaminants using titania nanotubes, *Chemical Engineering Journal*, Volume 310, Part 2, 2017, Pages 525-536, ISSN 1385-8947, https://doi.org/10.1016/j.cej.2016.06.098
30) Abbas, S. H., Ismail, I. M., Mostafa, T. M., & Sulaymon, A. H. (2014). Biosorption of heavy metals: a review. *J. Chem. Sci. Technol*, *3*(4), 74-102
31) Bayomie, O.S., Kandeel, H., Shoeib, T. *et al.* Novel approach for effective removal of methylene blue dye from water using fava bean peel waste. *Sci Rep* **10,** 7824 (2020). https://doi.org/10.1038/s41598-020-64727-5
32) Mohamed, S., El-Sayed, M.M.H., Removal of imidacloprid pesticide using nanoporous activated carbons produced via pyrolysis of peach stone agricultural wastes, *Chem. Eng. Comm.* 2020, doi: 10.1080/00986445.2020.1743695.
33) Ajay K Kashyap, Tripti Agarwal. Removal of salicylic acid from aqueous solutions by magnetic biosorbent synthesized from pineapple peel. *Pharma Innovation* 2019;8(1):502-504
34) Donald Raoul, Tchuifon & George Ndifor A Anagho Solomon Gabche, Nche & Joseph Mbadcam, Ketcha. (2015). 1- Adsorption of salicylic and sulfosalicylic acid onto powdered Activated Carbon prepared from Rice and Coffee Husks..*International Journal of Current Engineering and Technology*. 5. 1641-1652.

35) Essandoh, M., Kunwar, B., Pittman, C. U., Mohan, D., & Mlsna, T. (2015). Sorptive removal of salicylic acid and ibuprofen from aqueous solutions using pine wood fast pyrolysis biochar.*Chemical Engineering Journal, 265*, 219-227. doi:10.1016/j.cej.2014.12.006
36) Torrellas, S. Á., García Lovera, R., Escalona, N., Sepúlveda, C., Sotelo, J. L., & García, J. (2015). Chemical-activated carbons from peach stones for the adsorption of emerging contaminants in aqueous solutions. *Chemical Engineering Journal*, 279, 788-798. doi:10.1016/j.cej.2015.05.104
37) Álvarez, S., Ribeiro, R. S., Gomes, H. T., Sotelo, J. L., & García, J. (2015). Synthesis of carbon xerogels and their application in adsorption studies of caffeine and diclofenac as emerging contaminants. *Chemical Engineering Research and Design*, 95, 229-238. doi:10.1016/j.cherd.2014.11.001
38) Atomssa, T. & Gholap, A. V. Characterization of caffeine and determination of caffeine in tea leaves using UV-visible spectrometer. *African J of Appl*. Chem. 7, 22–31 (2015).
39) Simbaqueba, J. (2017). Analysis of Fusarium oxysporum effectors shared between strains that infect cape gooseberry and tomato
40) Shahat, M. (2018, March 05). Personal interview [Personal interview]
41) García-Mendieta, A., Olguín, M. T., & Solache-Ríos, M. (2012). Biosorption properties of green tomato husk (physalis philadelphica lam) for iron, manganese and iron–manganese from aqueous systems. *Desalination*, *284*, 167-174. doi:10.1016/j.desal.2011.08.052
42) Pavia, D. L., Lampman, G. M., Kriz, G. S., & Vyvyan, J. A. (2014). Introduction to Spectroscopy. Cengage Learning.
43) Jalvandi, Javid. (2016). Novel chemical and physical approaches for sustainable drug release from biodegradable electrospun nanofibres. 10.13140/RG.2.2.26541.69607.
44) Zhou, Weilie & Apkarian, Robert & Wang, Zhong & Joy, David. (2006). Fundamentals of Scanning Electron Microscopy (SEM). 10.1007/978-0-387-39620-0_1.
45) Stefanaki, E.-C. (2008). Electron Microscopy: The Basics. Physics of Advanced Materials Winter School
46) Webb P. (2003), Introduction to Chemical Adsorption Analytical Techniques and their Applications to Catalysis." *MIC Technical Publications*.
47) Scanning Electron Microscope—Radiological and Environmental Management—Purdue University.(n.d.).Retrieved December 11, 2020, from https://www.purdue.edu/ehps/rem/laboratory/equipment%20safet /Research%20Equipment/sem.html
48) (Project), ACOL, and Sandie Lindsay. High Performance Liquid Chromatography. J. Wiley for Thames Polytechnic, Chichester, 1992
49) Snyder, L. R., Kirkland, J. J., & Dolan, J. W. (2011). Introduction to Modern Liquid Chromatography. John Wiley & Sons

50) Llewellyn P, Bloch E, and Bourelly S. (2012), Characterization of Solid Materials and Heterogeneous Catalysts: From Structure to Surface Reactivity, 1st Edition. 2012 *Wiley-VCH, Weinheim*,
51) Atkins P and de Paula J. ATKINS' (2006) PHYSICAL CHEMISTRY. 8th. Great Britain: Oxford University Press
52) Chiou, Cary. (2003). Fundamentals of the Adsorption Theory. 10.1002/0471264326.ch4.
53) Surface Area and Porosity Determinations by Physisorption. (2020). Elsevier. https://doi.org/10.1016/C2018-0-00544-7
54) Ayawei, N., Ebelegi, A. N., & Wankasi, D. (2017, September 5). Modelling and Interpretation of Adsorption
55) Butt, H., Graf, K., & Kappl, M. (2003). Physics and chemistry of interfaces. Weinheim: Wiley-VCH.
56) Leddy N. (2012) "SURFACE AREA AND POROSITY." Centre For Microscopy and Analysis.
57) Durán-Valle C.J (2012). Techniques Employed in the Physicochemical Characterization of Activated Carbons, Lignocellulosic Precursors Used in the Synthesis of Activated Carbon - Characterization Technique sand Applications in the Wastewater Treatment
58) Naumov S.(2009) "Hysteresis Phenomena in Mesoporous Materials." University of Leipzig, Dissertation
59) Adsorption isotherm models. (n.d.). Gas Adsorption Technology. Retrieved December 6, 2020, from https://gasadsorptiontech.wordpress.com/tag/adsorption-isotherm-models/ Yang, Shuang & Chen, Guojun & Lv, Chengfu & Li, Chao & Yin, Na & Yang, Fei & Xue, Lianhua. (2017). Evolution of nanopore structure in lacustrine organic-rich shales during thermal maturation from hydrous pyrolysis, Minhe Basin, Northwest China. *Energy Exploration & Exploitation*. 36. 10.1177/0144598717723647
60) Khoshnevisan, K., & Barkhi, M. (2015). Zeta potential (https://doi.org/10.13140/RG.2.1.4554.3844)
61) Nanocomposix.eu. (n.d.). CHR6. Zeta Potential Measurements. Nanocomposix.Eu. Retrieved December 6, 2020, from https://nanocomposix.eu/pages/chr6-zeta-potential-measurements
62) Atkins, P. W. (1998). Physical chemistry (6th ed.). Oxford: Oxford University Press.
63) Levin, A., Alenichev, M., Masalov, V., Sukhinina, N., & Emelchenko, G. (2018). Developing of Standard Reference Materials of the Electrokinetic (Zeta) Potential of Nanoparticles. Nan*otechnologies in Russia*,13, 90 https://doi.org/10.1134/S1995078018010068
64) Nechifor, G., Pascu, D., PASCU, M., Alina, C., Bunaciu, A. A., & Aboul-Enein, H. (2013). Study of adsorption kinetics and zeta potential of phosphate and nitrate ions on a cellulosic membrane. *Revue Roumaine de Chimie*, 58, 591–597.
65) Pavia, D. L., Kriz, G. S., Lampman, G. M., & Engel, R. G. (2015). A Small Scale Approach to Organic Laboratory Techniques. Cengage Learning

66) Girard, K. K., & Sinha, N. K. (2006). Cranberry, Blueberry, Currant, and Gooseberry. In Handbook of Fruits and Fruit Processing (pp. 369–390). John Wiley & Sons, Ltd. https://doi.org/10.1002 /9780470277737.ch21
67) Essa, H.L.; Guirguis, H.A.; El-Sayed, M.M.H.; Rifaat, D.; Abdelfattah, M.S. Ultrasonically-Extracted Marine Polysaccharides as Potential Green Antioxidant Alternatives. *Proceedings* **2020**, *67*, 23. https://doi.org/10.3390/ASEC2020-07606
68) Abou El Azm, N. Fleita, D., Rifaat, D. Mpingirika, E.Z., Amleh, A., **El-Sayed***, **M.M.H.**, Production of bioactive compounds from the sulfated polysaccharides extracts of *Ulva lactuca*: Post-extraction enzymatic hydrolysis followed by ion-exchange chromatographic fractionation, *Molecules* **2019**, 24, 2132, doi: 10.3390/molecules24112132
69) Pakhra V. & Srivastava V, Adsorption of benzoic acid and salicylic acid onto granular activated carbon, International Conference on Chemical, Civil and Environment engineering (2012)

8.Appendix

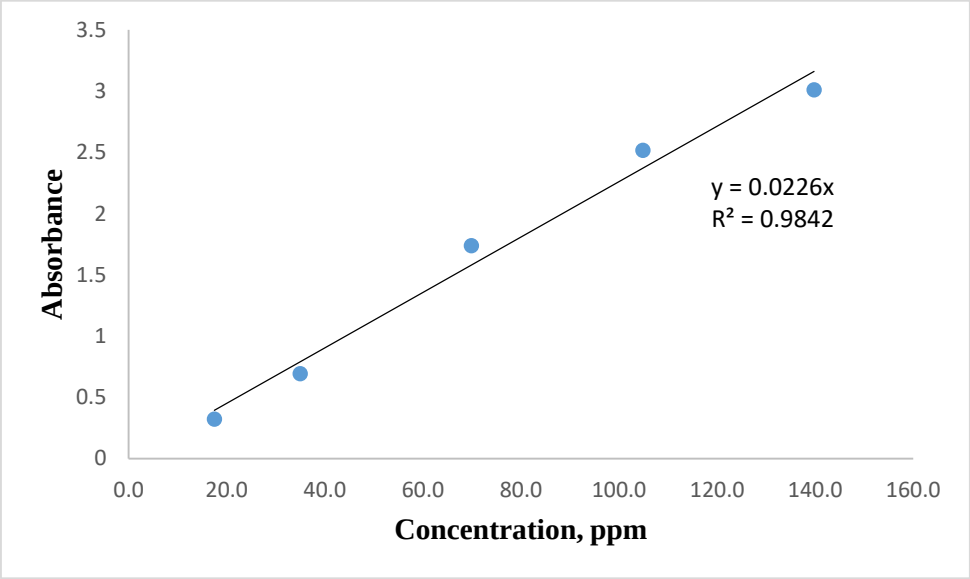

Figure 8.1 Calibration Curve for SA for UV-Spectrophotometer

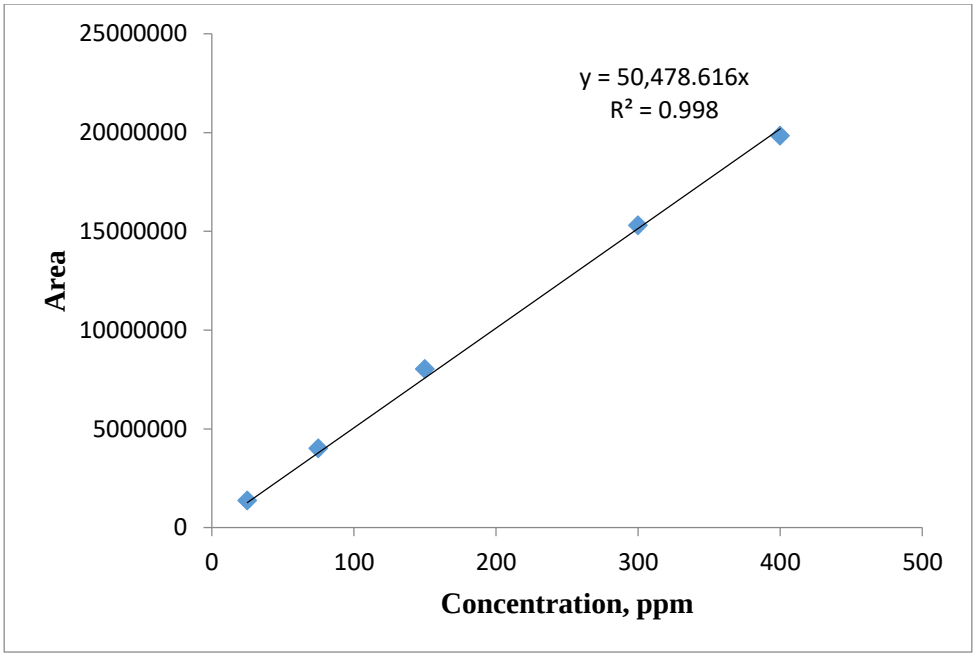

Figure 8.2 Calibration curve for CA for HPLC

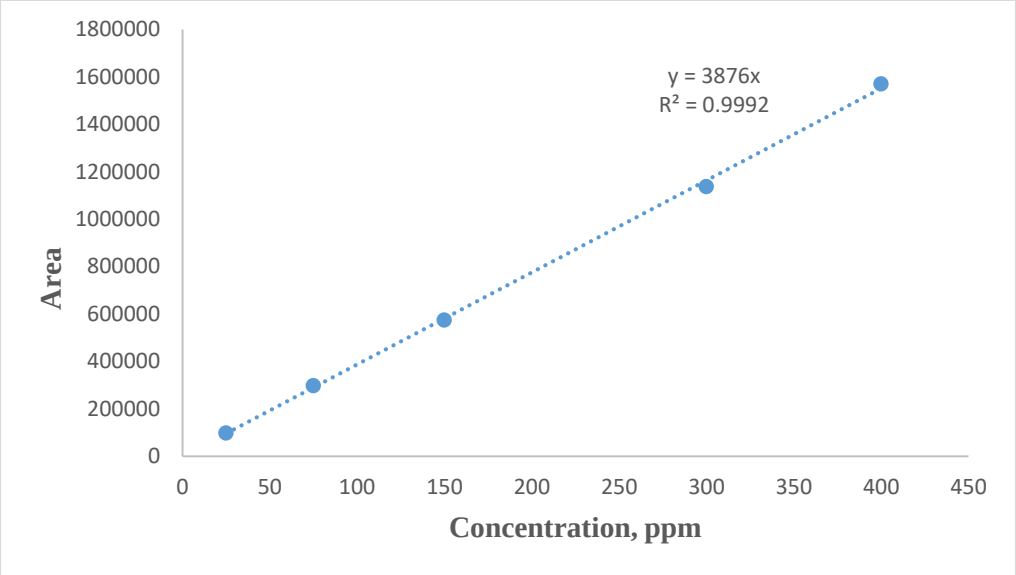

Figure 8.3 Calibration Curve of SA for HPLC

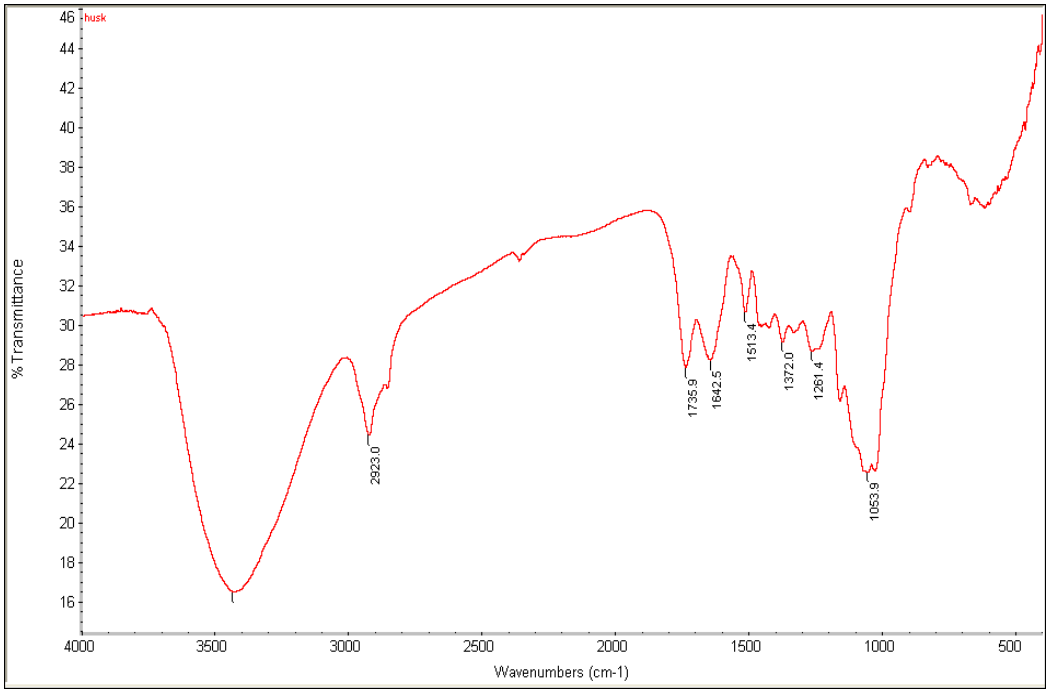

Figure 8.4 IR spectrum of H before adsorption

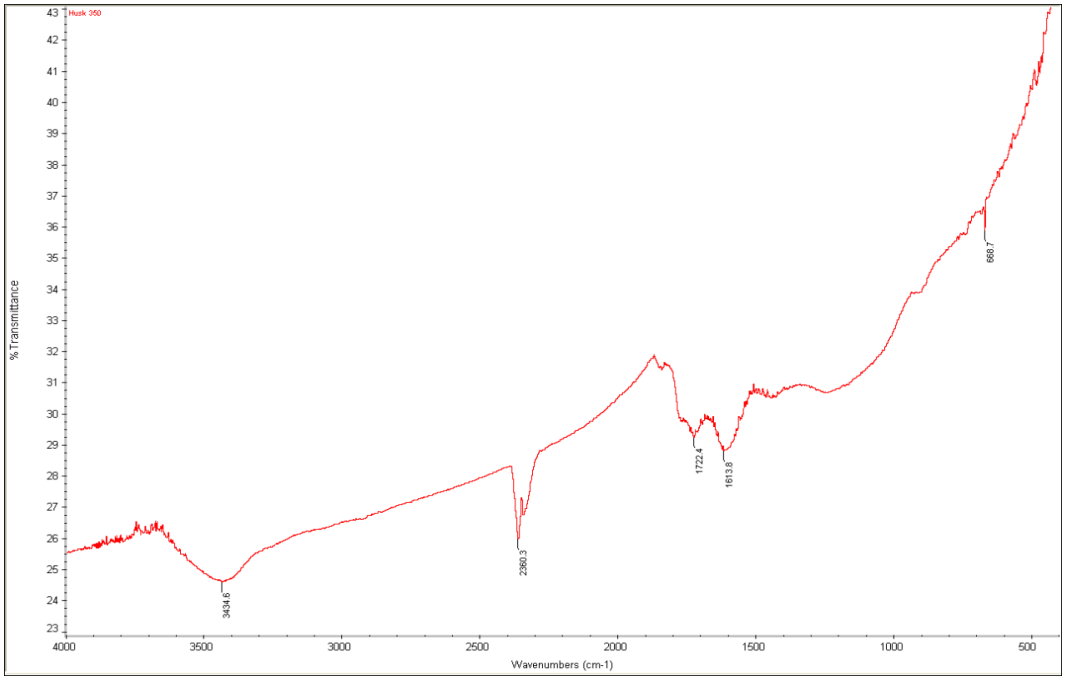

Figure 8.5 IR spectrum of H350 before adsorption

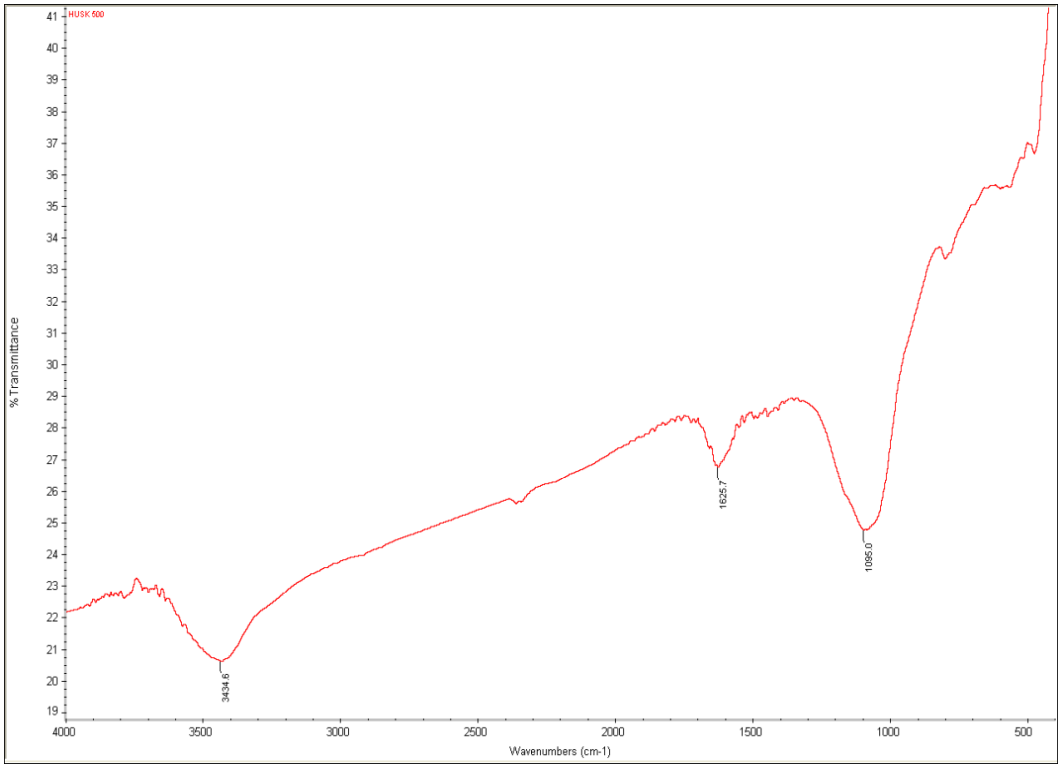

Figure 8.6 IR spectrum of H500 before adsorption

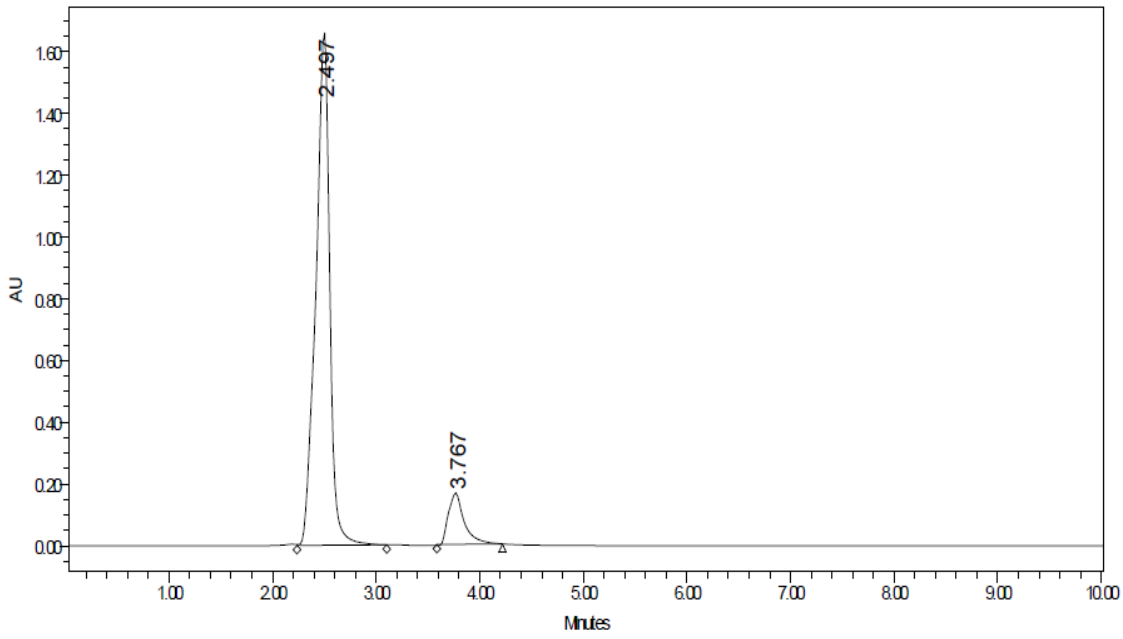

Figure 8.7 HPLC spectrum for a binary system of SA and CA at a wavelength of 275 nm